# Understanding the mechanism of $^{177}$Lu- PSMA617 radioligand therapy and evaluating its potential role in the treatment of metastatic castrate-resistant prostate cancer (mCRPC)

**By**

**Jay Joshi**

**B.Sc., California State University of Bakersfield, 2016**

**A Thesis Submitted in Partial Fulfillment of the Requirements of the Degree of**

**MASTER OF SCIENCE**

**In the Department of Biochemistry and Microbiology**



**University of Victoria**

Understanding the mechanism of $^{177}$Lu- PSMA617 radioligand therapy and evaluating its potential role in the treatment of metastatic castrate-resistant prostate cancer (mCRPC)

By
Jay Joshi
B.Sc., California State University of Bakersfield, 2016

## Supervisory Committee

Dr. Julian J. Lum, Supervisor
*Department of Biochemistry and Microbiology*

Dr. Lisa Reynolds, Departmental Member
*Department of Biochemistry and Microbiology*

Dr. Martin Boulanger, Departmental Member
*Department of Biochemistry and Microbiology*

Dr. Devika Chithrani, Outside Member
*Department of Physics and Astronomy*

# Abstract

Prostate cancer (PCa) is the most common cancer in men and the third leading cause of cancer-related deaths in Canadian men. Despite hormone and radiation therapies, most patients progress to late-stage metastatic castrate-resistant prostate cancer (mCRPC). $^{177}$Lu-PSMA617 radioligand therapy (rLT) is a radioactive biochemical substance that targets the human prostate-specific membrane antigen (hPSMA). This rLT has been used in compassionate trials in mCRPC patients and has been demonstrated significant clinical efficacy. However, recent findings suggest that this efficacy is short-lived, and most patients exhibit tumor recurrence. Here we establish a murine model to study the anti-tumor effects and the corresponding immune response of $^{177}$Lu-PSMA617 rLT on prostate cancer. We generated a doxycycline-inducible hPSMA-expressing murine prostate cancer (hPSMA TRAMP-C2) cell line with high binding responses to PSMA617. Using this system, we evaluated the *in vitro* and *in vivo* binding of $^{177}$Lu-PSMA617 to the hPSMA TRAMP-C2 cell line. Here, we show that the hPSMA TRAMP-C2 cell line expresses hPSMA upon doxycycline induction and that $^{177}$Lu-PSMA617 can bind to its target *in vitro* and *in vivo*. Together, these results show that the developed hPSMA TRAMP-C2 cell line can be used to investigate therapeutic and immunological responses targeted against hPSMA in prostate cancer.

# Table of Contents

## List of Figures

# Dedication

This thesis is first and foremost dedicated to all persons afflicted with prostate cancer. Secondly, I would like to also dedicate this thesis to my entire Joshi family.

# Acknowledgments

I would like to begin by thanking my supervisor Dr. Julian Lum. I appreciate him taking me on as a graduate student and supervising me throughout my master's degree. He was not only a mentor to me in the lab but also a guiding hand in a lot of my decisions I made and will make as I move forward. He has an intense passion for science and infinite energy to pursue it which I can only learn to be inspired from. He has been patient with me since the first day I started in the lab, as I performed experiments that yielded mediocre results. I think I've come a long way as a researcher and as a person, and I thank him for his contributions to my development.

I would also like to thank a few other members of the Deeley Research Centre (DRC), Nils Pavey, Eunice Kwok and Marisa Kilgour. Nils Pavey initially started as my lab mentor, but overtime has become one of my best friends and I am very lucky to have met him during my time at DRC. He is a brother to me and was always willing to help me, and anyone else who needed it. Eunice Kwok was a member of our sister "Nelson" lab but was integral in my experience as a scientist and made me more diligent in being involved with extracurricular activities at DRC and at UVIC. Marisa Kilgour and I were the only two graduate students when I started my program. Throughout our program, she has taught me to be a better scientist and has become one of my closest friends. All three of them contributed greatly not only to my research experience but also made me feel at home in a new country. I would also like to show my appreciation for other members of the aptly named "Lum Lab Legends" that have played a big role during my time at DRC. I truly appreciate the other members of DRC who played a big role in my personal development as a scientist and a better human being.

I would also like to extend my thanks to the members of my committee, Drs. Lisa Reynolds, Devika Chithrani and Martin Boulanger. They have each contributed to the direction and completion of my research and I thank them for their mentorship.

I would also like to my thank my gurus HDH Mahant Swami Maharaj and HDH Pramukh Swami Maharaj. My friends and family also deserve significant acknowledgement for their support and understanding throughout this journey. I would like to thank them for their enduring encouragement throughout my academic journey. They have always believed in me which has helped me believe in myself. I would also like to acknowledge my sister who might be younger but still an inspiration to me. Finally, my parents deserve a great deal of thanks for immigrating to the west without any help and allowing me the opportunity to pursue my dreams. I look forward to pursuing the next stage of my life that I have acquired due to your sacrifices.

# Additional Acknowledgments

Due to the multi-disciplinary nature of this project and the grant that was funded to carry out the experimental work, multiple groups and individuals worked together on aspects of my thesis. I wish to acknowledge their contributions by listing them below as well as indicating at the beginning of each appropriate chapter of my thesis. However, I wish to point out that all experiments were discussed and designed as a team, and the results were also discussed together.

**Chapter 2:**

- **Figure 8:** Helen Merkens performed the *in vitro* binding-response experiment (Figure 8A) and Marin Simunic was responsible for performing the *in vivo* experiment with the $^{18}$F-DCFPyL ligand.
- **Figure 9:** The PET/CT image scans were captured by Marin Simunic after evaluating the *in vivo* $^{18}$F-DCFPyL binding response.

**Chapter 3**

- **Figure 11A:** The TRAMP-C2 cells were irradiated using Truebeam linear accelerator with the help of Adria Devlinger and Tim Turcotte at BC Cancer Victoria.
- **Figure 11B:** Helen Merkens treated the hPSMA TRAMP-C2 cells with $^{177}$Lu-PSMA617 and collected the lysates. These lysates were then utilized to perform western blot experiments.

**Chapter 4**

- **Figure 14:** Helen Merkens treated the developed hPSMA TRAMP-C2 cells with $^{177}$Lu-PSMA617 and collected the supernatants. These supernatants were utilized to quantify HMGB1 levels post-treatment.

**Chapter 5**

- **Figure 17:** The TRAMP-C2 cells were irradiated using Truebeam linear accelerator with the help of Adria Devlinger and Tim Turcotte at BC Cancer Victoria.

# Chapter 1: Introduction

## Summary of Prostate Cancer

Prostate cancer (PCa) is the most common cancer in Canadian men. Recent analysis suggests that 1 in 7 men will be diagnosed with prostate cancer in their lifetime [1, 2]. PCa progresses slowly during early stages but can be aggressive and lethal during late stages [1]. Although PCa has one of the highest five-year survival rates compared to other cancers, treatments for patients with late-stage PCa are ineffective [1, 3, 4]. The current standard-of-care treatments are only effective during the early stages of PCa. These treatment options become ineffective as the disease progresses to a hormone-dependent state. Androgen deprivation therapy (ADT) is often prescribed to patients at this stage of PCa [5, 6]. However, patients receiving ADT advance to a hormone-independent state known as castrate-resistant prostate cancer (CRPC) [2, 4]. Patients with CRPC rapidly advance to the final stage of PCa known as metastatic castrate-resistant prostate cancer (mCRPC), for which there is currently no cure [2, 4]. This clinical problem forms the rationale for my thesis aimed at developing effective, novel therapies that can be used to treat patients with mCRPC.

## 1.1. Diagnosis

Prostate cancer is a slow growing disease and symptoms may not present themselves for many years [1, 3, 7]. The diagnosis of PCa is based on microscopic evaluation of prostate tissue acquired through a needle biopsy. A primary and secondary Gleason grade (on a scale of 1 to 5) are attributed to the sample based on most dominant histological patterns observed [8, 9]. The diagnosis is further stratified into low, intermediate and high-risk based on the sum of the Gleason scores and prostate specific antigen (PSA) levels in the blood. Combined Gleason scores

of 8, 9 or 10 can lead to death in significantly shorter amount of time compared to lower sums (≤ 6) [10, 11]. A study conducted on untreated cancer patients by Albertsan *et al.* showed that men with tumors of Gleason score 5 had 6 - 11% mortality rate at 20 years post-diagnosis [8, 10]. In the same 20-year follow-up analysis, this mortality rate slowly increased to 70% (Gleason score 7-8) and 87% (Gleason score 10) with few patients surviving past 15 years post-diagnosis [10]

Technological advances have allowed the diagnostic field to generate innovative imaging technologies that enhance diagnostic performance. The most notable has been the multiparametric magnetic resonance imaging (MRI). A prospective study of 1003 men who had received prostate biopsies found that targeted biopsies through MRI-ultrasound fusion identified 30% more cases of Gleason score ≥ 4 + 3 disease compared to systemic prostate biopsies [11, 12]. New molecular biomarkers that classify tumor aggressiveness have also become available. Using biopsy tissue, a cell cycle progression score based on 31 genes can be utilized to predict clinical outcome [13]. There has also been increased interest in diagnosing with positron emission tomography (PET) scans. Various radiotracers such as $^{18}$F-fluciclovine PET-CT and $^{11}$C-choline PET-CT provide ≥80% sensitivity in PCa [14]. Recently, PET-CT and PET-MRI based on prostate-specific membrane antigen (hPSMA; an enzyme overexpressed in PCa cells) showed favorable sensitivity to existing modalities, particularly in patients with low PSA levels and for detection of distant bone metastases [4, 12**,** 15].

## 1.2. Prostate Specific membrane antigen

Prostate specific membrane antigen (hPSMA), also known as glutamate carboxypeptidase 2 or N-acetyl-L-glutamate peptidase I, is a type-II membrane protein highly expressed on prostate cells compared to other sites in the body [16, 17, 18]. This expression of hPSMA increases significantly as PCa progresses to later stages [16, 17, 18].

hPSMA has a three-part structure including: a 19-amino-acid (AA) internal portion, a 23AA transmembrane and a 707AA external portion [18, 19]. It is known to have enzymatic activities and acts as a glutamate-preferring carboxypeptidase [18, 19].

One unique characteristic of hPSMA is that its known to have an internalization signal that allows the surface protein to enter the cell as an endosome. This characteristic makes it an attractive target for diagnosing and treating PCa with hPSMA-targeting agents [5, 19]. As mentioned, hPSMA is known to be highly expressed in PCa, particularly in poorly differentiated, metastatic, castrate-resistant carcinomas [19, 20]. These two characteristics can help distinguish local versus advanced/metastatic PCa and target distant metastatic sites.

Over the past two decades, hPSMA's unique characteristics have been exploited to generate antibodies and ligands that can target this protein. One of the first agents targeting hPSMA was a monoclonal antibody called mAb 7E11 used to detect hPSMA on the human prostate cancer cell line LNCaP [19, 20]. The next generation of antibodies were further improved to target the extracellular portion of hPSMA which could be internalized by hPSMA-expressing cells [19, 20]

## 1.3. Treatments in Prostate Cancer

Once the PCa stage and aggressiveness are assessed, treatments are recommended based on patient's risk assessment, age of the patient, and doctor's recommendation. Low-risk patients are recommended active surveillance to monitor progression; intermediate- to high-risk patients are suggested radical prostatectomy, various levels of radiation therapy (RT) and androgen-deprivation therapy (ADT) [1, 8, 21]. For patients who fail multiple lines of treatment and progress to mCRPC (bone metastases), there are no viable treatment options available. Currently there are many new therapies in development that may benefit patients in the future.

### 1.3.1. Active Surveillance and watchful waiting

As a measure to provide the most effective treatment option to patients, active surveillance (AS) was introduced. Patients diagnosed with low-risk or with localized disease are recommended active surveillance (monitoring for PCa without going through therapy) [8, 21, 22]. Active surveillance includes multiple PSA testing, physical examinations and prostate biopsies with an intent to cure the disease. Watchful waiting consists of treating symptoms for only palliative intent. Active surveillance is also suggested to low-risk patients for better quality of life. A trial performed by Prostate Testing for Cancer and Treatment randomized 1643 men (ages 50 to 69) with diagnosed localized PCa into AS (n=545), surgery (n=553), or radiation (n=545). There was no significant difference in the mortality rate at 120 months between the three groups [8, 12]. Even though 50% of AS group had to receive treatment in the future, they were reported to have better quality of life compared to the other two groups [12].

### 1.3.2. Radical Prostatectomy

Radical Prostatectomy (RP) is a surgical procedure in which the whole prostate and seminal vesicles are removed. This is an effective treatment option for patients whose cancer has not yet spread outside the prostate (stages I and II). The surgery can be performed with open or laparoscopic surgery. The type of surgery is left to the surgeon's discretion although men undergoing laparoscopic surgery have lower blood-loss and shorter recovery time compared to open surgery [8, 9, 24]. There has been no concrete evidence to suggest if one surgical procedure is better than the other [8, 9].

Once the prostate is removed and if the cancer is still localized, PSA levels can drop to zero. A randomized controlled trial reported that RP led to increased reduction in mortality rate compared to the AS group only if the tumor was completely removed [8, 24]. A study performed

by the Scandinavian Prostate Cancer Group randomized 695 men to surgery or watchful waiting with 76% of the patients having a palpable tumor [8, 25]. The results showed that benefits of surgery became more significant over time. In 10 to 18 years post-diagnosis, clinicians saw significant reductions in metastases and need for ADT [25].

### 1.3.3. Radiation Therapy in PCa

Radiation therapy (RT) has been a standard therapy option for patients with localized tumor. RT includes a treatment in which ionizing radiation is utilized to kill cancer cells [6, 26]. It is widely used as a primary treatment for PCa but can also be used as an adjuvant treatment. RT can be delivered as external beam radiation therapy (EBRT), brachytherapy or as systemic radiation therapy [26, 27].

EBRT utilizes a high-energy radiation from an external source to deliver a radiation load to the tumor. For an accurately targeted-radiation, three small gold markers are used to visualize the exact location of the prostate before the radiation is delivered [6, 28]. Although there are many different modalities through which EBRT can be delivered, most patients are recommended 3-dimensional conformal radiation therapy (3D-CRT) or intensity modulated radiotherapy (IMRT) and more recently through volumetric modulated arc therapy (VMAT) [6, 26, 27]. These modalities were developed to ensure a targeted and effective dosage to the tumor while decreasing damage to nearby healthy tissue.

The radiation dosage is measured in Grays (Gy). A standard clinical dosage for conformal radiotherapy is 74 Gy given in 2 Gy doses or “fractions” to the prostate. Once the patient receives radical prostatectomy, this radiation load is reduced to 66 Gy [29, 30]. Dose escalation has been shown to reduce PSA levels but has not shown significant improvement in overall survival [30].

Brachytherapy is another method for delivering radiation dosage [31, 32. 33]. Instead of using an external radiation source, radioactive seeds are placed in the prostate, and the dosage is administered as internal radiation [32]. Brachytherapy implants can be either temporary or permanent depending on the radiation dosage. Brachytherapy is mostly used for low-to high-risk patients and can be divided into two groups: high-dose rate (HDR) and low-dose rate (LDR) [33, 34]. LDR is utilized for patients classified as low-risk. HDR brachytherapy is recommended for high-risk patients and is used together with EBRT to boost the radiation dose to the tumor site [32, 33, 34].

Systemic radiation therapy is a developing treatment option for patients with metastasized PCa [27, 35]. In this treatment, a radioactive substance, such as radioactive iodine or a radioactively labeled monoclonal antibody is administered to the patient, which circulates through the blood to reach distant tumor sites [36]. PCa metastasizes through the lymph node and later to the bone. Radium-223 dichloride is a type of approved systemic radioisotope that particularly targets bone metastases in PCa patients [26, 36]. It is primarily an alpha emitter (energy range 5 - 7.5 MeV) with a half-life of 11.4 days [26, 36]. This treatment has been shown to improve overall survival by 3.6 months compared to standard treatment options [36]. Since Radium-223 only targets bone metastases, other non-bone tumor metastases (lymph nodes) are unaffected [7, 26, 36]. Although this treatment has been successful in patients, more effective treatment options are needed for patients with mCRPC.

### 1.3.4. Androgen Deprivation Therapy

Androgen deprivation therapy (ADT) continues to be the first-line treatment for patients with mCRPC. Prostate cells rely on the androgen receptor (AR) signaling pathway [1]. This

pathway is important for development and function of normal prostate cells and plays an important role in growth of malignant PCa cells.

ADT is utilized to limit or deplete the action of androgens on malignant prostate cells. This can be achieved through surgical (bilateral orchiectomy) or chemical castration. Surgical castration involves the removal of testes which reduces the hormone levels. Chemical castration delivers approved drugs that act on hypothalamus-pituitary-gonadal (HPG) axis. Beginning in the hypothalamus, luteinizing hormone-releasing hormone (LHRH) signals to the pituitary gland to release luteinizing hormone (LH) which induces release of androgens [37, 38]. The anterior-pituitary gland can also secrete adrenocorticotropic hormone (ACTH) which stimulates the adrenal glands to release androgens. This axis, together with the testes produces all the body's androgen supply [37, 38]

LHRH agonists and antagonists act on the HPG axis to limit the production of LH and thus, depleting the androgens produced by the testes [38, 39]. Although this treatment can be effective in metastatic PCa patients, some advance to the more lethal stage of mCRPC [38, 39]. There have been advances to develop next-generation ADT treatments such as Abiraterone and Enzalutamide [40, 41]. These agents have shown mixed success in PCa patients that have progressed to mCPRC [40. 41. 42]. Another downside to these treatments is the prevalence of adverse events and related toxicity during treatment [40, 41].

## 1.3.5. New Advances in PCa Treatment

New developments using hPSMA's characteristics have included generating a new type of therapy, known as radioligand therapy (rLT) [42, 43, 44, 45, 46]. In the past, radionuclides such as Iodine-131 ($^{131}$I) were bound to hPSMA ligands to test their ability to target and kill hPSMA expressing carcinoma cells [43, 44, 47]. These $^{131}$I-labeled hPSMA ligands showed

promise thorough tumor-shrinkage in distant metastatic tumor sites [43, 47, 48]. The success in these studies led to development of other radionuclides such as Lutetium-177 ($^{177}$Lu) that could be bound to hPSMA ligands such as PSMA617 [43, 46, 49, 50]. Beginning with a compassionate trial in Germany, $^{177}$Lu-PSMA617 became an attractive therapy molecule to use for patients with mCRPC [43, 48, 51]. Ideally, the emission characteristics of the radionuclide should be the exact size to target the tumor lesions and limit the exposure to the surrounding healthy tissue. $^{177}$Lu is a β-emitting particle (490 keV) with a tissue penetration range of <2 mm [43, 48, 49, 51]. This shorter range of $^{177}$Lu provides a better irradiation load than other radionuclides such as $^{90}$Y (Figure 1). Also, $^{177}$Lu has a relatively long half-life of 6.73 days that allows for high activity of $^{177}$Lu-PSMA617 in PCa cells. During the decay, $^{177}$Lu emits $\beta^-$ particles at 497 keV and low-energy gamma photons at 208 keV to get to the stable ground state of $^{177}$Halfnium (Figure 1; 51).

| Radionuclide | Physical $T_{1/2}$ (days) | Radiation type (MeV) | Particle range (mm) |
|---|---|---|---|
| $^{131}$I | 8 | $\beta$ (0.6), $\gamma$ (0.364) | 2 |
| $^{90}$Y | 2.67 | $\beta$ (2.28) | 12 |
| $^{67}$Cu | 2.58 | $\beta$ (0.54), $\gamma$ (0.185) | 1.8 |
| $^{186}$Re | 3.77 | $\beta$ (1.08), $\gamma$ (0.131) | 5 |
| $^{177}$Lu | 6.7 | $\beta$ (0.497), $\gamma$ (0.208) | 1.5 |

The ideal radionuclide for targeted therapy is persistent, short range and powerful. Lu$^{177}$ compared favourably to other $\beta$ emitters.

**Figure 1. Different radionuclides used in targeted therapy and their characteristics. Borrowed from *Emmet et al. 2017*.**

There have been various PSMA peptides and conjugates that have been labeled with $^{177}$Lu, and which have been used for clinical use as therapy in patients with mCRPC. One of these conjugates include PSMA-DKFZ-617 or PSMA617 [43, 50]. This conjugate has been the most widely used in patients that have received therapy. It is a small-molecule peptide that is chemically conjugated with $^{177}$Lu. PSMA617 was generated as a novel theragnostic (therapy and diagnostic) compound consisting of 3 parts: a glutamate-urea-lysine pharmacophore, DOTA chelator capable of binding to $^{177}$Lu and a linker to connect the 2 entities [43, 46, 50, 51]. The linker is an important component of the compound as it impacts the internalization potency as well as the pharmacokinetic properties that has an impact on the therapeutic result [43, 46, 51].

$^{177}$Lu-PSMA617 has steadily been a main subject in prospective clinical trials. A cancer center in Australia identified 50 men out of 76 eligible for the trial. These patients had previously received treatment including docetaxel (84%), cabazitaxel (48%), enzalutamide and/or abiraterone (90%). These patients were treated with intravenous administration of $^{177}$Lu-PSMA617 every 6 weeks for a total of 4 cycles. The median overall survival (OS) was 13.3 months with PSA decline ≥ 50% in 32 of the 50 patients, including 22 patients with ≥ 80% decline [43, 52]. The overall survival of patients with mCRPC treated with standard treatments ranges from 2-5 months [2]. Various trials with $^{177}$Lu-PSMA617 have shown similar results in patients, with high response rates and low-level toxicity [43, 46, 47, 50, 52]. Although $^{177}$Lu-PSMA617 has shown to be effective, many patients seem to relapse [43, 52]. This novel treatment although effective, has been poorly studied in terms of the process by which it induces cell death and its ability to induce the immune system.

## 1.4. Immunogenic Cell Death (ICD)

Induced-cytotoxicity from radiation causes production of damage-associated molecular patterns (DAMPS). The release of DAMPS is part of a type of cell death called immunogenic cell death (ICD) [53, 54, 55]. According to current research, ICD relies on the ability of the treatment to induce cytotoxicity while also activating the coordinating release of immunogenic signals. These signals are released by the above mentioned, DAMPs. These molecules are not usually found to interact with the immune system in normal physiological conditions [53, 54, 55]. These molecules are either released or presented on the plasma membrane during a stress response or upon cellular cytotoxicity (Figure 2). The released DAMPs bind to the pattern recognition receptors (PRRs) expressed on antigen presenting cells (APCs) such as dendritic cells and macrophages. Currently, three DAMPs have been studied to play a key role in ICD: calreticulin, high mobility group box 1 (HMGB1) and ATP [53, 54, 55].

Calreticulin (CRT) is an endoplasmic-reticulum (ER) chaperone protein that becomes exposed on the cell surface during ICD stimulation [56, 57, 58]. This signaling pathway includes an ER stress module that results in arrest of protein synthesis and an apoptotic module that cleaves caspase-8 and activates a consequent cascade of downstream apoptotic events [57, 58]. Once translocated to the surface, CRT binds to lipoprotein receptor related protein 1 (LRP1) delivering a phagocytic signal to the APCs such as dendritic cells (DCs) [56, 57, 58].

The release of HMGB1 from the cells undergoing ICD, requires permeabilization of the plasma and nuclear membranes [59, 60, 61]. HMGB1 is a non-histone chromatin-binding nuclear protein. The release of HMGB1 has been well known to initiate potent immune responses through binding interactions with receptors such as TLR2 and TLR4 of various immune cells. A recent study found that HMGB1-deficient malignant cells treated with ICD inducers failed to

elicit an adaptive immune response [59, 60, 61]. This shows that HMGB1-TLR2/4 interactions play a significant role in ICD-induced cell death [59, 60, 61].

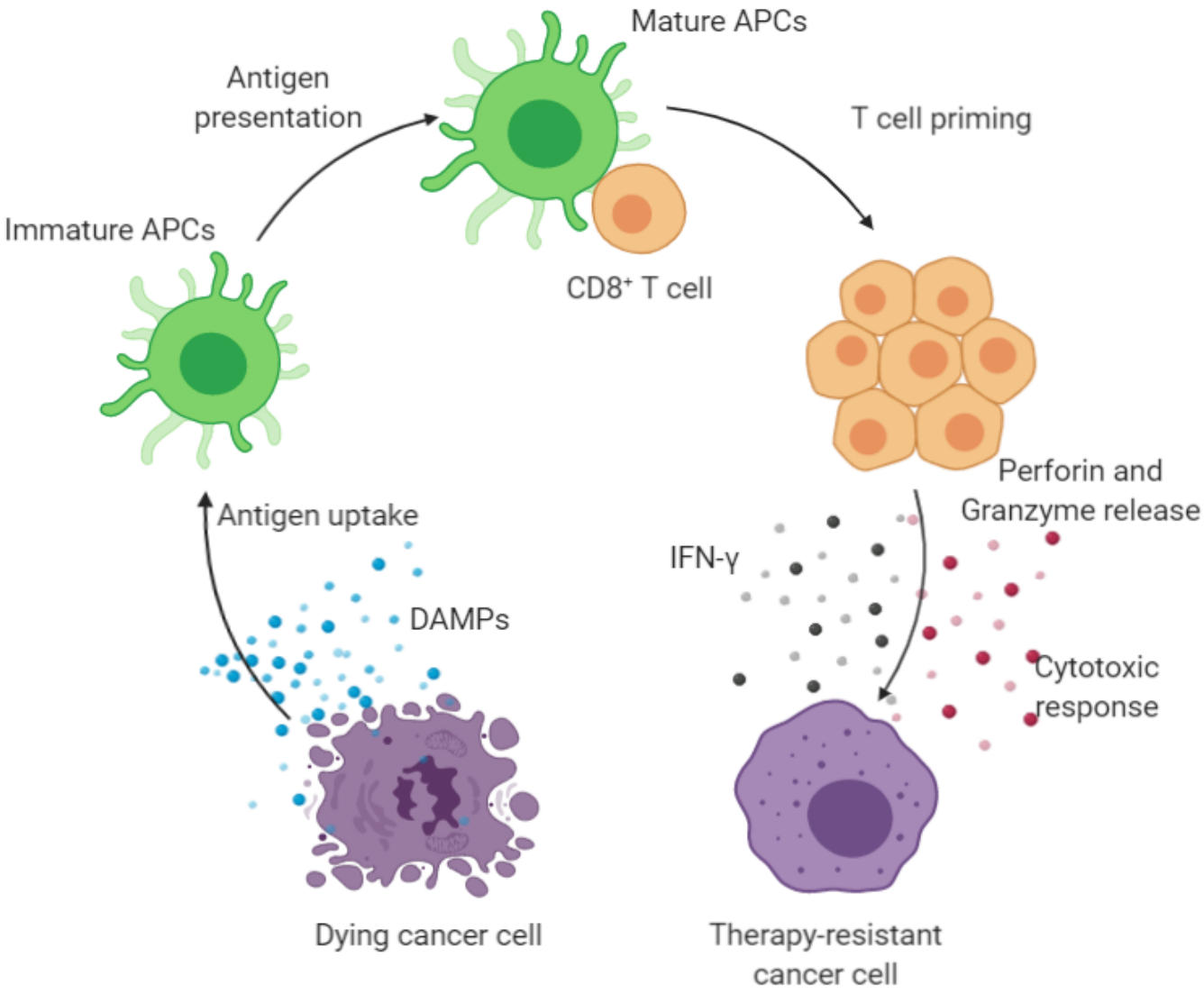


**Figure 2. Immunogenic cell death is induced through release of damage associated molecular patterns (*DAMPS*)**

There is evidence to suggest that radiation induces ICD. Many studies have shown that radiation can induce an "abscopal" response [62, 63]. Abscopal effect is a term used to describe radiation-induced anti-tumor response in distant metastatic sites [62, 63]. This response is evidence for involvement of the immune system in eliciting the distant anti-tumor response [62,

63, 64]. Although this phenomenon has been studied in the context of other ionizing radiations, there is no evidence that shows if $^{177}$Lu-PSMA617 can induce ICD.

## 1.5. Apoptosis

Apoptosis is a type of programmed cell death (PCD) that involves a coordinated and energy-dependent process involving different cascading events that end with elimination of the cell [65, 66]. This type of PCD normally occurs during development and acts as a homeostatic mechanism to maintain healthy cell populations [65, 66]. It is also an important defense mechanism when the cells are damaged by diseases such as cancer or by pathogens. In patients with cancer, irradiation or chemotherapy has been shown to induce apoptosis [66, 67]. These types of cancer treatment can lead to DNA damage in some cells, resulting in apoptotic cell death [66, 68].

As mentioned earlier, apoptosis involves highly controlled and complex mechanisms. Currently, three main mechanisms of apoptosis have been described in the literature: intrinsic/mitochondrial pathway, extrinsic/death-receptor pathway and the perforin/granzyme pathway [69, 70, 71]. The perforin/granzyme pathway is another mechanism that suggests that T-cell mediated cytotoxicity can induce apoptotic cell death [65]. Although all three mechanisms involve unique initiation steps, they all converge to the execution step of caspase-3 cleavage, which leads to DNA fragmentation, degradation of nuclear proteins, expression of phagocytic ligands, concluding with uptake by phagocytic cells [66, 68, 69, 71].

Caspases also known as cysteine aspartic proteases play critical roles in regulating different stages of apoptosis [ 66, 72, 73]. Caspases exhibit proteolytic activity that allows them to cleave proteins at aspartic acid residues. Once caspases are activated during apoptosis, there is an irreversible commitment to cell death [66, 72, 73]. This proteolytic cascade that involves a

chain-like activation of caspases amplifies the apoptotic signaling pathway leading to a faster cell death. All the identified caspases have been categorized into initiation (caspase-2, -8, -9, -10), effector (caspase-3, -6, -7) and inflammatory (caspases-1, -4, -5) caspases [72, 73, 74]. Both intrinsic and extrinsic pathways converge at the execution phase that includes activation of effector caspases such as caspase-3. These effector caspases induce activation of cytoplasmic endonucleases and proteins that can degrade nuclear and cytoskeletal proteins [66, 72, 73]. Caspase-3 is a key effector caspase and is activated by either of initiator caspases found in intrinsic (caspase-9) and extrinsic (caspase-8) pathway [66, 73, 75].

The intrinsic pathway involves a distinct arrangement of non-receptor-mediated stimuli that produce intracellular signals and are mitochondrial-initiated events [66, 76, 77]. Negative or positive signals can stimulate the intrinsic pathway of apoptosis. Example of negative signals includes absence of growth factors, hormones and cytokines that can lead to loss of apoptotic suppression and activation of PCD [66, 76]. Positive signals that can lead to apoptosis include cellular stresses such as radiation, hypoxia, viral infections and surpluses of free radicals. These stimuli can cause changes in the inner mitochondrial membrane leading to procaspase-9 activation and formation of an "apoptosome" [66, 76]. Downstream effects of this pathway include caspase-3 cleavage and DNA fragmentation [66, 76, 77].

The extrinsic pathway of apoptosis involves various transmembrane receptor-ligand interactions [66, 76]. One of those interactions is through the engagement of death receptors that are members of the tumor necrosis factor (TNF) receptor family with their respective ligands. The primary apoptosis-inducing ligands include TNF-α, lymphotoxin-α, FasL/CD178 and TNF-related apoptosis-inducing ligand (TRAIL) [66, 76, 77]. After binding interactions, downstream signaling leads to formation of signaling complexes such as the death inducing signaling

complex (DISC) resulting in activation of procaspase-8. Once caspase-8 is activated, execution phase of apoptosis is initiated [66, 76, 77].

## 1.6. Tumor Immune Landscape

As mentioned earlier, augmenting the tumor-cytotoxicity by increasing the anti-tumor immune response could potentially result in an even more effective treatment for PCa. The immune system plays a crucial role in control as well as progression of cancer. The immune system is constantly searching for foreign pathogens and even dangerous self-cells, including precancerous and cancerous cells through a process called immunosurveillance [78, 79]. Once the immune system has identified these entities, these transforming cells are quickly eliminated in a process called cancer immunoediting [78, 79, 80]. Even though the immune system has methods to stop cancer cells from replicating, some tumor variants gain the ability to survive the selective pressure imposed by the immune system [80, 81].

In a tumor microenvironment, one can find varying subsets of immune cells called tumor-infiltrating lymphocytes (TILs). As tumors develop, this microenvironment and the presence or absence of TILs can play an important role in a patient's prognosis [81, 82]. Different types of cancer and a patient's own biology can impact the density of TILs. Some of the immune cells found among the TILs include: $CD8^+$ T cells, $CD4^+$ T cells and antigen presenting cells (APCs) [80, 81].

There are two arms of the immune system, innate and adaptive, that must communicate to elicit a T cell response. Cells from the innate immune system recognize foreign pathogens through PRRs, phagocytose them and migrate to nearby lymph nodes [78, 79, 80]. These foreign pathogenic proteins are processed into fragmented peptides by APCs such as DCs, macrophages and B lymphocytes [78, 81]. These peptides are presented on the surface of APCs in

transmembrane complexes called major histocompatibility complex (MHC). There are two classes of MHCs, MHC class I is presented on all nucleated cells while MHC class II is presented only on APCs [78, 80]. During a process called T cell priming, the APCs present their peptides to naive $CD8^+$ and $CD4^+$ T lymphocytes [78, 81].

$CD4^+$ or helper T cells play an important role in providing the appropriate signals to guide the adaptive immune response. $CD4^+$ T cells secrete cytokines such as interleukin-2 (IL-2) interferon-gamma (IFN-$\boldsymbol{\gamma}$) and tumor necrosis factor-α (TNF-α) which aids APCs activate naive $CD8^+$ T cells into effector cells [80, 81]. $CD8^+$ effector cells direct a cell-mediated immune response. They act by targeting malignant cells and inducing cell-mediated apoptosis. An immunological synapse forms between the T cell and the target cell through TCR-MHC class I engagement. This leads to a cascade of signaling events that stimulates release of IFN-$\boldsymbol{\gamma}$, granzymes and perforin [78, 80, 81].

### 1.6.1 Checkpoint Blockade and Agonists

Following activation, these T cells up-regulate the expression of many surface molecules such as programmed death-1 (PD-1), and OX40 [82, 83, 84]. These molecules play important roles *in vivo*, and they can serve as markers to detect activated T cells *in vitro* and *in vivo*. PD-1 expression on naive T cells is induced on TCR activation and functions to suppress T cell activity. This inhibition is solely dependent on PD-1 binding with its corresponding ligands, PD-L1 and PD-L2 [82, 84, 85]. As mentioned earlier, to limit the malignant cell growth, immune cells can impose a selective pressure on the tumor cells. Some tumor variants gain the ability to avoid elimination through mechanisms of tumor escape such as downregulating MHC class I and expressing these checkpoint ligands such as PD-L1 [82, 83, 85].

In contrast to PD-1, which suppresses T cell function, OX40 is known to promote T cell effector function [86, 87]. OX40 or CD134 is a co-stimulatory marker expressed on activated $CD4^+$ and $CD8^+$ T cells but not naive T lymphocytes [86, 87]. OX40 signaling on T cells is induced after engagement with its corresponding ligand, OX40L [86, 87]. This ligand is not constitutively expressed but can be induced on APCs. Although TCR signals can be sufficient to induce OX40 expression, APC-derived cytokines like interleukin (IL)- 1, IL-2 and TNF can further modulate the kinetics of their expression. Interaction between OX40 and OX40L can play an important role in clonal expansion and proliferation of $CD4^+$ and $CD8^+$ T cells [86, 87, 88].

Checkpoint blockade and agonists have been gaining fast ground in the clinical field due to their ability to induce the immune system leading to better patient outcome. The most prevalent type of checkpoint therapies targets the PD-1/PDL-1 interaction [83, 89]. Clinical response with anti-PD1/anti-PD-L1 has been insignificant or minimal in PCa compared to other cancer types like melanoma [83, 89, 90]. There are several hypotheses for lack of success including the low density or even absent immune cell infiltration in PCa. This is largely due to the immunosuppressive microenvironment of the prostate [91, 92]. With the failure of PD-1/PDL-1 checkpoint inhibitors, researchers have started looking at other T cell engagements that could be exploited. OX40/OX40L engagement supports T cell survival and proliferation by enhancing IL-2 production [87, 88]. Several anti-OX40 agonists have been developed that can augment the OX40 signaling pathway in T cells. Studies have shown that anti-OX40 agonists induce significant increase in proliferation in conventional T cells [93, 94]. This engagement also stimulated increased production of IL-2 cytokine [93, 94]. Still a developing treatment, anti-OX40 agonists show a lot of promise and could be used in conjunction with other treatments in mCRPC for an augmented anti-tumor response.

# 1.7 Hypothesis and Objectives

### 1.7.1 Hypothesis

I have hypothesized that 177Lu- PSMA617 causes apoptosis and induces immunogenic cell death.

### 1.7.2 Objectives

1.7.2i. The first objective of my thesis was to develop an inducible hPSMA TRAMP-C2 cell line.

1.7.2ii. The second objective of my thesis was to determine the mechanism and kinetics of $^{177}$Lu-PSMA617 induced cell death in TRAMP-C2

# Chapter 2: Doxycycline-inducible human PSMA expression in a mouse prostate cancer cell line to study responses to $^{177}$Lu-PSMA617

## 2.1 Acknowledgements

I would like to start this chapter by thanking Marin Simunic and Helen Merkens for their assistance with this project. The team in Vancouver, BC utilized the cell lines developed in this chapter to perform binding response experiments (Figure 8) and perform the *in vivo* experiment in immunodeficient mice (Figure 9).

## 2.2 Abstract

Prostate cancer is the most common cancer in men and the third leading cause of cancer-related deaths in Canadian men [95]. Despite hormone and radiation therapies, most patients progress to late-stage metastatic castrate-resistant prostate cancer (mCRPC). $^{177}$Lu-PSMA617 radioligand therapy (rLT) is a radioactive biochemical substance that targets the human prostate-specific membrane antigen (hPSMA). This rLT has been used in compassionate trials in mCRPC patients and has been demonstrated significant clinical efficacy [96, 97]. However, recent findings suggest that this efficacy is short-lived, and most patients exhibit tumor recurrence [96]. Here we establish a murine model to study the anti-tumor effects and the corresponding immune response of $^{177}$Lu-PSMA617 rLT on prostate cancer. We generated a doxycycline-inducible hPSMA-expressing murine prostate cancer (hPSMA TRAMP-C2) cell line with high binding responses to PSMA617. Using this system, we evaluated the *in vitro* and *in vivo* binding of $^{177}$Lu-PSMA617 to the hPSMA TRAMP-C2 cell line. Here, we show that the hPSMA TRAMP-C2 cell line expresses hPSMA upon doxycycline induction and that $^{177}$Lu-PSMA617 can bind to its target *in vitro* and *in vivo*. Together, these results show that the developed hPSMA TRAMP-

C2 cell line can be used to investigate therapeutic and immunological responses targeted against PSMA in prostate cancer.

## 2.3 Introduction

Prostate cancer is the most common cancer in men in Canada. In 2017, an estimated 21,300 men were diagnosed with prostate cancer [95]. The diagnosis is based on the microscopic evaluation of the prostate tissue. A Gleason score from 1 to 5 is designated based on examination of these samples [98]. The Gleason score is based on the appearance and architecture of the cells. The final diagnosis is based on the sum of Gleason patterns, results from a digital rectal exam (DRE) and prostate-specific antigen (PSA) levels [98]. Patients are diagnosed with low, medium or high-risk prostate cancer and a variety of treatments are considered.

In patients with localized prostate cancer, there are three treatment options: active surveillance, surgery and radiation therapy. Active surveillance includes regular PSA testing and prostate biopsies to monitor disease burden [99]. Surgery and radiation therapy are the most effective treatment options for patients with more advanced stages of cancer. When patients advance to metastatic prostate cancer, surgery and radiation therapy become less effective. Androgen deprivation therapy (ADT) and chemotherapy continue to be the major treatment options for patients at this stage [100, 101]. Prostate cells rely on androgens to grow, proliferate and function normally, thus ADT is effective against “androgen sensitive” cancer cells [101]. Unfortunately, these prostate cancer cells can mutate to become insensitive to the treatment and most patients advance to the next stage of prostate cancer, known as advanced metastatic castrate-resistant prostate cancer (mCRPC) [101, 102] During this stage of prostate cancer, the tumor metastasizes to various sites in the body and to the bone [102]. As the tumor metastasizes to the bone, treatment options for these patients become limited.

Prostate-specific membrane antigen (hPSMA) is an extracellular transmembrane protein found on prostate cells. When prostate cells become cancerous, hPSMA is overexpressed 1000-fold in prostate cancers [103, 104]. This localized overexpression of hPSMA on malignant prostate cells makes it an effective target for prostate cancer therapy. Although antibodies against hPSMA have been promising, therapeutic effects have been modest [104].

Recently, targeted radioligands such as $^{177}$Lu-PSMA617, have shown promise in treating mCRPC [97, 105, 106]. This therapy involves the systemic delivery of a radiolabeled carrier ($^{177}$Lu) to cancer sites via a tumor targeting agent (PSMA617). A non-randomized trial showed sustained PSA levels (with no significant toxicities) in ~60% of heavily pre-treated patients (n=30) receiving $^{177}$Lu-PSMA617 [107]. The response to $^{177}$Lu-PSMA617 is not fully explained by the delivered radiation dose and may involve the stimulation of the immune system.

Although there is evidence that suggests the local RT can potentially elicit an anti-tumor response, it may be insufficient to trigger a robust response in mCRPC [26, 27]. Systemic rLT would target both prostate and bone lesions, maximizing immunogenic cell death (ICD) and increasing antigen spread [108]. ICD is a form of cell death that activates the immune system and may induce an effective anti-tumor response [53]. This could help prime naive immune cells that could be further activated with checkpoint blockade/agonists.

Currently, the scientific field lacks properly developed mouse prostate cancer model to study PSMA-targeted therapy [8]. Here, we report the development of hPSMA TRAMP-C2 cell line and its utilization in studying the binding responses to $^{177}$Lu-PSMA617. The hPSMA TRAMP-C2 cell line was also used to evaluate the mechanism of cell death induced by $^{177}$Lu-PSMA617.

# 2.4 Methods and Materials

### 2.4.1 Cell line and culture conditions

The generation of TRAMP-C2 mouse prostate cancer cell line by Foster, *et al.* has been previously described [109]**.** Briefly, the authors harvested a heterogeneous 32-week tumor from the C57BL/6J transgenic adenocarcinoma mouse prostate (TRAMP) model. The TRAMP mouse model was generated to study the development and progression of prostate cancer in mice. The harvested cells were passaged and tested for their ability to form tumors in syngeneic mice [109]. One of the clones that had tumorigenic capability and showed intense androgen receptor staining was referred to as TRAMP-C2.

The TRAMP-C2 lines used in this report were acquired from American Type Culture Collection (ATCC). These TRAMP-C2 cells were cloned to express hPSMA upon doxycycline (DOX) induction (Figure 3). Human PSMA-expressing TRAMP-C2 (hPSMA TRAMP-C2) cells were maintained in DMEM High Glucose Medium containing fetal bovine serum (FBS ; 5%), Nu-Serum IV (5 %), bovine insulin (0.005 mg/mL), dehydroepiandrosterone (DHEA; 10 nM), penicillin (100U/mL) and streptomycin (100 μg/mL (all items from Fisher Scientific). All cells were maintained at 37$^{o}$C, 20% $O_2$, and 5% $CO_2$ in a water-jacketed Forma Scientific Incubator.

HEK293T (293T) cells were used to generate lentivirus for the transduction and generation of the hPSMA TRAMP-C2 cell lines. 293T cells were cultured in DMEM High Glucose Medium containing 4 mM L-glutamine, and sodium bicarbonate (Sigma-Aldrich, D5796); 10% Fetal Bovine Serum (FBS); 100 units/mL penicillin G sodium & 100 μg/mL streptomycin sulfate. 293T cells were also maintained at 37$^{o}$C, 20% $O_2$, and 5% $CO_2$ in a water-jacketed Forma Scientific Incubator.

LNCaP cells were derived from the metastasized prostate tumor in the lymph node of a 50-year-old male [19, 20]. These cells acted as my positive control for hPSMA expression. LNCaP cells were cultured in Roswell Park Memorial Institute (RPMI) 1640 (Gibco) medium containing FBS 10%; penicillin (100U/mL) and streptomycin (100 μg/mL; all items from Fisher Scientific). The LNCaP cells were maintained at 37°C, 20% $O_2$, and 5% $CO_2$ in a water-jacketed Forma Scientific Incubator.

### 2.4.2 Gene ration of DOX-inducible hPSMA TRAMP-C2 clones using Lenti-X 3G Tet-On Inducible System

The Lenti-X 3G Tet-On inducible system is a gene expression system for mammalian cells. The Lenti-X 3G Tet-On includes a transactivator-expression vector and promoter-expression vector [110]. Target cells that express the Tet-On 3G transactivator protein and contain a gene of interest (e.g. hPSMA) under the control of a TRE3G promoter will express high levels of hPSMA only when cultured in the presence of a tetracycline [110]. DOX is a preferred effector for Tet-On systems as it has a good tissue distribution, low toxicity and a known half-life [111]. There were three main steps required to create a DOX-inducible expression system that utilizes a lentiviral approach (Figure 3). This included cloning hPSMA into the pLVX-TRE3G vector, producing lentiviral supernatants and co-transducing TRAMP-C2 cells with Tet-On 3G virus and TRE3G virus.

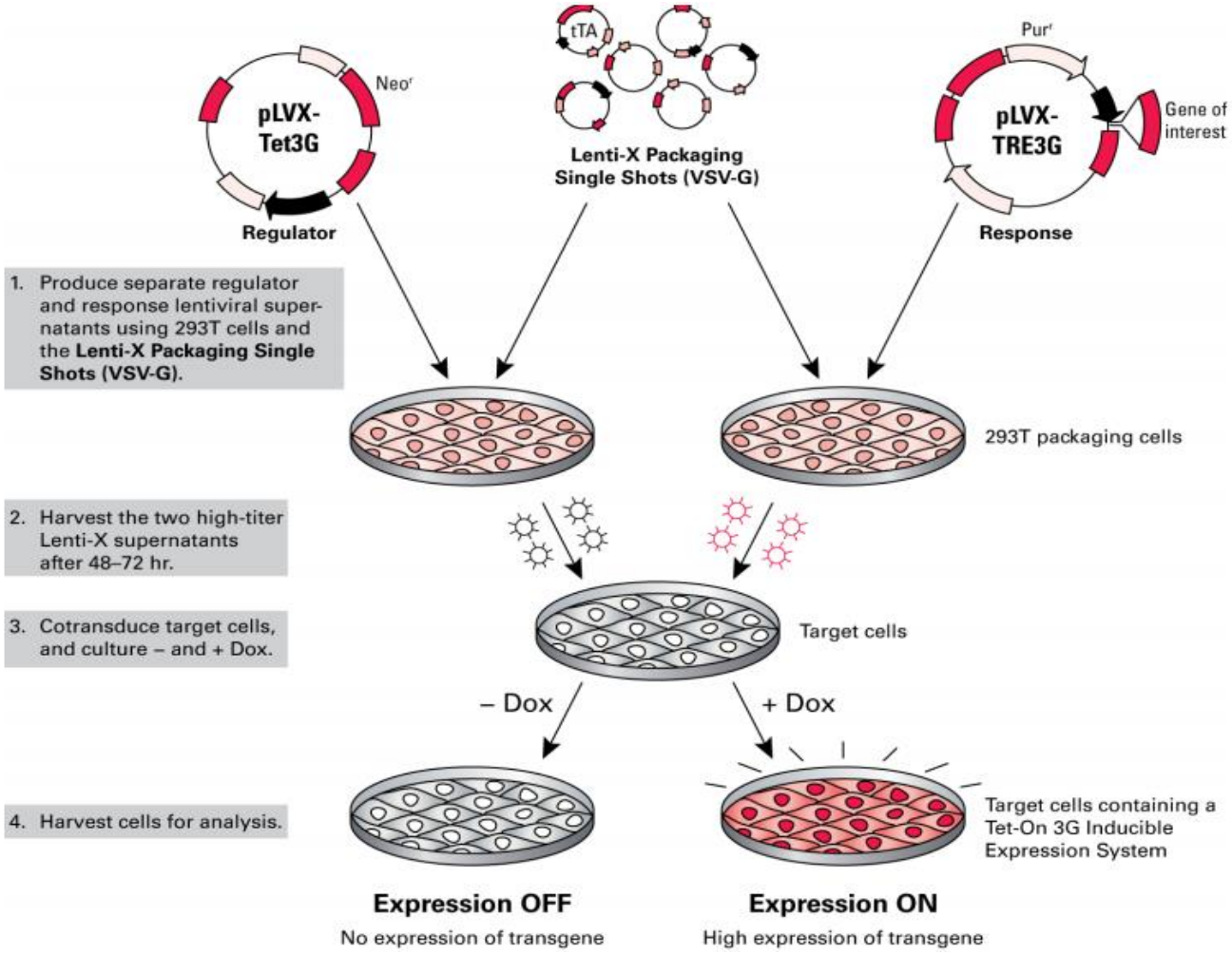


**Figure 3. Lenti-X 3G inducible expression protocol. (Adapted from Takara Bio. 25)**

### *2.4.2i Cloning hPSMA into pLVX-TRE3G vector*

To create hPSMA pLVX-TRE3G expression vector, hPSMA was sub-cloned out of an expression plasmid (EX-G0050-Lv205), kindly provided by our collaborator Dr. Francois Bénard. The expression plasmid contained the hPSMA insert between restriction sites BamHI and EcoRI of the multiple cloning site (MCS). To isolate the hPSMA insert, the expression plasmid was digested with EcoRI and BamH1 enzymes acquired from New England Biolabs (NEB) to generate two non-compatible ends, thus allowing the insert to be cloned directionally. The restriction digests reported in this thesis were all performed according to the protocol provided by NEB. The target pLVX-TRE3G plasmid was also digested with EcoRI and BamH1

enzymes (Figure 4A). The hPSMA insert was ligated into the pLVX-TRE3G plasmid according to the protocol provided by NEB. The ligated product was transformed into *E. coli* strain for plasmid amplification and verification. Transformed colonies that were resistant to puromycin and Geneticin (G418) were verified by performing restriction digests and performing gel electrophoresis to verify the sequence insertion of hPSMA in the pLVX-TRE3G vector.

### *2.4.2ii Lentiviral production of co-transduction of TRAMP-C2 cells*

Lentiviral production was done according to the protocol provided Clonetech, utilizing their proprietary Lenti-X packaging shots. To produce lentivirus, 293T cells were cultured in 10 cm dishes for 24 hours until they reached 70% confluency. In a sterile microfuge tube, 7 µg of the lentiviral vector plasmid DNA (PSMA pLVX-TRE3G and pLVX-Tet3G) were diluted with water to a final volume of 600 µl (Figure 4A, 4B). The diluted DNA was added to a tube of Lenti-X Packaging Single Shots and vortexed at high speed. The samples were incubated at room temperature for 10 minutes before being added dropwise to the cell culture dishes. The transfected samples were incubated at 37ºC, 20% $O_2$, and 5% $CO_2$ in a water-jacketed Forma Scientific Incubator. After 12 hours, fresh complete growth medium was replaced in both dishes and incubated at 37ºC, 5% $CO_2$ in a water-jacketed incubator. The lentiviral supernatants were harvested at 72 hours after the start of transfection. The collected supernatants were filtered through 0.45-µm filter to remove cellular debris. The filtered lentiviral supernatants were stored at -80ºC before being used for viral transduction.

### *2.4.2iii Viral transduction of TRAMP-C2 cells*

Finally, to generate the DOX-inducible hPSMA TRAMP-C2 cell line, lentiviral supernatants were used to transduce wildtype (WT) TRAMP-C2 cell line, TRAMP-C2 cells were plated 18 hours before transduction to reach 70% confluency. pLVX-Tet3G and hPSMA pLVX-

TRE3G lentiviral supernatants were slowly thawed on ice. Lentiviral supernatants were combined and added to the TRAMP-C2 cells at a 1:1 ratio with polybrene (4 µg/mL). The cells were transduced for 12 hours at 37ºC, 5% $CO_2$ in a water-jacketed incubator. The lentiviral-culture medium was discarded and replaced with fresh growth medium. After resting the cells for 24 hours, they were treated with G418 (500 µg/mL) and puromycin (3 µg/mL) antibiotics for two weeks. The resulting population of hPSMA TRAMP-C2 cells after a 2-week treatment with antibiotics was referred to as the "bulk population".

### 2.4.3 DOX-induction of hPSMA TRAMP-C2 bulk population

As explained earlier, this inducible system is dependent on DOX, a tetracycline that initiates transcription after binding to the Tet-On 3G transactivator protein. To achieve the highest level of hPSMA expression, a DOX dosage experiment was performed. hPSMA TRAMP-C2 bulk cells were plated in 6-well plate 24 hours pre-DOX treatment to achieve 60% confluency. DOX was added to the wells at varying concentrations between 0-1 µg/mL. The cells were incubated with DOX for 18 hours and their hPSMA expression was validated through flow cytometry. (see below)

### 2.4.4 Generation of hPSMA TRAMP-C2 clones

To generate hPSMA TRAMP-C2 clones that have stable hPSMA expression after DOX induction, we started by DOX-inducing the bulk population as mentioned in the earlier section. The DOX-induced hPSMA TRAMP-C2 bulk cells were harvested and prepared for flow cytometry and cell sorting. The harvested bulk cells were washed with phosphate buffered saline (PBS) and centrifuged at 1250 RPM for 5 minutes at 4ºC. These cells were then stained with viability dye (e450; eBiosciences; 1 µg/mL) for 20 minutes at 4ºC. The cells were washed again with PBS and treated with anti-human PSMA antibody (Biolegend; clone LNI17; 0.5 µg/mL) for

20 minutes at 4ºC. The cells were prepared for cell sorting by resuspending them in 500 µL TRAMP-C2 culture medium. Flow cytometry samples were run on a BD Influx Cell Sorter or BD FACSAriaII. The "bulk" hPSMA TRAMP-C2 cells were isolated into single-cell clones that were cultured in multiple 96-well plates. This method was used to generate a clonal population arising from a single cell.

Over the next two weeks, these single cells were treated with G418 (500 µg/mL) and puromycin (3 µg/mL) to isolate clones that have "medium" and "high" level hPSMA expression. Four clones were isolated from 25 clones that were tested. Two clones were validated to be "medium" expressors while the other two were "high" expressors. All future experiments were done with these four isolated clones.

### 2.4.5 Validating protein expression through Immunoblotting

For immunoblotting of hPSMA, hPSMA TRAMP-C2 cells were induced with doxycycline for 18 hours. For immunoblotting, hPSMA TRAMP-C2 cells were treated with $^{177}$Lu-PSMA617. The cells were lysed in Radioimmunoprecipitation assay (RIPA) buffer (50 mM Tris-HCl pH 7.4, 1% NP-40, 0.25% Na-deoxycholate, 150 mM NaCl, 1 mM EDTA) containing complete protease inhibitor cocktail, and phosphatase inhibitor cocktail for 30 min at 4ºC. Lysates for $^{177}$Lu-PSMA617-treated samples were collected 1, 24, 48, 72- and 120-hours post-treatment. The samples were centrifuged at 13,000 g for 15 min at 4ºC after which supernatants were collected and stored at -80ºC. Lysates were quantified using BCA assay (Thermo Fisher) and equal amounts were loaded onto 4-12% gradient SDS-PAGE gels (Invitrogen). Protein was transferred onto nitrocellulose membranes and immunoblots for hPSMA (D4S1F; 1:1000; Cell Signaling) and GAPDH (14C10; 1/1500; Cell Signaling) were performed using their respective antibodies (Cell Signaling).

### 2.4.6. Evaluating the *in vitro* and *in vivo* binding response to an hPSMA ligand (BC Cancer—Vancouver)

To understand the binding responses for each hPSMA TRAMP-C2 clone, cells were plated in 24-well plates with TRAMP-C2 medium and treated with doxycycline for 18 hours. Media was removed and cells were incubated with HEPES-buffered saline for one hour at 37°C. Cells were treated with $^{18}$F- labelled 2-(3-(1-Carboxy-5-((6-(18F)fluoro-pyridine-3-carbonyl)-amino)-pentyl)-ureido)-pentanedioic acid (DCFPyL) in a constant 1 nM concentration and incubated at 37°C for one hour. The cells were trypsinized and transferred into biodistribution tubes. The radioactivity bound to the cells was measured with a ɣ-counter for 1 minute per tube.

To evaluate if the response observed *in vitro* was also viable in an immunodeficient mouse model, immunodeficient mice were inoculated with hPSMA TRAMP-C2 clones. 10 x $10^6$ cells in 200-250 µl of media and Matrigel (1:1) of each of the four clones ("parental clones": 1, 14, 16 and 19) were subcutaneously inoculated in the area dorsocaudomedial to the acromiotrapezius muscle of male NOD.Cg-Rag1$^{tm1Mom}$ Il2rg$^{tm1Wjl/}$SzJ ("NRG", NOD-Rag1$^{null}$ IL2rg$^{null}$, NOD rag gamma) mice of 12 weeks of age and older (Jackson Laboratory, Bar Harbor, ME, USA), using a 25 gauge needle. The mice were maintained in a pathogen-free animal facility with restricted access on a 12:12 light cycle, monitored for tumor size (measured as volume through length, width and thickness of the tumor), weight and general signs of illness following protocol A16-0290-Mus-03 of the BCCRC Animal Resource Centre. Five to eight weeks post-inoculation, mice with tumor volume of at least 200 mm$^3$ were selected for *in vivo* imaging and biodistribution studies with $^{18}$F-labelled radiotracer DCFPyL and pre-treated with 50 mg DOX/kg of body weight in 200-250 µl of PBS intraperitoneally, 36-48 hours prior to the study. Additional mice were selected as controls and did not receive the antibiotic prior to the study.

# 2.5 Results

### 2.5.1 hPSMA was integrated into the Lenti-X 3G inducible expression system

To develop a hPSMA TRAMP-C2 that expresses human PSMA on DOX induction, plasmid containing the folate hydrolase I gene (*FOLH1;* encodes hPSMA) into the Lenti-X 3G inducible expression system. The genomic size of hPSMA is reported to be 2253 base pairs (bp). The hPSMA segment was located between restriction sites EcoRI and BamH1 in the expression plasmid (EX-G0050-Lv205) provided by Dr. Francois Bénard. hPSMA was isolated from the expression plasmid by performing a restriction digest (Figure 4C). This insert was ligated into the pLVX-TRE3G plasmid that was digested with EcoRI and BamH1 respectively (Figure 4D). The insertion of hPSMA in pLVX-TRE3G was validated by performing a final restriction digest on the vector products acquired after transformation in *E. coli* (Figure 4D).

### 2.5.2 hPSMA expression is non-dependent on DOX dosage concentration

Post-transduction**,** we examined the concentration of DOX required to obtain the highest hPSMA expression in the bulk hPSMA TRAMP-C2 population. We tested multiple doses of DOX at 0, 0.2, 0.4, 0.6, 0.8 and 1 μg/mL (Figure 5). Using flow cytometry, I found that 36.0% of the DOX treated cell population became positive for surface expression hPSMA at 0.2 μg/mL. In this experiment, WT TRAMP-C2 acted as my negative control while LNCaPs acted as my positive control. There was no significant difference in expression of hPSMA ($p>0.05$) between all other tested concentrations (Figure 5A, B). This suggested that the system was not concentration-dependent, where an increasing concentration would lead to increased expression. Rather, once the cells were treated with a lower dosage of DOX, the cells still retained high hPSMA expression (Figure 5A, B). We also did not observe any DOX-related toxicity in these

cells even at higher concentrations. To be consistent in our experiments and for simplicity, we decided to use 1 µg/mL as the standard DOX concentration for all future experiments.

**A.**

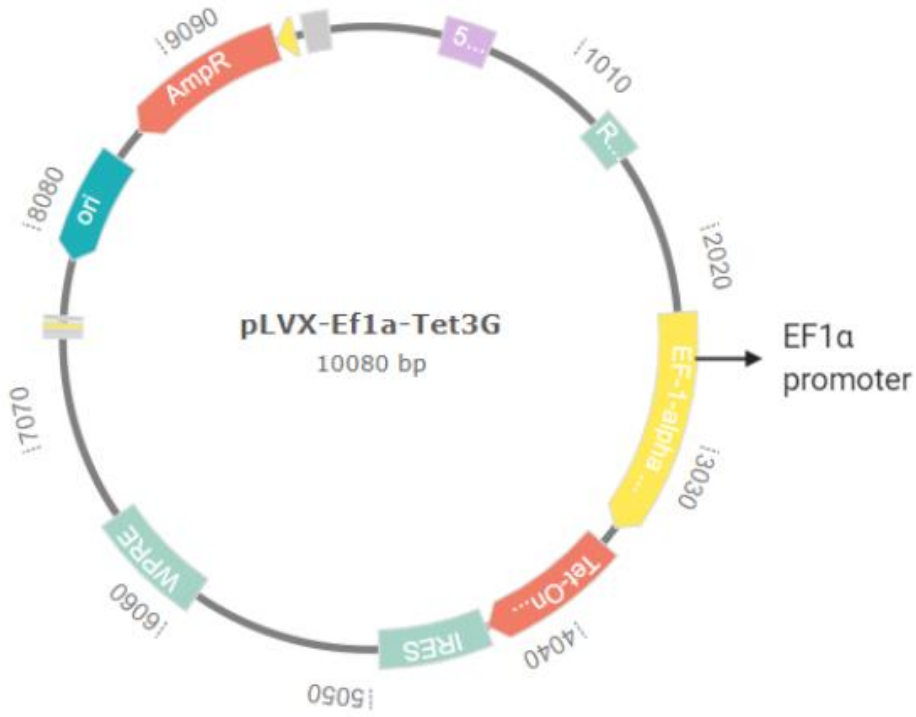


**B.**

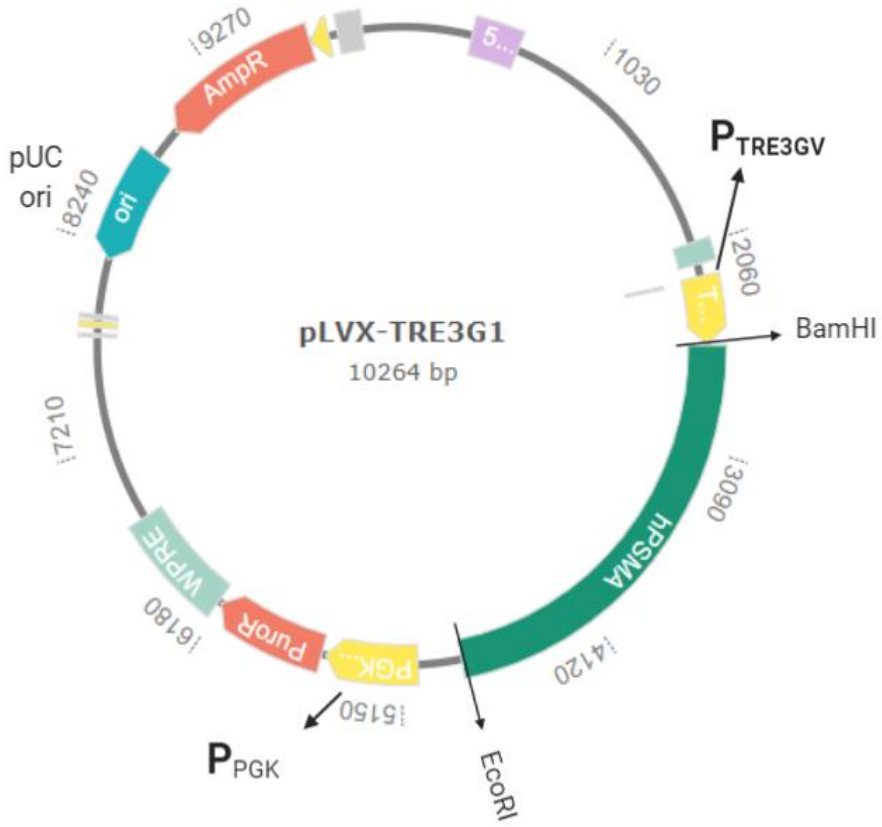

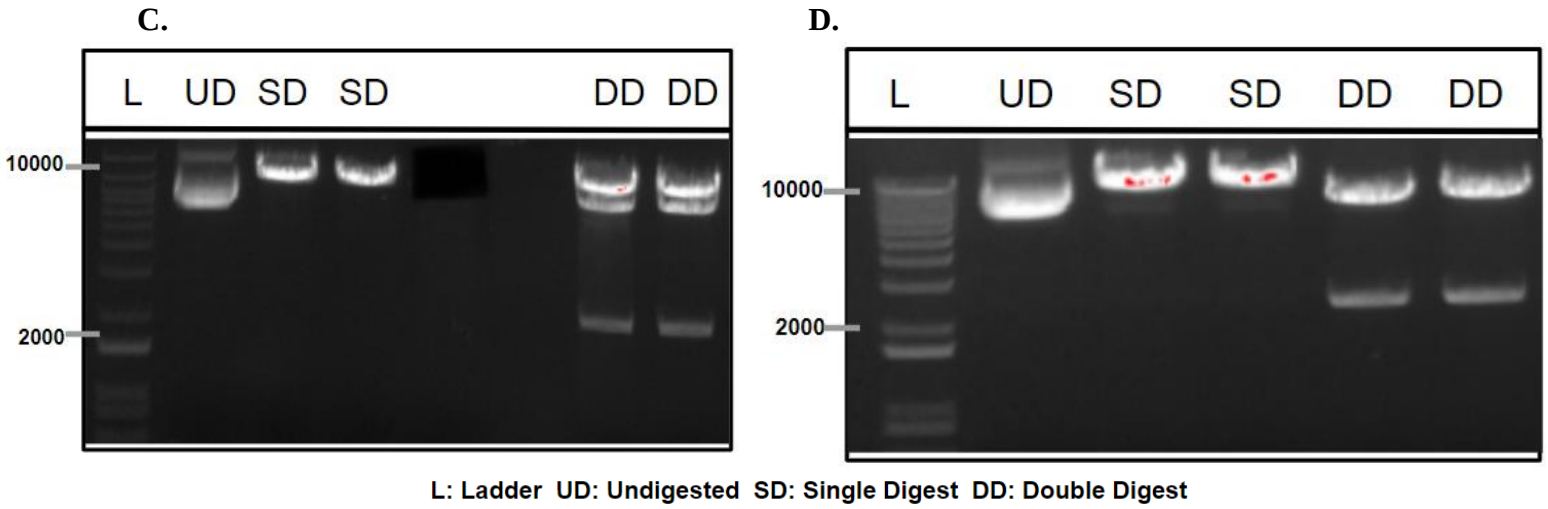


**Figure 4. hPSMA was integrated into the pLVX-TRE3G plasmid**. (A/B) Plasmid maps for pLVX-EF1a-Tet3G and pLVX-TRE3G Lenti-X vectors. (C) Restriction digest of hPSMA from the expression plasmid. (D) Restriction digest of the vectors derived after bacterial transformation. hPSMA has a genomic size of 2253 bp.

### 2.5.3 Four hPSMA TRAMP-C2 clones were isolated from the bulk population

For all future experiments, we wanted to have clonal populations of hPSMA TRAMP-C2 cells that would all express hPSMA at comparable levels. To generate these clones, the bulk population was DOX-induced, and the single-cell populations were isolated into 96-well plates. Out of this bulk population, 25 isolated clones had varying expression levels of hPSMA after DOX induction (Figure 6). Even though these clones were able to express hPSMA, some of the clones had slower growth or inconsistent hPSMA expression (Figure 6). Finally, after further antibiotic selection and multiple passages, four clones were isolated from the earlier 25 clones.

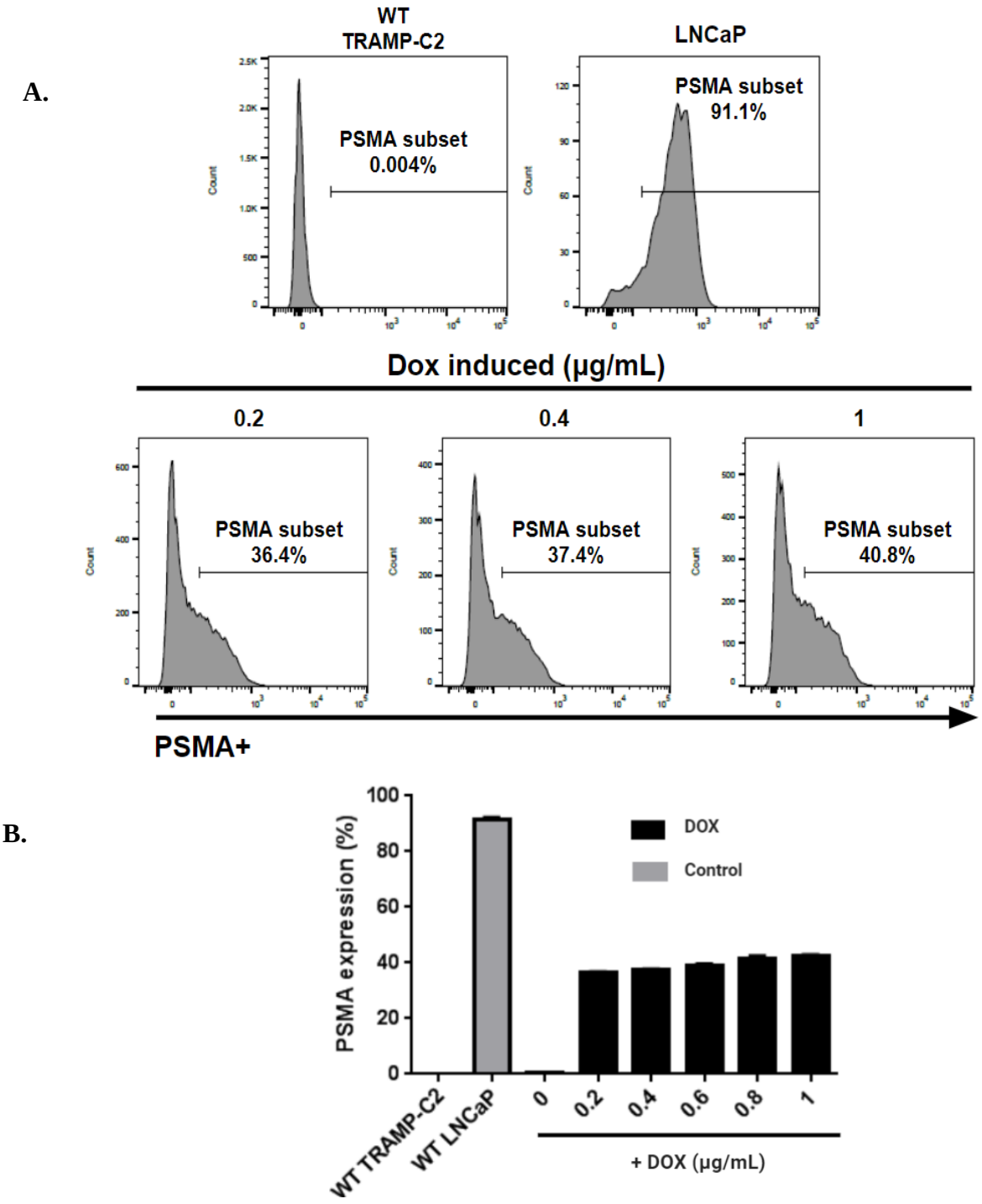


**Figure 5. Doxycycline (DOX) induces PSMA expression hPSMA TRAMP-C2 cells. (**A) Histograms and corresponding (B) bar graph showing hPSMA expression post-DOX induction at 0-1 µg/mL concentrations in hPSMA TRAMP-C2 cells, WT TRAMP-C2 and WT LNCaPs. (Tet-On +PSMA: hPSMA TRAMP-C2 cells + DOX; Controls: WT TRAMP-C2 cells and LNCaP cells + DOX; N=3, Error bar =SD; NS= p-value> 0.05, * = p-value<0.05, ** = p-value<0.01, *** = p-value<0.001)

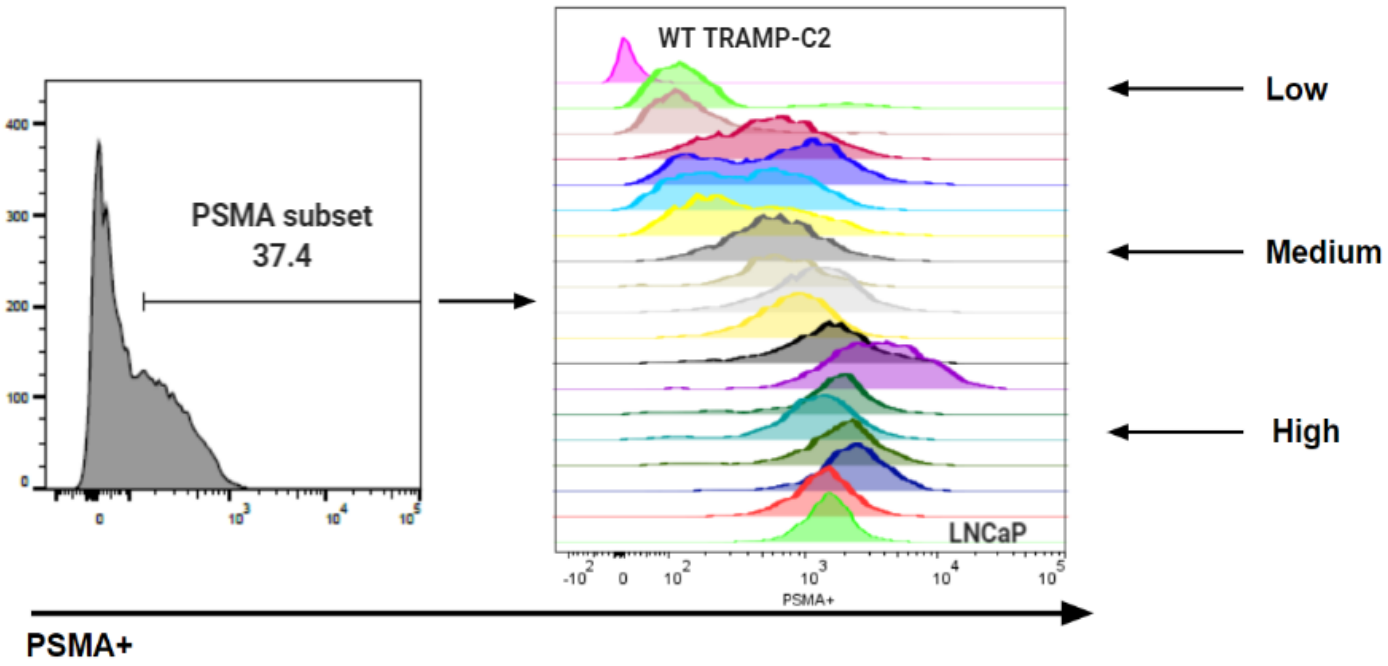


**Figure 6. Single-cell sorting to generate hPSMA TRAMP-C2 clones.** hPSMA TRAMP-C2 "bulk" cells were single-cell sorted to generate hPSMA TRAMP-C2 clones. These clones expressed hPSMA at low, medium and high intensity levels. Each colored histogram demotes a different clone. (Purple at top: WT TRAMP-C2; Green at bottom: LNCaPs)

These four clones had consistent "medium" or "high" hPSMA expression after DOX induction and their doubling time was consistent with the WT TRAMP-C2 cell line (Figure 7). These clones were tested against WT TRAMP-C2 (negative control) and LNCaPs (positive control; Figure 7). The expression of the clones was also validated against non-induced clones (Figure 7). All four clones had a significant difference in hPSMA expression compared to WT TRAMP-C2 ($p<0.001$). To evaluate the significance of hPSMA expression on PCa cells, we wanted to have some clones that expressed at "medium" levels and other clones that would express hPSMA at "high" levels. Clones 1 and 16 were designated to be "high" expressors while

clones 14 and 19 were identified as “medium” expressors (Figure 7A). “Medium” expressors had significantly lower expression ($p<0.001$) than “high” expressors and my positive control. I also observed no significant difference between the “medium” expressing clones 14 and 19. Non-induced (orange) and isotype control (blue) had identical hPSMA expression profile.

I also wanted to validate the hPSMA expression of these clones through immunoblotting. I tested one of each “medium” and “high” population and found that DOX-induced hPSMA expression in these clones (Figure 7B). For this experiment, TRAMP-C2 lysates acted as my negative control while LNCaP lysate was my positive control. GAPDH acted as my experimental control. In contrast to flow cytometry analysis, I found that the non-induced samples exhibited hPSMA expression even though no cell surface expression was observed. Once I developed these four clones, I wanted to test their ability to interact with an $^{177}$Lu-PSMA617 ligand.

### 2.5.4 hPSMA TRAMP-C2 is capable of binding to DCFPyL *in vitro*

Once the induced expression was confirmed through flow cytometry and immunoblotting, I wanted to assess the binding response of the expressed hPSMA to $^{18}$F-DCFPyL through positron emission tomography/computed tomography (PET-CT) scan. $^{18}$F-DCFPyL is a urea-based radiotracer composed of hPSMA targeting agent (DCFPyL) and a positron emitting isotope (Fluorine 18). This radiotracer was used as a substitute for $^{177}$Lu-PSMA617 for preliminary binding experiments. The hPSMA TRAMP-C2 clones were successfully able to bind $^{18}$F-DCFPyL post DOX-induction. Clone 14 and 16 had significantly higher binding responses ($p<0.01$) than Clone 1 and 19 (Figure 8A). We wanted to validate if $^{18}$F-DCFPyL could also bind *in vivo*. There was also a significant difference in ligand binding between the uninduced TRAMP-C2 cells versus DOX-induced clones (Figure 8, $p<0.001$)

**A.**

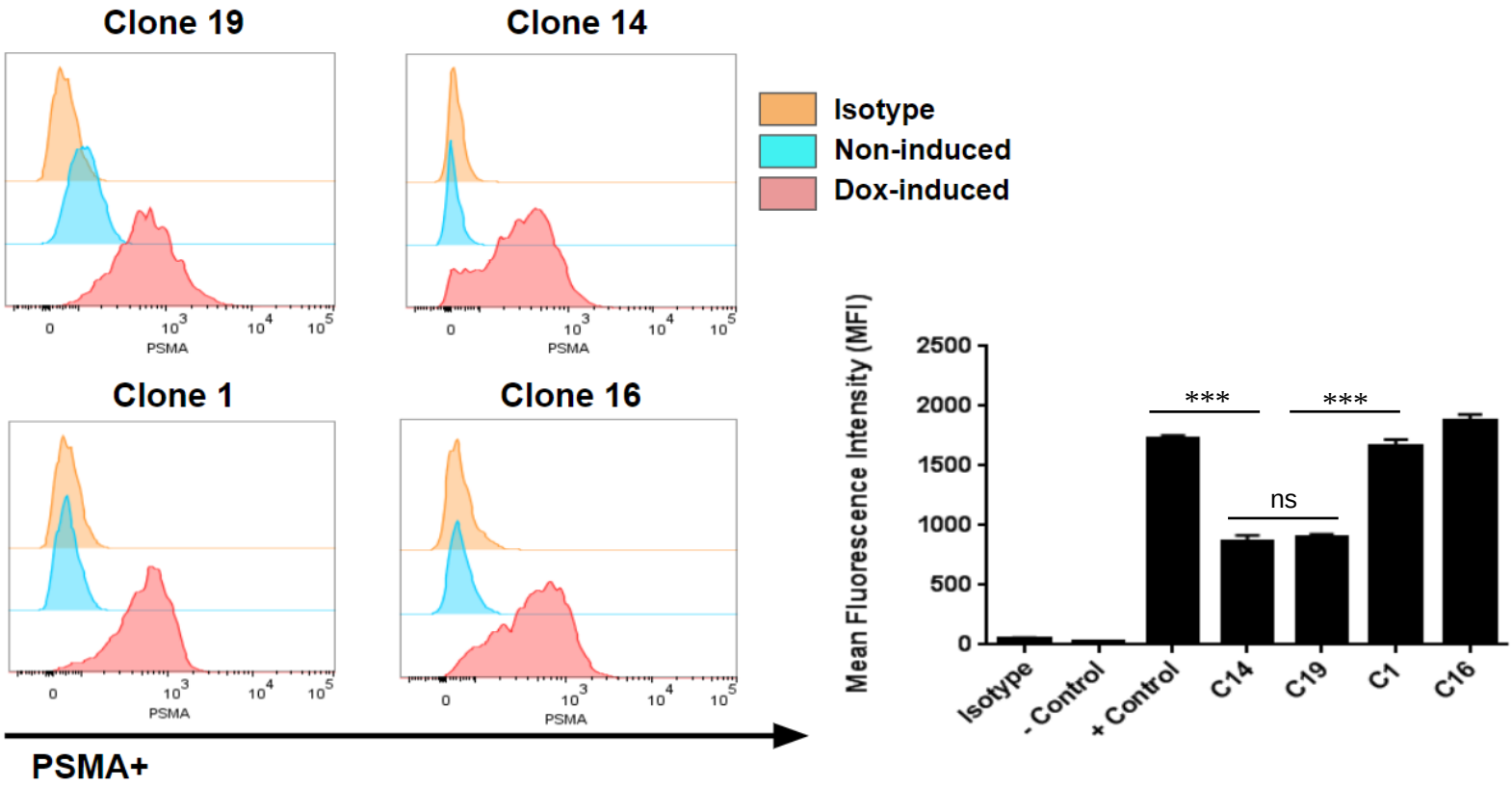


**B.**

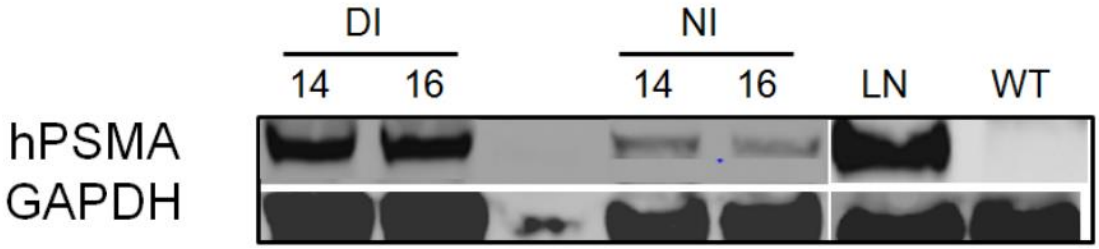


**Figure 7. Four hPSMA expressing clones were isolated from the "bulk" population.** Transduced TRAMP-C2 cells were single-cell sorted to acquire clonal populations of hPSMA expressing cells. Four clones were isolated after cell sorting. (A) Histograms and corresponding bar graph showing the 4 clones acquired after single-cell sorting. Clones 1 and 16 were "high" hPSMA expressing clones while clones 14 and 19 were "medium" expressing clones (Orange: isotype control, Blue: non-induced, red: DOX-induced). N=3, Error bar =SD (B) Western blots were performed to verify protein expression in clones 14 and 16. (NI: non-induced, DI: DOX-induced; LN: LNCaP (positive control); WT: WT TRAMP-C2 (negative control); GAPDH: experimental control; NS= p-value> 0.05, * = p-value<0.05, ** = p-value<0.01, *** = p-value<0.001)

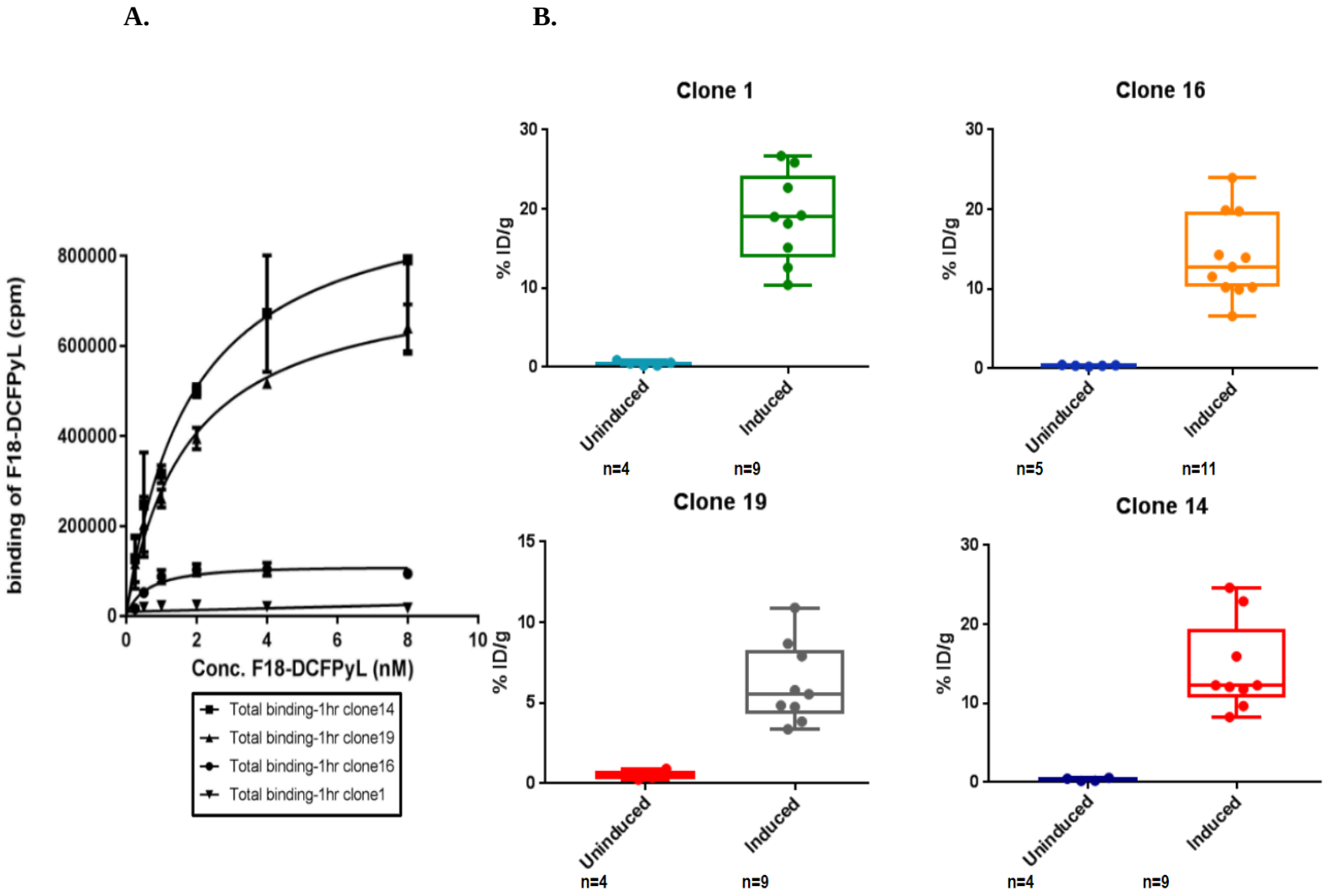


**Figure 8. $^{18}$F-DCFPyL binding response to hPSMA TRAMP-C2 in-vitro and in-vivo.** Binding response was quantified using 18F-DCFPyL ligand on hPSMA expressing TRAMP-C2 clones in vitro and in-vivo. (A) The clones were DOX-induced for 18 hours. These clones were incubated with $^{18}$F-labelled DCFPyL ligand for 1 hour and harvested to analyze binding response to $^{18}$F-DCFpyL. (B) hPSMA TRAMP-C2 clones inoculated in NRG mice express hPSMA upon doxycycline-induction. Unpaired t-tests for all four clones showed a p-value of <0.0001 when comparing radioactivity uptake of $^{18}$F-DCFPyL, a PSMA-binding radiotracer in mice with or without pre-treatment with doxycycline. Significantly lower (p=0.0001, unpaired t-test) uptake was seen with clone 19 (mean uptake = 6.96% ID/g) when compared to clones 1, 14 and 16 combined (mean uptake = 15.43 % ID/g).

### 2.5.5 hPSMA TRAMP-C2 is capable of binding to $^{18}$F-DCFPyL *in vivo*

Post treatment of NRG mice with $^{18}$F-DCFPyL, we observed significantly increased ($p<0.001$) uptake levels compared to non-induced mice (Figure 8B). Clone 1, 16 and 14 showed an increased $^{18}$F-DCFPyL uptake ($p=0.0001$) compared to Clone 19 (Figure 8B). This biodistribution response was confirmed with PET-CT images of 4 mice, each inoculated with a different clone. PET-CT images were collected before and after induction with DOX. The standardized uptake value used in PET scans uses the unit %ID/g. This unit can be explained as % injected dose/ body weight (g) of the mice. Visualization of tumors signified $^{18}$F-DCFPyL uptake and this response was only observed after the mice were treated with DOX (Figure 9). Physiological uptake was also observed in normal tissues including the urinary bladder, kidneys, and salivary glands**.**

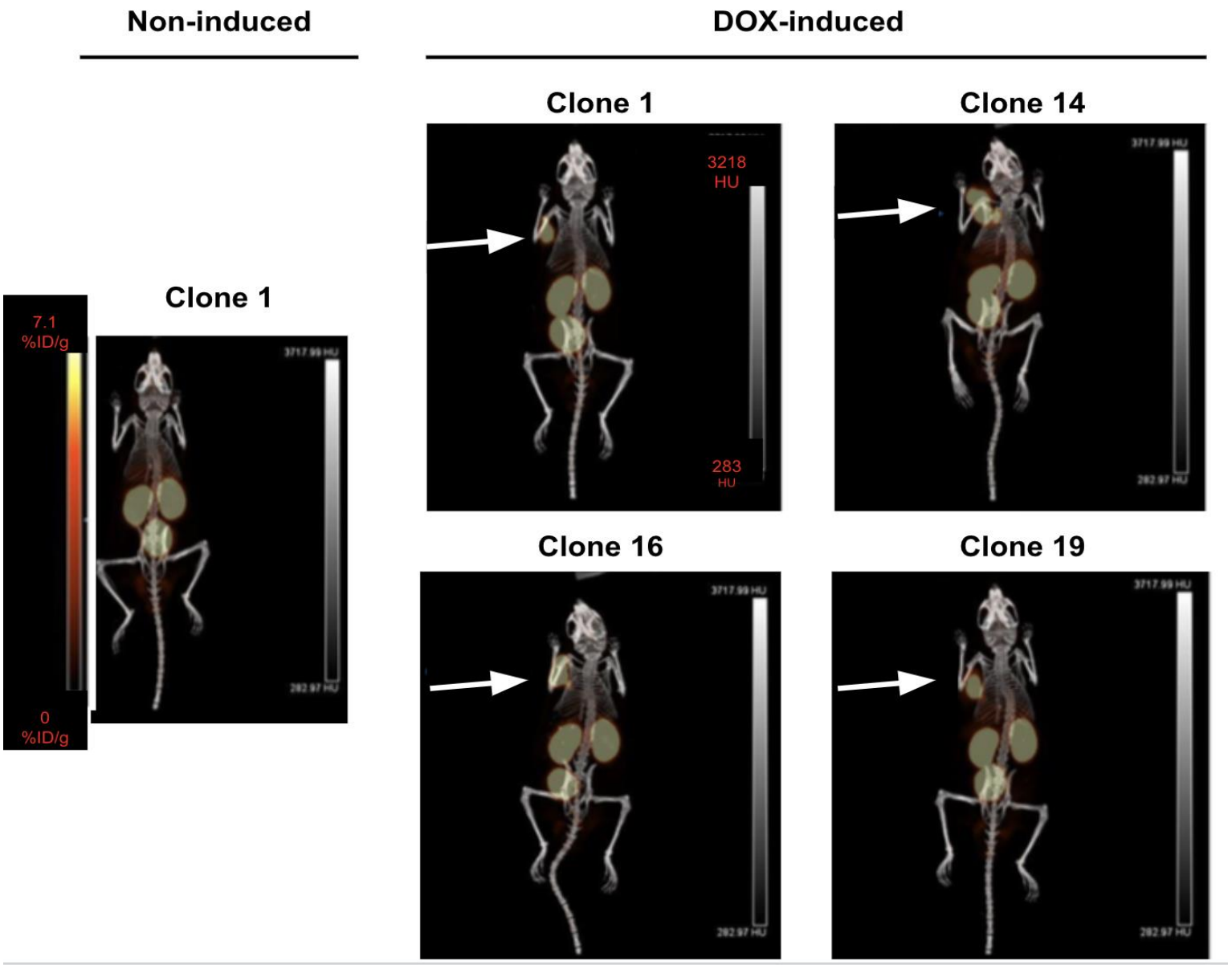


**Figure 9. PET/CT images comparing 18F-DCFPyL uptake in non-induced and DOX-induced hPSMA TRAMP-C2 tumors.** Comparison of PET-CT images before (left) and after (right) doxycycline-induction in 4 mice, each inoculated with one of the four transfected TRAMP-C2 clones: 1, 14, 16 and 19. All mice received intravenously 5 +/- 0.86 MBq of $^{18}$F-DCFPyL one hour before imaging. Corresponding to all images are spectrum bars of 283-3218 Hounsfield unit (HU) for CT (grey scale), and 0-7.1% ID/g for PET (yellow/red tones). White arrows indicate tumor sites (%ID/g: % injected dose/body weight).

## 2.6 Discussion

To develop a mouse model to study the effects of $^{177}$Lu-PSMA617 on PCa tumors, we had to generate a mouse PCa cell line that could express hPSMA. It would be pertinent to ensure that hPSMA was not constitutively expressed due to possible foreign-antigen immune response. For this reason, I developed the hPSMA TRAMP-C2 cell line that would express the transmembrane protein only on DOX induction. To generate this cell line, I utilized the Lenti-X Tet-On 3G Inducible Expression System which is a tetracycline-inducible gene expression system. This system allows you to control expression of your gene on tetracycline (DOX) induction.

The first step to generating these cell lines included generating vectors with my target cDNA (FOLH1). This would allow for further transcription and translation of hPSMA in WT TRAMP-C2 cell lines. The cloning of hPSMA into the Lenti-X system was verified by gel digests and the protein expression was further verified through flow cytometry and western blots. These vectors were utilized for viral transduction into WT TRAMP-C2 cells. Through this transduction we acquired a primary "bulk" population that could express hPSMA post-induction with DOX (Figure 5). Using these cells, I evaluated the concentration of DOX required to express high levels of hPSMA in this "bulk" hPSMA TRAMP-C2 cells. It was interesting to notice that this expression was not concentration dependent and the expression plateaued around ~40% with higher dosages of DOX (Figure 5). I was concerned about DOX-induced toxicity but noticed high viability in our cells (data not shown). This allowed me to utilize a higher DOX-concentration (1 µg/mL) for the next experiments.

Although I had a "bulk" hPSMA TRAMP-C2 cell line, I wanted a population that had similar levels of hPSMA expression which would allow for easier analysis in future experiments and consistency. From this "bulk" population, I was able to isolate 25 clonal populations that had

varying hPSMA expression post-induction with DOX (Figure 6). These populations varied in terms of their cellular growth and hPSMA expression. We noticed that some clones had very high hPSMA expression but were slow growing while others had lower hPSMA expression but were fast-growing (Figure 6). Out of these 25 clones, we isolated four clones that had a similar doubling time but varying hPSMA expression. Clones 1 and 16 were "high" hPSMA expressing clones while clones 14 and 19 were noted as "medium" expressing clones (Figure 7A). While performing experiments we needed to verify that there was not hPSMA being expressed without DOX-induction. To ensure this, performed flow-cytometry experiments for cell-surface expression and western blots for total expression. Through flow-cytometry experiments, we found no hPSMA expression in non-induced and expected level of expression in DOX-induced cells. This was also the expected result for our western blot experiments but after analysis we found low-level expression in non-induced hPSMA TRAMP-C2 cells (Figure 7B).

Initially it was unclear why the results between flow experiments and western blots were different as the hPSMA TRAMP-C2 cells tested came from the same culture conditions. One possibility is that the low-level expression may be due to tetracyclines found in fetal bovine serum (FBS) that was use in the TRAMP-C2 culture medium. To control for this, we acquired tetracycline-free (Tet-free) FBS but still noticed similar levels of non-induced hPSMA expression. Another ingredient in TRAMP-C2 medium is Nu-serum which also contains tetracyclines. Unfortunately, a source of Tet-free Nu-serum was not available. Therefore, I was unable to fully rule out the possibility of Tet contamination in the culture media. Another possible explanation could be related to different forms of hPSMA. A review by Heston *et al.*, noted PSMA gene mapped to 2 identical regions: one of chromosome 11p11.2 and the other on 11q14.3. The 11q14.3 PSMA was designated as PSMA-like [112]. They also noted that PSMA-

like protein lacks the transmembrane domain and thus only found as a cytosolic protein [112]. This property also allows for clinical targeting of the transmembrane hPSMA without interference [112]. Therefore, it is possible that the antibody I used for western blot may also be binding to the cytosolic PSMA-like protein. As I had noticed no surface-level expression without DOX-induction when verifying with flow cytometry, I decided to move further and analyze if the DOX-induced hPSMA can bind to its corresponding ligands.

We performed our binding-response experiments using $^{18}$F-DCFPyL ligand. This experiment acted as a verification process to verify that hPSMA ligands can bind to DOX-induced hPSMA on these clones. The results from this response correlated well with my previous experiments. We found no hPSMA-$^{18}$F-DCFPyL binding in non-induced clones while much higher binding-response was noted with DOX-induced hPSMA clones. In our initial analysis it seemed that the "medium" clones 14 and 19 had a significantly increased binding compared to our "high" expressing clone 16 (Figure 8A). After further analysis with our collaborators in Vancouver, we concluded that the 6-fold difference between clone 16 and "medium" clones was due to the differences in cell concentration between the two clones. Fewer cells/well were used in this assay for clone 16 than clone 14 and 19. This may have resulted in the visualized "lower" binding response. Once this binding-response was verified *in vitro*, we wanted to test it in an immunodeficient mouse model.

The *in vivo* experiment performed with immunodeficient mice resulted in similar and expected results. This experiment verified hPSMA inducibility *in vivo* and verified uptake of $^{18}$F-DCFPyL. Clone 19 showed significantly lower uptake levels compared to clones 1, 14 and 16 (Figure 8B). It is unclear why this difference was noticed between the clones. Even though clone 14 is a "medium" expressing clone, it had similar uptake levels compared to clone 1 and 16

("high" expressing clones). This result is even more peculiar considering that clone 19 had a high binding response *in vitro*. It is unclear if the number of passages during cell culture between the *in vitro* and the *in vivo* experiment changed the biology of the cell resulting in a lower uptake. It is also interesting to note that clone 1 had lower binding response during the *in vitro* binding-response experiment but had similar uptake response to clone 14 and 16. It is unclear what may have resulted in these different responses and should be studied further. The $^{18}$F-DCFPyL uptake was verified with PET/CT scan images of the DOX-treated mice. With the PET/CT images, there was significant difference in binding at tumor sites between non-induced and DOX-induced mice (Figure 9). We also noticed uptake of the $^{18}$F-DCFPyL ligand in salivary glands, urinary bladder and kidneys. The uptake in urinary bladder and kidneys can normally be attributed to the release of radionuclide through the renal system. Salivary glands have been known to have low level hPSMA expression which may have contributed to the observed uptake [113]. It is important to note that we did not observe any radionuclide attributed toxicity in these mice.

This array of experiments show support towards a promising PCa mouse model that can be used to study the effects of different hPSMA-targeted therapies and most importantly $^{177}$Lu-PSMA617 radioligand therapy. Recently, there have been a few other mouse models that have been developed to study hPSMA response. One study established an immunocompetent model of PCa to investigate the impact of $^{177}$Lu-PSMA617 activity on organ distribution and efficacy of the compound. This group stably expressed hPSMA in RM1 murine carcinoma model to study therapeutic behavior of $^{177}$Lu-PSMA617 [16]. They found that high specific activity was associated with increased tumor uptake and more prominent DNA damage [16]. They also observed that hPSMA expression did not induce an adaptive immune response in the RM1 carcinoma model for 14 days post-inoculation in C57BL/6 mice [16].

The current FDA approved immunotherapies for PCa include cancer vaccines (Sipuleucel-T, PROSTVAC-F), checkpoint inhibitors (anti CTLA-4) [114]. One Phase III studies analyzing the effects of combining Ipilimumab (anti CTLA-4) with low dose radiation showed that Ipilimumab had no benefit in overall survival (OS), but slightly improved progression-free survival (PFS), suggesting possible antitumor activity [115]. Individually, PCa targeted immunotherapy trials have yielded modest results [89]. Early trials targeting the programmed death I (PD-1)/ programmed death ligand I (PDL-1) axis have failed to elicit effective responses in patients [89].

Most clinical trials involving $^{177}$Lu-PSMA617 have shown positive results with ≥50% decline in PSA levels and median increase in overall survival of 11.3 months [116]. This may be considered an effective outcome but unfortunately, many patients relapse with the disease and it remains unclear whether the treatment is unable to eradicate all the disease or if the cells can mutate to nullify the expression of PSMA [29, 116]. There is a growing recognition that combination therapy is necessary to overcome the immunosuppressive nature of PCa [117]. One of our future directions is to perform a combined therapy experiment with $^{177}$Lu-PSMA617 and a checkpoint agonist (anti-OX-40). In Chapter 5, I will discuss and present the data on the expression patterns of OX-40 and PD-1 in T cells for potential combinatorial treatment with $^{177}$Lu-PSMA617.

# Chapter 3: $^{177}$Lu-PSMA617 induces apoptosis in hPSMA TRAMP-C2 cells

## 3.1 Acknowledgments

I would like to start this chapter by thanking Tim Turcotte (BC Cancer- Victoria) and Adria Devlinger (BC Cancer- Victoria) for helping me perform Truebeam Irradiation on my cells. I would also like to thank Helen Merkens (BC Cancer, Vancouver) for collection of TRAMP-C2 lysates after treatment with $^{177}$Lu-PSMA617.

## 3.2 Abstract

Apoptosis is one of the cell-death modalities observed in cells as a response to irradiation and other cancer immunotherapies [65, 68]. In normal tissues, it plays an important role in maintaining cellular homeostasis [66, 69, 70]. Apoptosis involves a highly complex set of cascading molecular events that include activation of cysteine proteases known as caspases [35]. This type of programmed cell death involves two mechanisms: intrinsic and extrinsic pathways [66, 69, 69]. All the apoptotic events can be divided into four stages: induction, early, execution and late phase. Both pathways result in an important execution-step of caspase-3 cleavage [66, 118]. Although irradiation-induced apoptosis has been widely studied, the mode of cell death induced by radioligand therapy (rLT) requires clarification [67]. Here I investigated the mechanism of cell death induced by $^{177}$Lu-PSMA617 in TRAMP-C2 cells. Using immunoblotting, I investigated the cleavage of caspase-3 post-treatment with $^{177}$Lu-PSMA617 rLT. I show that $^{177}$Lu-PSMA617 induces apoptosis in TRAMP-C2 as evident by cleavage of caspase-3. These results provide the first evidence evaluating the mechanism of cell death induced by $^{177}$Lu-PSMA617 rLT.

## 3.3 Introduction

Apoptosis is a type of programmed cell death (PCD) that involves activation of caspases leading to cascading events that end with elimination of the cell [65, 70, 119]. This type of PCD normally occurs during development and acts as a homeostatic mechanism to maintain cell populations [66, 70, 120]. It is also an important defense mechanism when the cells are damaged by diseases such as cancer [119]. During cancer treatment, irradiation or chemotherapy can be used to induce apoptosis [66, 119]. These type of cancer treatments can lead to DNA damage in some cells, resulting in apoptotic cell death [69, 70, 121].

Caspases or cysteine aspartic proteases play critical roles in regulating different stages of apoptosis [66, 70, 120]. Caspases exhibit proteolytic activity that allows them to cleave proteins at aspartic acid residues [66, 120]. Once caspases are activated during different phases of apoptosis, there is an irreversible commitment to cell death [70, 122, 123]. This proteolytic cascade involves a chain-like activation of caspases that catalyzes the apoptotic signaling pathway leading to cell death. All the identified caspases have been categorized into three types: induction (caspase-2, -8, -9, -10), effector (caspase-3, -6, -7) and inflammatory (caspases-1, -4, -5) caspases [66, 122].

As mentioned earlier, apoptosis involves highly controlled and complex mechanisms. Currently, researchers have identified two main mechanisms of apoptosis: intrinsic (mitochondrial) pathway and extrinsic (death-receptor pathway) [66, 122, 123]. Both mechanisms involve the cleavage of caspase-3 which leads to DNA fragmentation, degradation of nuclear proteins, expression of phagocytic ligands, concluding with uptake by phagocytic cells [66, 123, 124].

The intrinsic pathway of apoptosis involves a distinct arrangement of non-receptor mediated stimuli that produce intracellular signals and are mitochondrial-initiated events [125].

These intracellular signals can act in a negative or positive manner. Furthermore, these negative or positive signals can stimulate the intrinsic pathway of apoptosis. Negative signals involve the withdrawal of growth factors, hormones and cytokines which can result in loss of apoptotic suppression and PCD activation [66, 125]. Positive signals that lead to apoptosis include cellular stresses such as radiation, viral infections and surpluses of free radicals [125]. These stimuli can cause changes in the inner mitochondrial membrane leading to procaspase-9 activation and formation of a large quaternary protein structure called the apoptosome [126]. Downstream effects of this pathway include caspase-3 cleavage and DNA fragmentation.

The extrinsic pathway of apoptosis involves transmembrane receptor-ligand interactions. This induction phase of the extrinsic pathway is activated when death receptors (members of the tumor necrosis factor (TNF) receptor family) bind with their respective ligands. The primary apoptosis inducing ligands include tumor necrosis factor alpha (TNF-α), lymphotoxin-α (LT-α), fatty acid synthetase ligand (FasL)/CD178 and TNF-related apoptosis-inducing ligand (TRAIL) [69. 127]. During the early phase, downstream binding interactions occur where signaling pathways are activated leading to formation of the death inducing signaling complex (DISC) resulting into activation of procaspase-8 [123, 127]. Once caspase-8 is activated, it initiates the execution-phase of apoptosis.

Both intrinsic and extrinsic pathways converge at the execution phase that includes activation of effector caspases such as caspase-3 [123, 128]. These effector caspases induce activation of cytoplasmic endonucleases and proteins that can degrade nuclear and cytoskeletal proteins (Figure 10). Caspase-3 is regarded as the key effector caspase and is activated by either

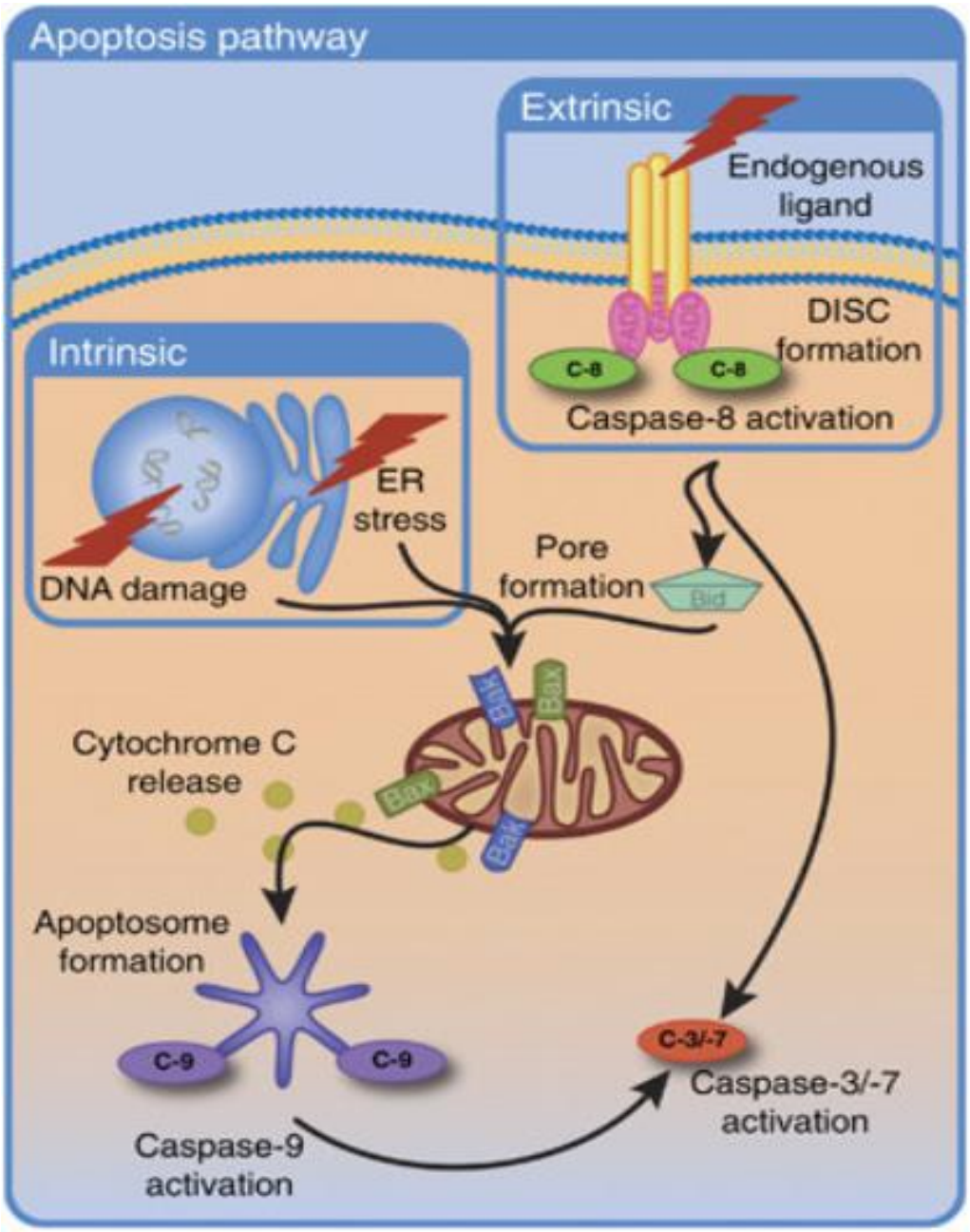


**Figure 10. Caspase-3 activation via the intrinsic and extrinsic pathway of apoptosis (Boland *et al.*, 2013)**

initiator caspases which are activated in the intrinsic (caspase-9) and extrinsic (caspase-8) pathway of apoptosis [66, 123, 128].

There have been many cancer therapies that can induce apoptosis in cancer cells. Some of these treatments target specific signaling mechanisms. The p53 transcription factor controls

DNA repair genes and apoptosis [129, 130]. Irradiation and chemotherapies induce this *p53* pathway leading to effective induction of apoptosis [66, 129, 131]. Targeted radioligand therapy such as $^{177}$Lu-PSMA617 rLT has not been studied for its role in activation of apoptosis. Although the role of irradiation in apoptosis has been widely studied, there are significant differences between the type of particles emitted from ionizing radiation versus $^{177}$Lu-PSMA617 radioligand therapy. Thus, here I report an investigation into the induction of apoptosis in previously generated (refer to Chapter 2) hPSMA TRAMP-C2 cells through $^{177}$Lu-PSMA617 rLT.

## 3.4 Methods and Materials

### 3.4.1 Cell line and culture conditions

The TRAMP-C2 lines used in this report were acquired from American Type Culture Collection (ATCC). These TRAMP-C2 cells were cloned to express hPSMA upon doxycycline (DOX) induction. Human PSMA-expressing TRAMP-C2 (hPSMA TRAMP-C2) cells were maintained in DMEM High Glucose Medium containing fetal bovine serum (FBS; 5%), Nu-Serum IV (5 %), bovine insulin (0.005 mg/mL), dehydroepiandrosterone (DHEA; 10 nM), penicillin (100 U/mL) and streptomycin (100 μg/mL (all items from Fisher Scientific). All cells were maintained at 37$^{o}$C, 20% $O_2$, and 5% $CO_2$ in a water-jacketed Forma Scientific Incubator.

### 3.4.2 Treatment with irradiation

hPSMA TRAMP-C2 bulk cells were plated in 6 well plate 24 hours pre-DOX treatment to achieve 60% confluency. DOX was added to the wells at 1μg/mL. The cells were incubated with DOX for 18 hours. The DOX-induced cells were trypsinized and harvested in 15 mL conical tubes with 10 mL TRAMP media. Cells were treated with irradiation at 0, 10, 20 and 30 Gy

doses with a 6 MV photon beam delivered by a Truebeam linear accelerator (Varian Medical, Palo Alto). The radiation was prescribed to the center column of the tubes and the dose delivery was verified with an ionization chamber.

### 3.4.3 Treatment with $^{177}$Lu-PSMA617 radioligand – Vancouver, BC

Our collaborators at BC Cancer- Vancouver, performed this experiment by plating hPSMA TRAMP-C2 bulk cells were in 6 well-plates, 24 hours pre-DOX treatment to achieve 60% confluency. DOX was added to the wells at 1μg/mL. The cells were incubated with DOX for 18 hours. The DOX-induced cells were treated with $^{177}$Lu-PSMA617 (0.01 mCi). Lysates were collected from samples on days 1, 4 and 7 post-$^{177}$Lu-PSMA617 treatment.

### 3.4.4 Validating caspase-3 cleavage through immunoblotting

For immunoblotting cleaved caspase-3, hPSMA TRAMP-C2 cells were treated with $^{177}$Lu-PSMA617. The cells were lysed in RIPA buffer (50 mM Tris-HCl pH 7.4, 1% NP-40, 0.25% Na-deoxycholate, 150 mM NaCl, 1 mM EDTA) containing complete protease inhibitor cocktail, and phosphatase inhibitor cocktail for 30 min at 4$^{o}$C. The samples were centrifuged at 13,000 g for 15 min at 4$^{o}$C after which supernatants were collected and stored at -80$^{o}$C. Lysates were quantified using a bicinchoninic (BCA) assay (Thermo Fisher) and equal amounts were loaded onto 4-12% gradient SDS-PAGE gels. Protein was transferred onto nitrocellulose membranes and immunoblotted for pro-caspase 3 (D3R6Y, dilution 1/1000), cleaved caspase-3 (ASP175, 1/1000), GAPDH (D16H11, 1/2000) and β-actin (13E5, 1/2000) using their respective antibodies (all antibodies were acquired from Cell Signaling).

# 3.5 Results

### 3.5.1 Validation of cleaved caspase-3 antibody post-irradiation

To examine if $^{177}$Lu-PSMA617 induces apoptosis in hPSMA TRAMP-C2 cell lines, I performed a western blot using irradiation. In this experiment, non-irradiated (0 Gy) hPSMA TRAMP-C2 cell-lysates served as the negative control while GAPDH was used as a loading control. In this control experiment, 0 Gy lane yielded no detectable cleaved caspase-3. In contrast, all three dosages (10, 20 and 30 Gy) of irradiation resulted in apoptotic induction (Figure 11A). The hPSMA TRAMP-C2 cells treated with 30 Gy irradiation dosage showed increased caspase-3 cleavage compared to the other dosages. This experiment was used as a control for analysis of caspase-3 cleavage in $^{177}$Lu-PSMA617 treated hPSMA TRAMP-C2 lysates. For the next experiment, the 30 Gy irradiated hPSMA TRAMP-C2 cells served as the positive control.

### 3.5.2 $^{177}$Lu-PSMA617 induces apoptosis in hPSMA TRAMP-C2 cells

Next, we wanted to examine if a similar response could be observed from $^{177}$Lu-PSMA617 treated hPSMA TRAMP-C2 cells. For this experiment, we had two groups: non-treated and $^{177}$Lu-PSMA617 treated samples. We also wanted to test the kinetics of apoptotic induction. For $^{177}$Lu-PSMA617 treated samples (0.01 mCi), lysates were collected day 1, 4 and 7 post-treatment. In this experiment, β-actin served as the loading control. The negative control for this experiment were the non-irradiated (0 Gy) hPSMA TRAMP-C2 cells while the 30 Gy irradiated cells acted as my positive control (Figure 11B). When all the non-treated and $^{177}$Lu-PSMA617 treated samples were assessed for caspase-3 cleavage, we found no caspase-3 cleaved bands in non-treated samples. However, there was clear evidence of apoptosis in $^{177}$Lu-PSMA617 treated samples as early as day 1 post-treatment (Figure 11B). All samples treated

with $^{177}$Lu-PSMA617 showed caspase-3 cleavage. This response was maintained over the time course of $^{177}$Lu-PSMA617 treatment. The pro-caspase 3 levels were also consistent in all samples.

**A.**

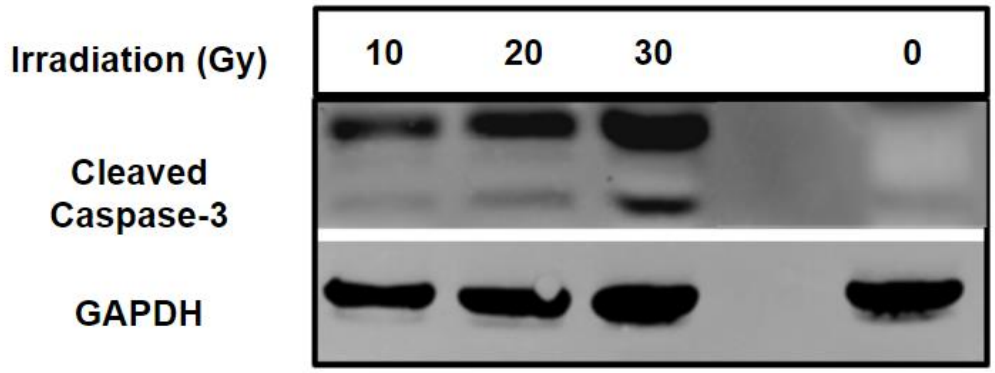


**B.**

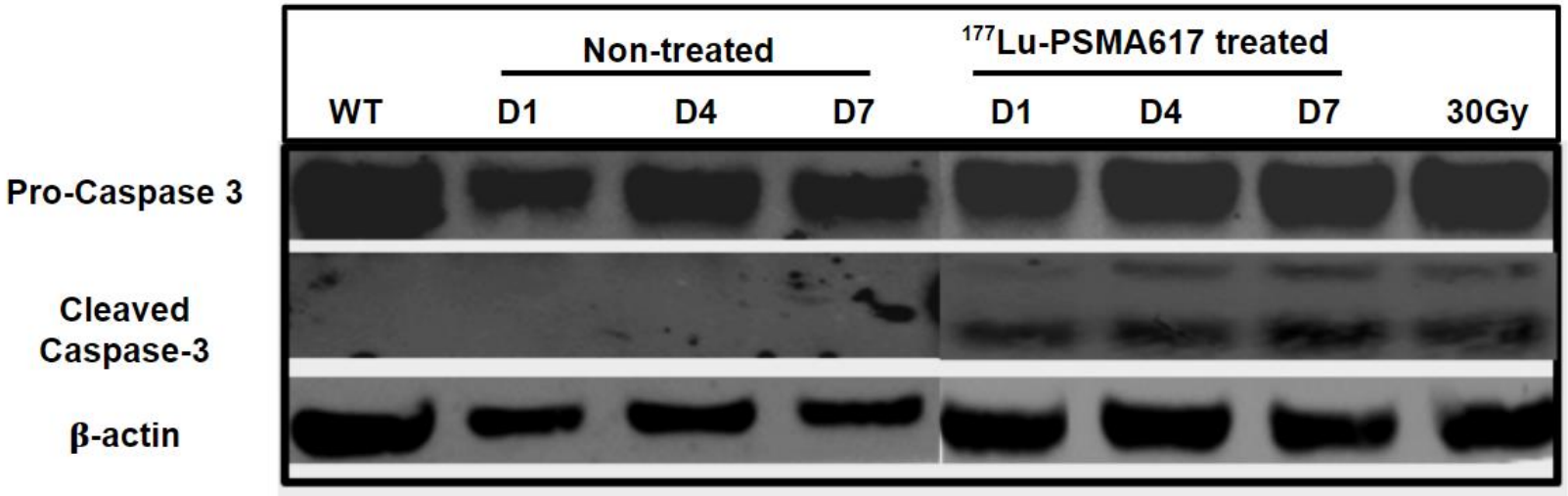


**Figure 11. Western blots were performed to assess apoptotic induction after treatment with irradiation and $^{177}$Lu-PSMA617 treatment.** (A) Western blot was performed to verify caspase-3 cleavage 24 hours post-irradiation at 10, 20, 30 Gy dosage. (B) Western blot was performed on non-treated and $^{177}$Lu-PSMA617 rLT treated cells. Lysates were collected day 1, 4 and 7 post-$^{177}$Lu-PSMA617 treatment. (30 Gy: irradiated control sample; WT: WT TRAMP-C2 (negative control); β-actin: experimental control; GAPDH: experimental control)

## 3.6 Discussion

Our aim with this experiment was to understand how $^{177}$Lu-PSMA617 rLT induces cell death in TRAMP-C2 cells. We collected lysates from hPSMA TRAMP-C2 cells treated with $^{177}$Lu-PSMA617 and performed western blots to assess the extent of apoptosis using cleaved caspase-3 as the key marker. To assess this, I used hPSMA TRAMP-C2 cells treated with irradiation as a positive control. Gamma irradiation has a well-described role in the induction of apoptosis. I used a clinical linear accelerator (LINAC) to expose hPSMA TRAMP-C2 cells with a photon energy of 6 megavoltage (MV). This emission is different from $^{177}$Lu-PSMA617 rLT as the $^{177}$Lu radionuclide is a β-emitting particle (490 keV). We tested three different irradiation dosages (10, 20, 30 Gy) to assess caspase-3 cleavage and consequently apoptosis in my hPSMA TRAMP-C2 cells (Figure 11A). We observed varying level of caspase-3 cleavage in all irradiated samples, although 30 Gy treated sample seemed to have the most distinct caspase-3 cleaved band after 24 hours. The non-irradiated sample resulted in no detectable cleaved caspase-3. Given this result, I decided to use the 30 Gy treated sample as my positive control for the next experiment.

The next experiment was to assess how $^{177}$Lu-PSMA617 rLT induces cell death in hPSMA TRAMP-C2 cells. For this experiment, our collaborators in Vancouver treated my cells with 0.01 mCi of $^{177}$Lu-PSMA617. They collected and prepared lysates for days 1, 4 and 7 post-treatment. This was done to assess not only the presence or absence of apoptosis but to also study the kinetics of induction. In this experiment, the pro-caspase 3 bands were present in all non-treated and treated samples. While analyzing the caspase-3 cleavage between non-treated and $^{177}$Lu-PSMA617 treated samples, we found cleaved caspase-3 bands only in $^{177}$Lu-PSMA617 treated cells. This supported the hypothesis that $^{177}$Lu-PSMA617 rLT induces apoptosis in hPSMA TRAMP-C2 cells (Figure 11B). An important observation was that this apoptotic

induction could be visualized as early as day 1 post-treatment. This result was correlative to what we observed with our irradiated samples in Figure 11A. The cleaved caspase-3 expression was also consistent in day 4 and day 7.

One of the significant hallmarks of cancer is the evasion of cell death by cancer cells. Targeting the apoptotic cellular death pathways may act as an effective treatment option for all cancers [131, 132]. Some of the key players recognized in apoptotic regulation include death receptors, B-cell lymphoma 2 (Bcl-2) proteins and caspases [132, 133]. The identification of these regulators has led to increased interest in developing targeted therapies to intervene with cell death. Different chemotherapies including cisplatin have been found to interact with Bcl-2 members [134]. Cisplatin has been found to transactivate the *bax* (translates for proapoptotic proteins such as BAX) gene through p53 pathway leading to apoptosis induction [134, 135].

Some of the other approaches have included mimicking extracellular death signals with recombinant ligands that could trigger apoptosis. The activation of a surface-level death receptor binding to the TRAIL ligand can lead to intracellular recruitment of the DISC resulting in the induction of caspase-8 activation and further downstream effects [66, 136, 137]. One study found that targeting the TRAIL pathway led to targeted killing of the tumor cells while leaving normal tissue unaffected [137, 138]. Other studies have shown that injection of TRAIL into immunodeficient mice that were challenged with colon carcinoma and human mammary adenocarcinoma led to tumor cell apoptosis, tumor-growth suppression and improved survival [137, 138, 139]. Pre-clinical safety tests have in non-human primates have shown no toxicity in these non-human primates [140]. Other approaches include using caspase-inhibitors or other small-molecule drug that can activate the caspase-related cascading events [137].

Previous studies with $^{177}$Lu-PSMA617 had shown effective cytotoxicity to prostate cancer cells but the specific type of cell death was still unknown [4, 16, 17]. Our data suggests that $^{177}$Lu-PSMA617 induces apoptotic cell death in TRAMP-C2 cells. It is still unclear if this apoptotic cell death is also able to induce a systemic immune response. If $^{177}$Lu-PSMA617 can induce immunogenic cell death, we might be able to combine $^{177}$Lu-PSMA617 with immunomodulatory treatments such as checkpoint inhibitors to develop a more effective treatment for PCa. This proposition is further reviewed in chapter 5 of my thesis.

# Chapter 4: $^{177}$Lu-PSMA617 induces immunogenic cell death in TRAMP-C2 cells

## 4.1 Acknowledgments

I would like to thank Helen Merkens (BC Cancer, Vancouver) for collection of supernatants from TRAMP-C2 cells treated with $^{177}$Lu-PSMA617.

## 4.2 Abstract

Immunogenic cell death is a type of cell death that induces the immune system [53, 54]. Cancer treatments such as chemotherapy and radiation can be effective in inducing cytotoxicity in cancer cells but may not always activate the immune system [53]. More importantly, the ability to assess the extent and temporal dynamics of ICD is a challenge due to the lack of the proper tools to study ICD [53, 54]. This type of cell death can be monitored by release of DAMPs (damage-associated molecular patterns) such as high mobility group box-1 (HMGB1) and calreticulin (CRT) [54]. I generated fluorescence-associated DAMP constructs that could be utilized to observe ICD in TRAMP-C2. Using this system, I observed translocation of DAMPs through microscopy post-ICD induction with CTX in TRAMP-C2.

I was able to quantify HMGB1 release into the cell culture supernatants and thus verify ICD release post-treatment with CTX and $^{177}$Lu-PSMA617. Collectively**,** these results showed that CTX and $^{177}$Lu-PSMA617 induce immunogenic cell death in TRAMP-C2 cell lines.

## 4.3 Introduction

Apoptosis and other programmed cell death modalities have been considered to not elicit an immune response [71]. However, various stimuli can induce a functionally specific type of apoptotic death that induces the adaptive arm of the immune system. This type of cell death is aptly named “immunogenic cell death” (ICD) [53, 54]. Some cellular stresses and stimuli can

engage the immune system that result in an immunogenic variant of cell death with biochemical properties of apoptosis [54]. Many chemotherapy agents such as cyclophosphamide (CTX), doxorubicin, mitoxantrone and epirubicin have been known to trigger ICD inducing release of tumor antigens from dying cancer cells [141]. CTX is a widely used chemotherapy agent for the treatment of hematologic and solid tumor malignancies including PCa [86, 142, 143]. CTX exhibits an immunomodulatory behavior by suppressing immune cells like regulatory T cells (T regs) and thus nullifying the immunosuppression in the tumor microenvironment [144].

ICD is reliant on the ability of the treatment to induce cytotoxicity while also activating the coordinating release of immunogenic signals [54, 145]. These signals are released by damage-associated molecular patterns (DAMPs) [145, 146]. These molecules are not usually found to interact with the immune system in normal physiological conditions [145, 146]. However, during ICD, these molecules are released into the extracellular space and can interact with antigen presenting cells (APCs) such as dendritic cells. These molecules, also referred to as DAMPs bind to the pattern recognition receptors (PRRs) expressed on these immune cells [145, 146]. Currently, three DAMPs have been found to play a key role in ICD: calreticulin, HMGB1 and ATP [53, 54].

Calreticulin (CRT) is well-studied ICD marker which, under normal cellular conditions, is found in association with endoplasmic-reticulum (ER) chaperone proteins. Upon exposure to cellular stress that stimulates ICD, CRT translocates from the ER onto the cell surface [147, 148]. This mechanism includes an ER stress-signaling module that results in arrest of protein synthesis and an apoptotic module resulting in activation of caspase-8 and consequent cascade of downstream apoptotic events [147, 148]. Once translocated to the surface, CRT binds to lipoprotein receptor related protein 1 (LRP1) on the surface of an antigen presenting cell (APCs),

leading to an intercellular cellular signal being delivered to induce phagocytosis of the dying cell [147, 148].

Another ICD molecule that has both cell release and translocation properties is the non-histone chromatin-binding protein HMGB1. Under ICD stimulating conditions, HMGB-1 is released from the nucleus and into the cytoplasmic space [53, 54]. Prolonged exposure to ICD agents ultimately results in extracellular release of HMGB-1. The release of HMGB1 has been well known to initiate potent immune responses through binding interactions with receptors such as toll-like receptor-2 (TLR-2) and TLR-4 found on various immune cells [149, 150]. A study done by *Yamazaki et. al* investigated these interactions and found that HMGB1-deficient malignant cells treated with ICD inducers failed to elicit an adaptive immune response in immunocompetent syngeneic mice. This effect was altered with administration of TLR-4 ligands [150]. This shows that HMGB1-TLR2/4 interactions play a key role in the initiation of ICD.

The central dogma of radiobiology suggests that radiation induces irreversible cytotoxic effects through production of DNA double-strand breaks [151]. This phenomenon can lead to apoptotic, necrotic or autophagic cell death [151]. There is evidence to suggest that radiation induces ICD [152]. Many studies have proposed that ICD may be caused due to an abscopal response from the radiation [153, 154]. Abscopal effect is a term used to describe radiation-induced tumor suppression in distant metastatic post-treatment of a target site [154, 155]. This response is evidence for involvement of the immune system in eliciting the distant anti-tumor response [152, 154, 155]. Although this phenomenon has been studied with ionizing radiation, it is still unclear if radionuclides (e.g., $^{177}$Lu-PSMA617) can induce ICD. Here I report my findings on the development of a novel technique to assess ICD and the induction of ICD by $^{177}$Lu-PSMA617.

# 4.4 Methods and Materials

### 4.4.1 Cell line and culture conditions

The TRAMP-C2 lines used for this study were acquired from ATCC. These TRAMP-C2 cells were cloned to express human PSMA (prostate specific membrane antigen) post-doxycycline (DOX) induction. The human PSMA-expressing TRAMP-C2 (hPSMA TRAMP-C2) cells were maintained in DMEM High Glucose Medium containing fetal bovine serum (FBS ; 5%), Nu-Serum IV (5%), bovine insulin (0.005 mg/mL), dehydroepiandrosterone (DHEA; 10 nM), 100 U/mL penicillin and 100 µg/mL streptomycin (all items from Fisher Scientific). All cells were maintained at 37$^{o}$C, 20% $O_2$, and 5% $CO_2$ in a water-jacketed Forma Scientific Incubator.

### 4.4.2 Generation of HMGB1-GFP and CRT-mCherry reporter plasmids

#### *4.4.2i Cloning HMGB1-GFP and CRT-mCherry into pef1α-ires-neo plasmid*

Previously, an undergraduate student (Xuan Wang) had generated DAMP-reporter gene constructs with a cytomegalovirus (CMV)-based promoter. The fluorescent markers used in this study were the green fluorescent protein (GFP) and a member of the monomeric red fluorescent proteins (mCherry). These plasmids had shown dual expression of HMGB1-GFP and CRT-mCherry post-transfection respectively [156]. It was noted that utilizing a CMV-based promoter led to a decreased expression over time post-transfection in TRAMP-C2 (data not shown). To improve transient expression, these plasmids were cloned into an ef1α-based promoter vector (pef1α-ires-neo).

To clone HMGB1-GFP and CRT-mCherry into pef1α-ires-neo vector, both fusion sequences were cloned out of the initial plasmid generated by Xuan Wang [156]. The expression plasmid contained the HMGB1-GFP and CRT-mCherry fusion sequences between restriction

sites NheI and NotI of the multiple cloning site (MCS). To isolate the inserts, the expression plasmids were digested with their respective restriction enzymes to generate two non-compatible ends, thus allowing the insert to be cloned directionally. The restriction digests reported in this paper were all performed according to the protocol provided by New England Biolabs (NEB). The target peF1α-ires-neo plasmid were also digested with NotI/NheI enzymes. The fusion inserts were ligated into the pef1α-ires-neo plasmid according to the protocol provided by NEB. The ligated products were transformed into *E. coli* for plasmid amplification and verification. Transformed colonies that were resistant to antibiotic selection were verified by performing restriction digests on the pef1α-ires-neo plasmid at their target-restriction sites respectively. The cloning protocol generated two plasmids: HMGB1-GFP pef1α-ires-neo and CRT-mCherry pef1α-ires-neo vectors.

#### *4.4.2ii Transfection of TRAMP-C2 cells with reporter plasmids*

To finally test expression of these reporter plasmids, a lipofectamine-based transfection was performed. To prepare, TRAMP-C2 cells were plated 18 hours pre-transfection to reach 70% confluency. Both reporter plasmids were transfected according to the Lipofectamine3000 ® protocol provided by ThermoFisher. The cells were transduced for 12 hours at 37ºC, 5% $CO_2$ in a water-jacketed incubator. The transfected-culture medium was discarded and replaced with fresh growth medium. After resting the cells for 24 hours, they were utilized for further experiments.

### 4.4.3 Fluorescence-microscope imaging to verify expression of HMGB1-GFP and CRT-mCherry post-transfection

Images of the transfected cells were collected using the EVOS LifeSciences fluorescent microscope (Invitrogen, EVOS FL Cell Imaging System).

### 4.4.4 DAPI-nuclear stain and ER-stain to verify plasmid localization

TRAMP-C2 cells were plated for 18 hours to reach 70% confluency and transfected with HMGB1-GFP and CRT-mCherry plasmids using Lipofectamine3000® (as per manufacturer's protocol). Cells were washed with phosphate buffer saline (PBS) three times and treated with 100 µM of 4′,6-diamidino-2-phenylindole (DAPI) and 50 µM ER-tracker dye (both dyes acquired from ThermoFisher). Cells were incubated at 37ºC for 20 mins. Cells were then washed with PBS and images of the stained cells were collected using LifeSciences fluorescent microscope (Invitrogen, EVOS FL Cell Imaging System).

### 4.4.5 CTX dosage-curve assessment for inducing cell death

To evaluate the most potent CTX dosage concentration for inducing cell death, TRAMP-C2 cells were plated in a 6-well plate (2 x $10^5$ cells/well). Cells were treated with CTX at 0, 30, 40, 45, 50 and 100 µg/mL for four days. Crystal violet assay was performed on days 0, 2, and 4 to monitor cell death. Cells were then washed with PBS and treated with crystal violet (0.2%). These cells were incubated at room temperature with crystal violet for 20 minutes. The wells were washed with PBS and treated with 1% SDS solution. The plate was placed on an orbital shaker until a homogenous solution could be observed. 100 µL from each well was then transferred to a 96-well plate and their absorbance was calculated using an absorbance reader at 560 nm (BioTek Industries).

### 4.4.6 CTX treatment to observe HMGB1 and calreticulin translocation

To observe qualitative translocation of ICD dependent molecules like HMGB1 and CRT, TRAMP-C2, cells were plated in a 6-well plate (2 x $10^5$ cells/well) for 18 hours to reach 70% confluency and transfected with HMGB1-GFP and CRT-mCherry plasmids using Lipofectamine3000® (as per manufacturer's protocol). Finally, cells were monitored for cell

death, images were collected using a fluorescent microscope (Invitrogen, EVOS FL Cell Imaging System).

To observe quantitative release of HMGB1, TRAMP-C2, cells were treated with CTX at 20 and 30 µg/mL for 72 hours (3 days). These cells were then monitored for cell death. Supernatants were collected on day 0, 1, 2 and 3 post-treatment. These collected supernatants were then analyzed for HMGB1 release using an HMGB1-ELISA kit (IBL international). Finally, cells were monitored for cell death, images were collected using a fluorescent microscope (Invitrogen, EVOS FL Cell Imaging System).

### 4.4.7 $^{177}$Lu-PSMA617 treatment to observe HMGB1 release in supernatants

To quantify HMGB1 levels in the supernatants, TRAMP-C2, cells were plated in a 6-well plate (2 x $10^5$ cells/well) for 18 hours to reach 70% confluency. The cells were treated with doxycycline (DOX) to induce hPSMA expression. These cells were treated with $^{177}$Lu-PSMA617 (0.01 mCi) and supernatants were collected on days 0, 1 and 4. The collected supernatants were then analyzed for HMGB1 release using an HMGB1-ELISA kit (IBL international).

### 4.4.8 Statistical Analysis

Comparisons of cell populations between treatment and control groups were performed on GraphPad (Graphpad Software Inc., CA, USA) using one-way ANOVA and Sidak's multiple comparisons test. P values correspond to the following representation of statistical significance. NS= p-value> 0.05, * = p-value<0.05, ** = p-value<0.01, *** = p-value<0.001, and **** = p-value<0.0001.

# 4.5 Results

### 4.5.1 HMGB1-GFP and CRT-mCherry were cloned into pef1α-ires-neo vector

To generate the two reporter constructs, I needed to isolate the gene inserts from the original expression plasmid. The insert size of HMGB1-GFP was 1400 bp while the insert size of CRT-mCherry was 2010 bp. The HMGB1-GFP and CRT-mCherry gene constructs were isolated from their original expression plasmid and cloned into an EF1-α based promoter (pef1α-ires-neo) vector (Figure 12A, 12B). These new fusion-constructs were validated by performing a final restriction digest on the vector products acquired after *E. coli* transformation.

### 4.5.2 CTX induces cellular toxicity in TRAMP-C2 cells

To validate if CTX can induce cytotoxicity in TRAMP-C2 cells and more importantly, induce ICD in these cells (Figure 13A), I performed a crystal violet assay (CVA) to investigate the concentration and kinetics of CTX-induced cell death. I treated cells with 0, 20, 30, and 40 µg/mL concentration(s) of CTX and monitored cell death every day of treatment for 3 days. I observed that CTX was able to induce cell death in TRAMP-C2 cells (Figure 13A, $p<0.001$). I found that there was a significant difference in cytotoxicity between each tested concentration of CTX and this was time dependent. I also observed a significant difference in cytotoxicity between each day for all concentrations (Figure 13A, $p<0.001$). I found that 30 µg/mL of CTX yielded 48% cell toxicity on day 2 increasing to 72% cytotoxicity by day 4 (Figure 13A, $p<0.001$). Therefore, I concluded that to observe a gradual but potent response, I needed to use CTX at concentrations lower than or equal to 30 µg/mL.

A.

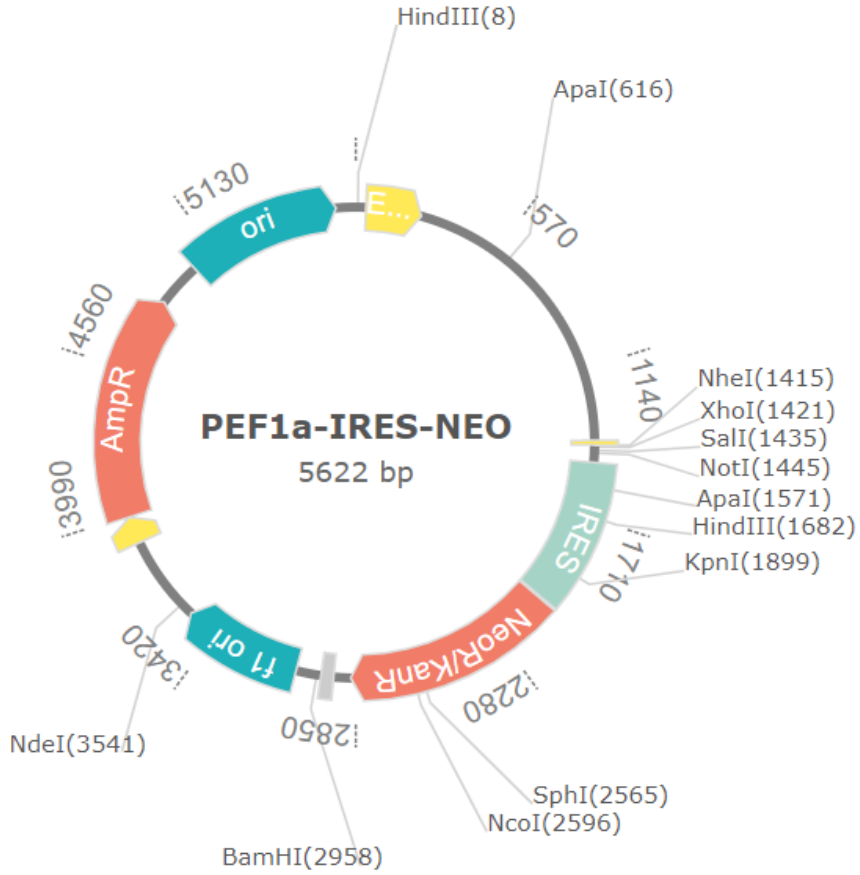


B.

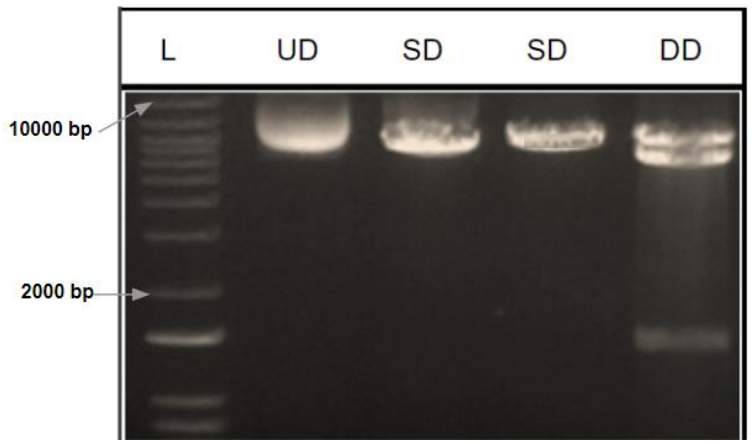


C.

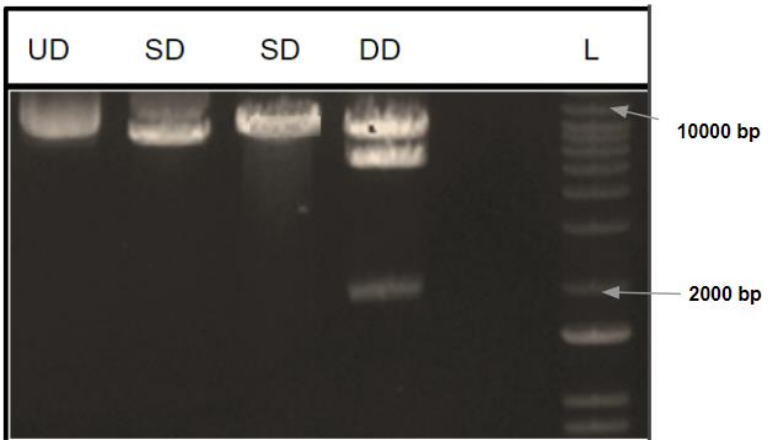


**Figure 12. HMGB1-GFP and CRT-mCherry cloned into plv-ef1α-neo vector.** (A) Plasmid maps for plv-ef1α-neo vector. Plasmid map was generated through GenScript. Restriction digest of (B) HMGB1-GFP and (C) CRT-mCherry derived after bacterial transformation. Genomic sizes of CRT-mCherry is 2010 bp; HMGB1-GFP is 1400 bp.

### 4.5.3 CTX induces ICD in TRAMP-C2 cells

Once CTX was validated to induce cytotoxicity in TRAMP-C2 cells, I assessed whether the doses established above would induce ICD. The TRAMP-C2 cells were treated with CTX at 20 µg/mL and 30 µg/mL and supernatants were collected on day 0, 1, 2 and 3 post-treatment. There was no significant difference observed between the untreated samples. There was a significant difference in HMGB1 concentrations between day 0 and 1 post-CTX treatment in both concentration groups (Figure 13B, $p<0.001$). This significant difference in HMGB1 concentration was also observed between day 1 and 2 in the 20 µg/mL (Figure 13B, $p<0.001$) concentration group but not in the 30 µg/mL group (Figure 13B, $p>0.05$). There was also a significant difference in HMGB1 concentrations between treated and non-treated groups (Figure 13B, $p<0.001$).

### 4.5.4 $^{177}$Lu-PSMA617 induces immunogenic cell death in TRAMP-C2 cells

Previously I had shown that $^{177}$Lu-PSMA617 induces apoptosis in TRAMP-C2 (refer to Chapter 3). In addition to this, I wanted to observe if $^{177}$Lu-PSMA617 could also induce ICD in TRAMP-C2. To investigate this, my colleagues in Vancouver treated TRAMP-C2 cells with $^{177}$Lu-PSMA617 (0.01 mCi) and supernatants were collected day 0, 2 and 4. These samples were shipped to Victoria where I performed the HMGB-1 ELISA. In this analysis, I found that $^{177}$Lu-PSMA617 increased HMGB1 levels in the supernatants post-treatment (Figure 14, $p<0.001$). Moreover, HMGB1 levels increased significantly between day 2 and day 4 post-treatment with $^{177}$Lu-PSMA617 (Figure 14, $p<0.001$). Although $^{177}$Lu-PSMA617 yielded high HMGB1 levels, there was still a significant difference between the control and treated samples for all timepoints (Figure 14, $p < 0.001$). In contrast, there was no significant difference in HMGB1 levels between any of the untreated samples as well all samples on day 0 (Figure 14, $p>0.05$).

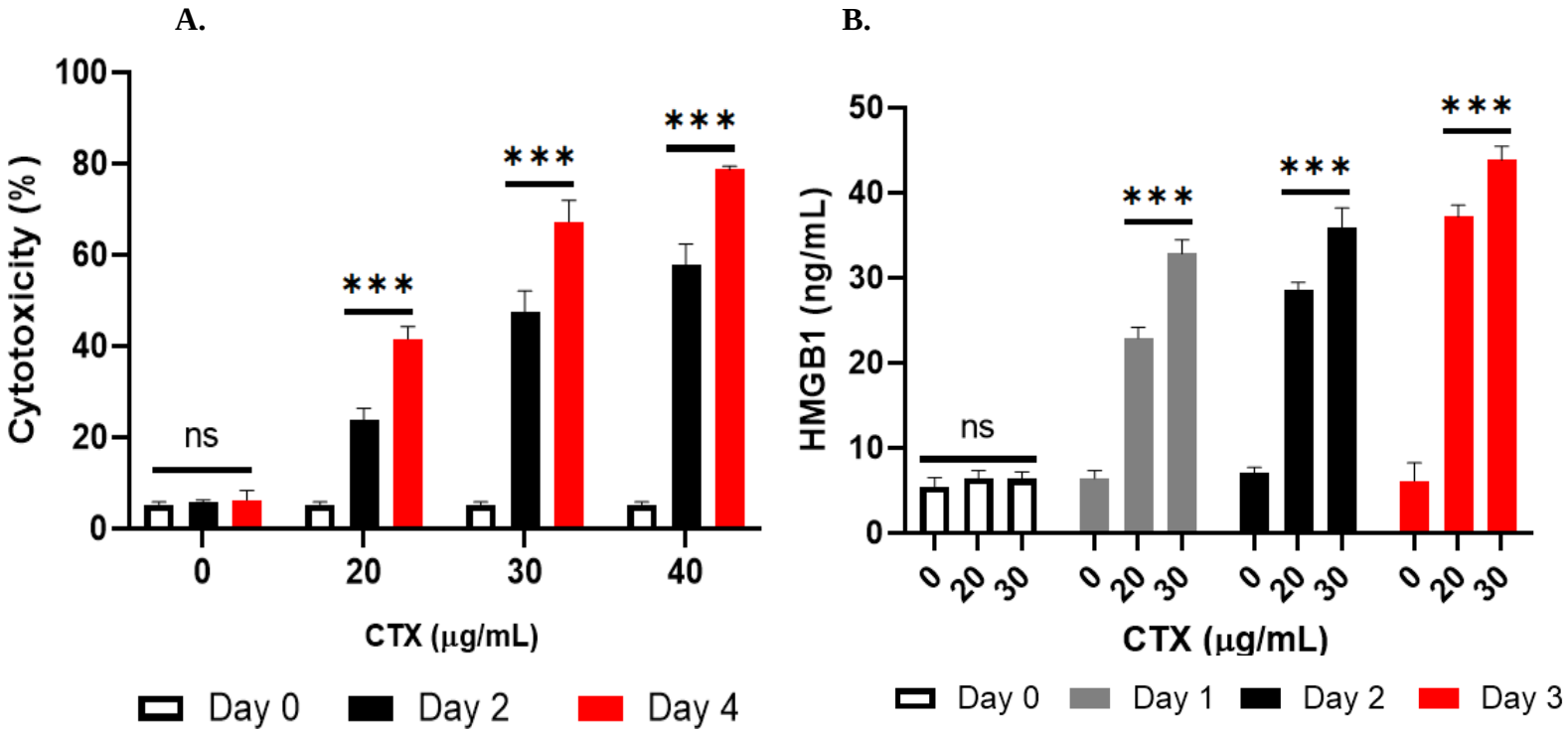


**Figure 13. CTX induces ICD in TRAMP-C2 cells.** (A) TRAMP-C2 cells were treated with CTX at 0, 20, 30 and 40 ug/mL. Crystal violet assay was performed on days 0, 2 and 4 post-treatment. Absorbance was read at 560 nm using a spectrometer. (B) TRAMP-C2 cells were treated with CTX at 20 and 30 ug/mL. Supernatants were collected and analyzed for HMGB1 using HMGB1-ELISA kit (IBL-international). Error bars = standard deviation, N=3.

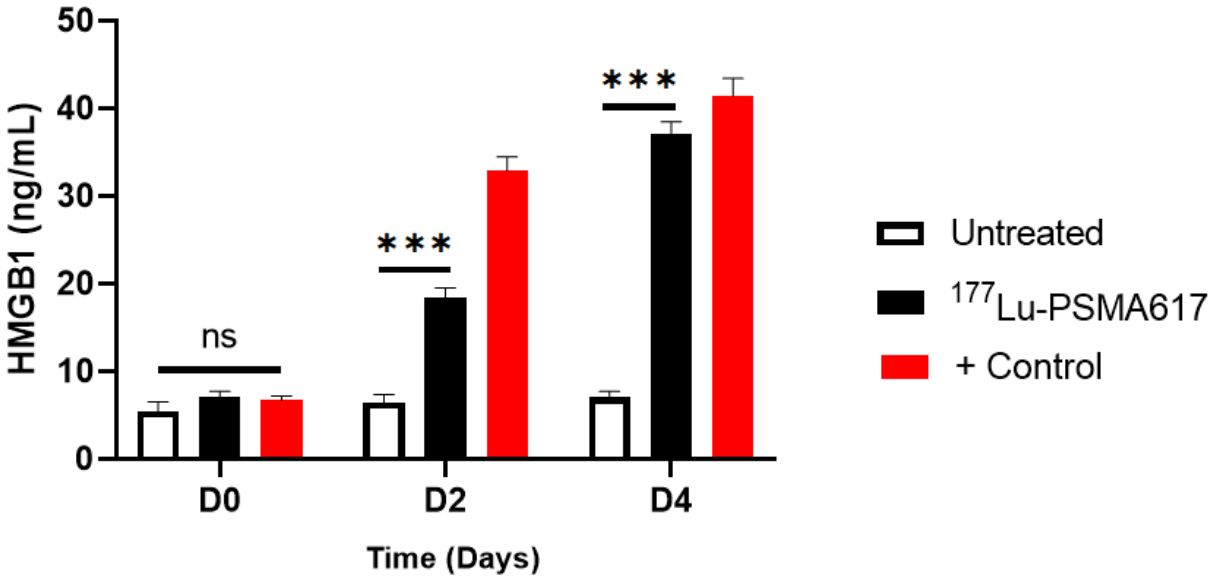


**Figure 14. $^{177}$Lu-PSMA617 induces immunogenic cell death in hPSMA TRAMP-C2 cells.** Cells were DOX-induced for 18 hours and treated with $^{177}$Lu-PSMA617 (0.01 mCi). Supernatants were collected day 0, day 1 and day 4. HMGB1 release in supernatants was quantified using HMGB1-ELISA kit (IBL international). Error bars = SD N= 3.

### 4.5.5 HMGB1-GFP and CRT-mCherry can be transiently transfected in TRAMP-C2 cells

I wanted to validate if these constructs were able to localize at their respective sites. HMGB1 is a nuclear protein while CRT acts a chaperone protein in the endoplasmic reticulum (ER) [53, 147, 149]. I performed transfections with these constructs on TRAMP-C2 cells. After 24 hours post-transfection, I used microscopy to assess the cellular localization of the two respective ICD markers. I verified this localization by performing a nuclear stain for the HMGB1-GFP construct and an ER-stain for the CRT-mCherry construct. The HMGB1-GFP transfection consisted of a no-stain control and a positive control where TRAMP-C2 cells were stained with the DAPI nuclear stain (Figure 15A). The CRT-mCherry transfection also had a no-stain control and positive control consisting of an ER-dye stain. After performing the DAPI nuclear stains, I found that the HMGB1-GFP transfections showed localized fluorescence in the nucleus (Figure 15A). After merging CRT-mCherry localization image with ER-tracker dye-stained images, I observed that CRT-mCherry was being localized to the ER. Finally, I wanted to validate if these reporter-plasmids could be transfected and visualized together. To investigate this, I performed dual transfections on TRAMP-C2 with HMGB1-GFP and CRT-mCherry plasmids (Figure 15B). I found that performing dual transfections did not disrupt their individual localizations and that those localizations could be visualized without interference from either plasmid.

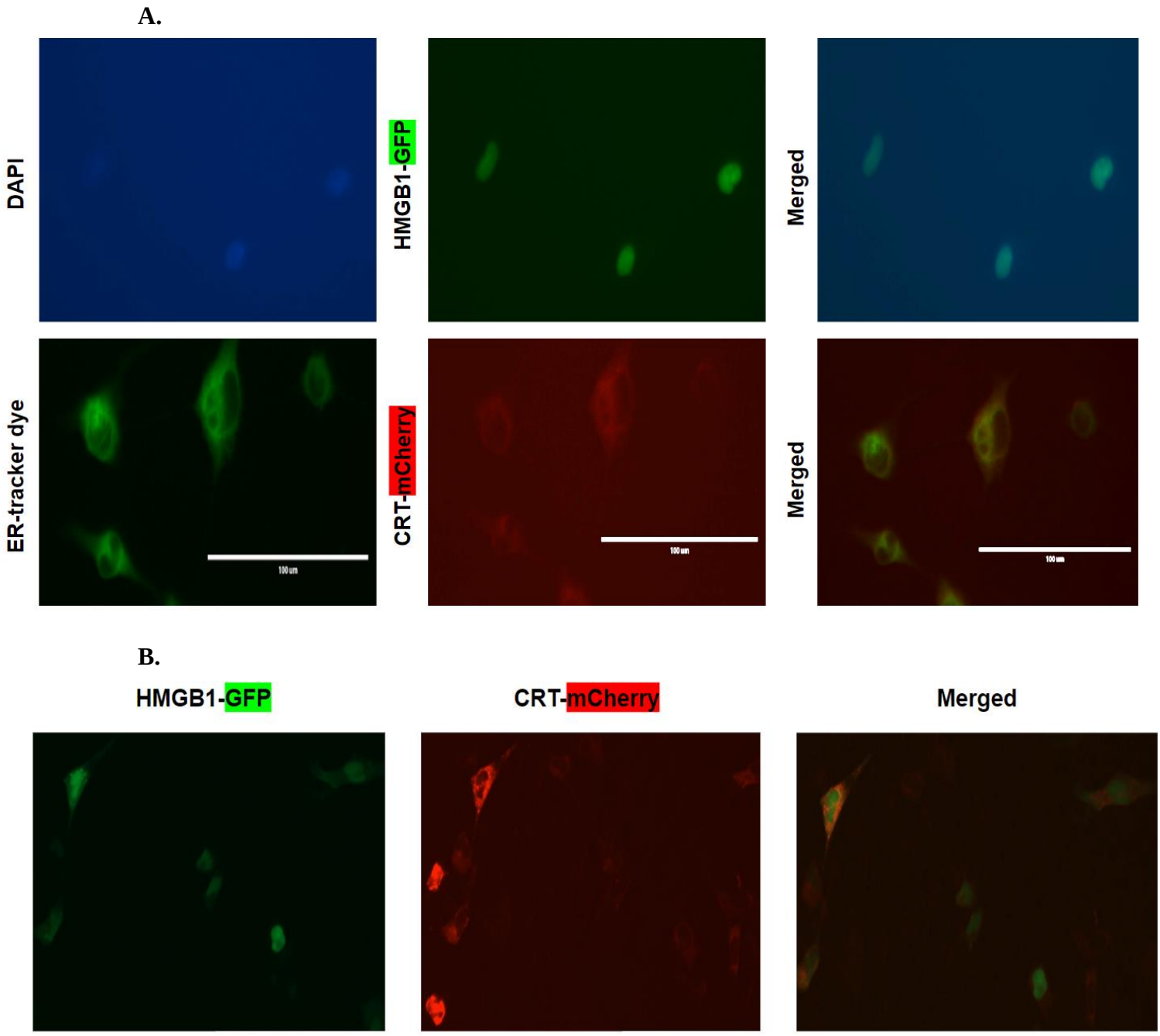


**Figure 15. HMGB1- GFP and CRT-mCherry constructs localize to their respected sites and can be dually transfected**. (A)TRAMP-C2 cells were transfected with HMGB1-GFP and CRT-mCherry plasmids and stained with either DAPI nuclear stain for HMGB1-GFP or ER-tracker dye for CRT-mCherry transfected TRAMP-C2 cells. Bar = 100 μm (B) HMGB1-GFP and CRT-mCherry constructs were dually transfected and visualized using fluorescent microscopy at 40 μm.

### 4.5.6 HMGB1-GFP and CRT-mCherry constructs to assess response to an ICD inducer

Once I validated that these constructs localize to their respective sites, I examined their response after treatment with an ICD inducer. An important aspect of these constructs was to observe if they would localize to the surface once treated with an ICD inducer such as CTX**.**

TRAMP-C2 cells that were transduced with HMGB1-GFP and CRT-mCherry constructs were treated with CTX (30 μg/mL). HMGB1-GFP transfected cell lines showed evidence of release from the nucleus (Figure 16A). CRT-mCherry transfected cell line showed large aggregations of calreticulin structures and evidence of translocation towards the plasma membrane (Figure 16A, 16B). Another significant difference between pre- and post-treated CRT-mCherry transfected cells was the size of the calreticulin blobs. The average area of the blobs in Day 0 CRT-mCherry image was 554 units$^2$ compared to the significantly larger ($p<0.01$) area of the blobs in Day 3 CRT-mCherry image at 6875 units$^2$ (Figure 16B).

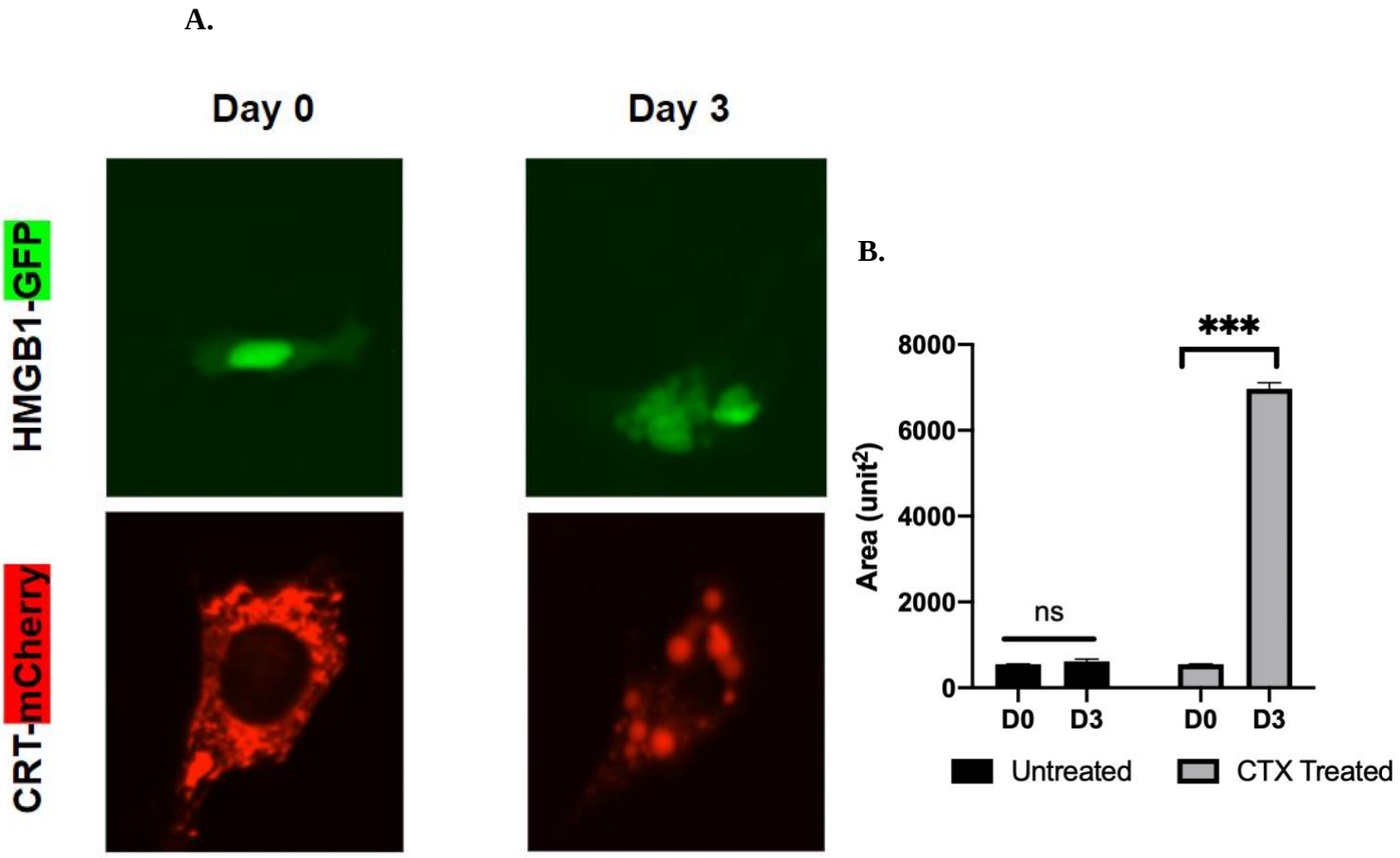


**Figure 16. DAMP trans-localization post-CTX treatment can be visualized. (**A) TRAMP-C2 cells were transfected with HMGB1-GFP and CRT-mCherry plasmids. Cells were treated with CTX at 30 μg/mL. Images were collected day 0 and day 3 post-treatment. (B) Bar graph depicting the area of the blobs. Values were quantified using Fiji Image Analyzer. Error bars= SD, N=3.

## 4.6 Discussion

Our aim with this experiment was to understand if $^{177}$Lu-PSMA617 can induce ICD in TRAMP-C2 cells. Another aim of this experiment was to design a new technique to visualize the translocalization of DAMPs post ICD-induction. This technique could help in understanding the kinetics of ICD and be used to combine different treatments that can augment the anti-cancer effects. To this end, I generated two DAMP-reporter gene constructs, HMGB1-GFP and CRT-

mCherry. TRAMP-C2 cells expressing these reporters were treated with CTX and $^{177}$Lu-PSMA617 to observe ICD through the release of DAMPs.

The first step to assess ICD in TRAMP-C2 cells was to assess if CTX would be able to induce ICD in TRAMP-C2 cells. I observed that CTX was able to cause ICD in TRAMP-C2 cells starting at concentrations of 20 μg/mL. This was an important observation as I realized that CTX was highly toxic to TRAMP-C2 cells. Once this dosage curve was determined, I used 20 μg/mL and 30 μg/mL as my testing concentrations. I observed that there was a significant increase in cytotoxicity between day 0 and day 2 in all tested concentrations (Figure 13). There was a significant difference ($p<0.001$) in cytotoxicity on day 2 between 20 μg/mL and 30 μg/mL concentrations. By day 2, 30 μg/mL concentration yielded ~50 % cell death. As my future experiments would last until day 4, I wanted a concentration that would yield ~80% cytotoxicity at the time. The 30 μg/mL concentration was chosen as the final concentration and my positive control for the future experiments (Figure 13).

Once I had confirmed that CTX was able to induce cytotoxicity in my TRAMP-C2 cells, I wanted to observe if this cytotoxicity could induce ICD. After treating my cells with CTX, I collected supernatants on days 0, 1, 2 and 3 post-treatment. I used the HMGB1-ELISA kit (IBL international) to quantify HMGB1 concentration in these samples. I noticed no significant difference ($p>0.05$) between the untreated samples for all treatment days. The HMGB1 levels followed a similar patter between the 20 μg/mL and 30 μg/mL concentrations where there was a significant increase between day 0 and day 1. With this set of experiments, I was able to confirm that CTX can induce cytotoxicity in TRAMP-C2 cells and can cause ICD as observed by the release of HMGB1 (Figure 13**).** One study done by Mikyskova *et al*. wanted to test a DC-based vaccine in combination with chemotherapy agents. In this study, approximately 8-week-old mice

with TRAMP-C2 tumors treated with CTX yielded a better therapeutic response than combined treatment as evaluated by histology comparisons of neoplasms [157]. Based on this article and my experiments, it could be integral to use CTX as a control for inducing immunogenic cytotoxicity in a TRAMP-C2 model. Although the end goal of this experiment was to understand if $^{177}$Lu-PSMA617 can induce ICD, CTX acted as a positive control for my later experiments.

While observing for ICD induced by $^{177}$Lu-PSMA617, the positive control (CTX at 30 μg/mL) resulted in a significantly increased HMGB1 levels on day 2. There was a significant difference in HMGB1 levels between day 2 and day 4 in TRAMP-C2 cells treated with $^{177}$Lu-PSMA617. Even though there was still a significant difference in HMGB1 levels on day 4 between CTX and $^{177}$Lu-PSMA617, the radioligand treatment still resulted in close HMGB1 levels to the control (Figure 14). As mentioned in section 4. 2, the release of HMGB1 is a strong indicator of ICD induction. Our results are the first to investigate this relationship between $^{177}$Lu-PSMA617 and its ability to induce ICD in TRAMP-C2. It would be essential to see how these results translate in *in vivo* mouse experiments. In the *in vivo* experiment performed by Mikyskova *et al*, the CTX dosage used was 200 mg/kg [157]. It could be important to understand what concentration of HMGB1 release is necessary to cause an effective immunogenic response.

Another aspect of this chapter was to generate two DAMP- reporter gene plasmids that could be utilized to visualize the cellular release of HMGB1 and CRT post-ICD induction. Once the plasmids were generated, I tested them by co-staining them DAPI (nuclear stain) for HMGB1 and ER-tracker dye for CRT. I found that HMGB1 translocated the same as DAPI nuclear stain. This result was similar to what I observed with CRT and ER-tracker dye (Figure 15). It verified that the constructs could be temporarily integrated in TRAMP-C2 cells. It would be interesting to observe if these constructs can be stably expressed or integrated into the genome through viral

transduction. An interesting observation I noticed was that I was able to co-transfect TRAMP-C2 cells with both HMGB1 and CRT constructs without noticing any cellular interference. When I visualized these cells, I did not notice any decrease in expression between the two constructs (Figure 15). With this set of experiments, I was able to verify that the constructs localize accurately in the cell and that dual transfections do not result in any visualization issues.

Using these constructs, I wanted to see if I could visualize the DAMP constructs reacting to the CTX treatment. I transfected TRAMP-C2 cells and treated them with 30 µg/mL of CTX. When I visualized the untreated TRAMP-C2 cells on day 0 and day 3, I found that both constructs were still localized to their sites. The interesting observation I noticed was the nuclear blebbing that had occurred by day 3 in the TRAMP-C2 cells treated with CTX (Figure 16). This effect corresponds to the breakdown of nucleus and could consequently point towards the translocation of HMGB1 to the extracellular space. I noticed a similar effect on day 3 with TRAMP-C2 cells that were transfected with CRT-mCherry and treated with CTX. I observed that by day 3, there were aggregates of CRT that had formed on the plasma membrane (Figure 16). Although, it is critical to note that this was from my first set of experiments treating the DAMP- reporter gene TRAMP-C2 cells with CTX. When I performed this experiment, I acquired a transfection rate of ~40% in all three replicates which resulted in reduced samples to verify the above-mentioned observations. It would be important to improve the transfection procedure or switch to a viral transduction that would result in a better expression of these constructs. It would also be integral to repeat this experiment with more replicates and verify the location of aggregates using cellular stains. As this is a novel observation, this experiment should also be performed with other ICD inducers for a more thorough analysis of the constructs.

As explained earlier in section 4. 2, the DAMP release after a cytotoxic treatment can lead to an adaptive immune response. It is important to study these DAMPs as they could act as adjuvants to current treatment options for not only PCa but other cancer types as well. One study investigated the CRT expression of high-grade serous carcinoma (HGSC) patients in relation with prognosis and functional orientation of the tumor microenvironment [158]. They found that CRT exposure on the surface of primary as well as metastatic HGSC cells is driven by treatment-independent ER stress-response [158]. They also found that patients with high CRT expression had significantly improved relapse-free survival (RFS) and overall survival (OS). High CRT expression was also correlated to T cell activation, T cell migration and cytotoxicity. Another interesting observation was that high CRT expression was associated with activated DC infiltration [158]. Studies like this show how ICD caused by current treatments can be augmented with novel therapies such as checkpoint inhibition or augmentation. One such possible experiment would be to use these constructs to visualize the movement of DAMPs post-treatment with a chemotherapy agent and learn the kinetics of ICD caused by that treatment option. After understanding the kinetics, the anti-cancer response can be augmented using immunotherapy agents such as checkpoint inhibitors or checkpoint agonists. This idea of using checkpoint agonists will be explored in Chapter 5.

# Chapter 5: Expression patterns of checkpoint markers present on T cells and TRAMP-C2 cells

## 5.1 Acknowledgements

I would like to start this chapter by thanking Tim Turcotte (BC Cancer- Victoria) and Adria Devlieger (BC Cancer- Victoria) for helping me perform Truebeam Irradiation on TRAMP-C2 cells.

## 5.2 Introduction

Cancer immunotherapy has become a rapidly developing field in the past decade. The regulation of immune checkpoints has become an important field of study regarding cancer immunotherapy [73,98, 159]. These immune checkpoints consist of various stimulatory and inhibitory pathways that aid in self-tolerance and assist in immune response [73, 98]. In cancer, these immune checkpoints are blocked or activated to inhibit the immune response against the tumor. There have been various immune checkpoint therapies that have been developed that block or stimulate the anti-tumor immune response [73, 85, 86].

As suggested in Chapter 1, the tumor microenvironment consists of a range of intricate interactions between the malignant cells, immune cells and the stroma [92, 160]. These group of immune cells include antigen presenting cells (APCs), natural killer cells (NK cells), and B and T lymphocytes [160]. As explained in section 1.5, $CD8^+$ effector cells direct a cell-mediated immune response [161]. An immunological synapse forms between the T cell and the targeted malignant cell through TCR-MHC class I engagement [162]. When this engagement occurs, the cancer cell attempts to suppress the immune response. One such method of suppression is through expression of inhibitory checkpoint markers such as programmed death ligand 1 (PD-

L1). The programmed cell death 1 protein (PD-1) expressed on T cells, and its ligand PD-L1 interact to induce T cell exhaustion, state that effectively halts the anti-tumor response [89, 163].

Checkpoint inhibitors are a class of drugs that block the interactions between checkpoint markers and their respective ligands. Many checkpoint inhibiters such as anti-PD-L1 and anti-PD-1 have been developed to relieve the suppressive effects caused by T cell-tumor cell interactions of these checkpoint molecules [83, 164]. This allows the T cells within the tumor to become reactivated and mount an effective anti-tumor response [83, 165]. One checkpoint marker that has been utilized towards PCa includes the cytotoxic T lymphocyte-associated protein 4 (CTLA-4). CTLA-4 is an immune checkpoint expressed on T cells that serves to contain T cell-mediated immune responses [166, 167]. CTLA-4 interacts with B7 family of ligands to inhibit T cell responses. Currently there are several other Food and Drug Administration (FDA) approved checkpoint inhibitors including Nivolumab (anti-PD-1) and Atezolizumab (anti-PD-L1) [83, 86, 159].

Targeting CTLA-4 with a monoclonal antibody results in enhanced T cell mediated responses and tumor eradication [166, 167]. Ipilimumab (anti-CTLA-4) has shown mixed results but has been more effective when combined with other treatments including surgery and vaccines [86, 167]. Although it is unclear what makes checkpoint blockade ineffective in PCa, some researchers suggest it may be the immunosuppressive tumor microenvironment [168, 169, 170]. Studies have shown that PCa patients have increased frequencies of $CD4^+$ T regulatory (T regs) cells in both the tumor and peripheral blood compared to healthy individuals [168, 169, 170]. As the name implies, regulatory T cells act by limiting the generation of innate and adaptive anti-tumor immunity. T regs release cytokines such as IL-10 and transforming growth factor beta 1 (TGF-β) that have a suppressive function. T regs have also been linked with disease

progression in PCa as studies show that patients at advanced stages had increased peripheral T regs population than individuals with early-stage disease [169, 170]. The studies also found increased T reg population in the tumor compared to the benign tissue from the same prostate [169]. The consensus seems to be that combinatory treatment modalities are required to amplify and overcome the inhibitory immune state of PCa [103, 169, 170].

Given the lack of clinical efficacy for these early checkpoint molecules, one alternative approach may be to target the co-stimulatory checkpoint markers. This strategy is different from derepressing negative signaling molecules because optimal T cell activation also requires positive co-stimulatory signals. One of these checkpoint molecules is the OX40 or CD137 molecule. This checkpoint molecule is a co-stimulatory marker expressed only on activated $CD4^+$ and $CD8^+$ T cells [87, 88]. Naive T lymphocytes lack expression of OX40 but can be induced after interaction with its cognate ligand [87, 88, 171]. Although not constitutively expressed, APCs can present OX40L to induce the OX40-OX40L pathway [87, 88, 171]. The expression of OX40 on T cells can be increased by using APC-derived cytokines such as interleukin-2 (IL-2) and tumor necrosis factor alpha (TNF-α).

Understanding these checkpoint markers, especially their expression patterns and ability to interact with other immune molecules can provide important insight on the rationale development of better combinatorial immune-based treatments for PCa.

## 5.3 Methods

### 5.3.1 Cell line and culture conditions

The TRAMP-C2 line used in this chapter was acquired from American Type Culture Collection (ATCC). The TRAMP-C2 cells were engineered to express hPSMA upon doxycycline (DOX) induction. Refer to Section 3.3.1 for cell culture method.

### 5.3.2 Treatment with irradiation

hPSMA TRAMP-C2 cells were plated in 10-cm plates 24 hours prior to the irradiation treatment to achieve 70% confluency. The cells were trypsinized and harvested in 10 mL TRAMP-C2 media. Cells were irradiated using a clinical linear accelerator (Truebeam, Varian Medical, Palo Alto) at 0 and 20 Gy doses. Post-radiation the cells were incubated for an additional 24 hours, washed with PBS, and harvested for flow cytometry analysis.

### 5.3.3 Treatment with interferon gamma (IFNγ)

hPSMA TRAMP-C2 cells were plated in 10-cm plate 24 hours pre-IFNγ treatment to reach 70% confluency. The cells were treated with IFNγ at 100 U/mL concentration and incubated for 24 hours. The cells were trypsinized and harvested for flow cytometry analysis.

### 5.3.4 Spleen harvest and splenocyte preparation

Male C57BL/6 wild-type mice were ordered from the Jackson Laboratory (ME, USA). All mice were at least 8 weeks of age for this experiment. Spleens harvested form mice were passed through 40 µm cell strainers to give single cell suspensions. Red blood cells were lysed with ACK lysis buffer and the remaining cells were washed with PBS at 2000 RPM for 10 minutes at 4°C. Next, the washed cells were suspended in complete media (RPMI-1640 media containing fetal bovine serum (FBS; 10%), 4-(2hydroxyethyl)-1-piperazineethanesulfonic acid (HEPES; 1%), sodium pyruvate (1%), penicillin-streptomycin (1%), L-glutamine (1%), and β-mercaptoethanol (0.1%)). Cells were suspended in 6-well plates that were conjugated with anti-CD3 and anti-CD28 antibodies (Abs) for plate-bound T-cell activation. 1 U/mL IL-2 was added to the plates. These cells were maintained at 37°C, 20% $O_2$, and 5% $CO_2$ in a water-jacketed Forma Scientific Incubator. Cells were harvested for flow cytometry analysis 72 hours post-activation. All animal protocols were approved by and conducted in accordance with the UVIC

Animal care Committee (ACC). I have received animal ethics and animal handling training and certification for all procedures.

### 5.3.5 Flow cytometry analysis

Separate cell suspensions were prepared from hPSMA TRAMP-C2 cells and activated splenocytes. For assessment of cell surface markers expression, cells were first stained with a fixable viability dye in order to only analyze live cells. Cells were then stained with fluorochrome-conjugated Abs in PBS containing 3% FBS. Samples were then run on the FACSCalibur (BD Biosciences, CA, USA) and analyzed using FlowJo V10 software (Tree Star Inc, OR, USA). Population gates for each experiment are discussed in the figure legend. Flow cytometry anti-mouse Abs were used for the following markers: CD3 (17A2), CD4 (GK1.5), CD8 (53-6.7), PD-1 (RMP1-30), PD-L1 (MIH5), OX40 (OX-86) (Biolegend Inc, USA).

### 5.3.6 Statistical Analysis

Comparisons of cell populations between treatment and control groups were performed on GraphPad (Graphpad Software Inc., CA, USA) using one-way ANOVA and Sidak's multiple comparisons test. P values correspond to the following representation of statistical significance. NS= p-value> 0.05, * = p-value<0.05, ** = p-value<0.01, *** = p-value<0.001, and **** = p-value<0.0001.

## 5.4 Results

### 5.4.1 TRAMP-C2 treated with IFNγ and irradiation showed increased PD-L1 expression

To observe changes in PD-L1 expression post-irradiation treatment, hPSMA cells were treated with IFNγ and 20 Gy irradiation. These cells were harvested and analyzed for PD-L1 expression using flow cytometry. My positive control for this experiment were the IFNγ-treated

hPSMA TRAMP-C2 cells. As expected, the PD-L1 isotype control showed no PD-L1 expression on hPSMA TRAMP-C2 cells. Treatment with IFNγ yielded PD-L1 expression in 96.8% of the TRAMP-C2 population with the significantly higher mean fluorescence intensity (MFI) of 1510 than 20 Gy irradiated sample (Figure 17A, 17B; $p<0.05$). In contrast, the untreated hPSMA TRAMP-C2 cells showed PD-L1 expression in 42% of the TRAMP-C2 population increasing to 56% post-irradiation treatment at 20 Gy (Figure 17A; $p<0.01$). There was also a significant difference in MFI between untreated and 20 Gy treated hPSMA TRAMP-C2 cells (Figure 17B, $p<0.001$).

### 5.4.2 Increased PD1 and OX40 expression is observed in activated T lymphocytes

To observe expression patterns of PD-1 and OX40 in activated T cells, splenocytes were harvested from spleens of adult C57BL/6 wild-type mice. These splenocytes were then activated with plate bound anti-CD3 and anti-CD28. These splenocytes were analyzed for PD-1 and OX40 expression before and after T cell activation (Figure 18, 19). The inactivated T cells from day 0 served as my negative control while activated T cells were my positive control. Isotype controls were used to draw population gates.

While analyzing PD-1 expression in activated T cells we observed that on day 0 there was no detectable PD-1 expression (Figure 18). This PD-1 expression increases significantly in both $CD4^+$ (~40%) and $CD8^+$ (~30%) T cell population ($p<0.001$, $p<0.001$). By day 2, PD-1 expression can be observed in ~70% of $CD4^+$ and $CD8^+$ T cells (Figure 18, $p<0.001$). This expression decreases significantly in both lymphocyte populations by day 3 ($p<0.001$). Although, PD-1 expression is significantly higher in $CD8^+$ T cells versus $CD4^+$ T cells on day 3 (Figure 18, $p<0.001$).

A similar result was observed when analyzing the OX40 expression pattern. We observed that less than ~10% of splenocytes had any OX40 expression on day 0 (Figure 19). The level of OX40 gradually increases starting on day 1, where about ~35% of $CD4^+$ T cells and ~25% of $CD8^+$ T cells show OX40 expression (Figure 19). On day 2, the OX40 expression increases significantly ($p<0.001$) and lowering significantly by day 3 ($p<0.001$). On day 2, 48% of all activated T cells express OX40 with almost 84% of $CD4^+$ and 82% of $CD8^+$ T cells expressing OX40 (Figure 19). This expression lowers significantly by day 3 with <20% of $CD4^+$ T cells and ~40% $CD8^+$ T cells expressing OX40 (Figure 19, $p<0.001$).

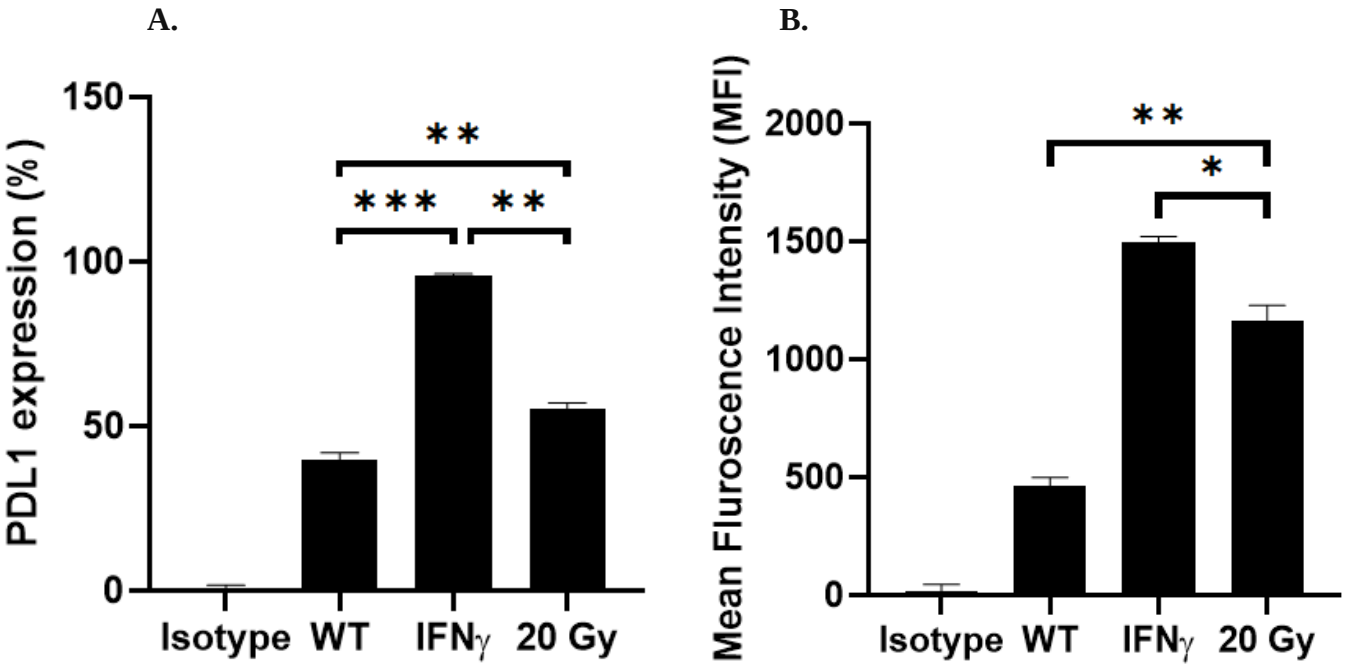


**Figure 17. Flow cytometry analysis was performed to assess PD-L1 expression post-irradiation treatment in hPSMA**. TRAMP-C2 cells. Cells were harvested 24 hours post-irradiation treatment and gated on viable cells. These cells were then analyzed for (A) PD-L1 ratio and (B) MFI in different conditions. (20 Gy: irradiated sample; WT: Untreated TRAMP-C2; IFNγ: experimental control; Isotype: PD-L1 isotype control, N=3, Error bar: SD)

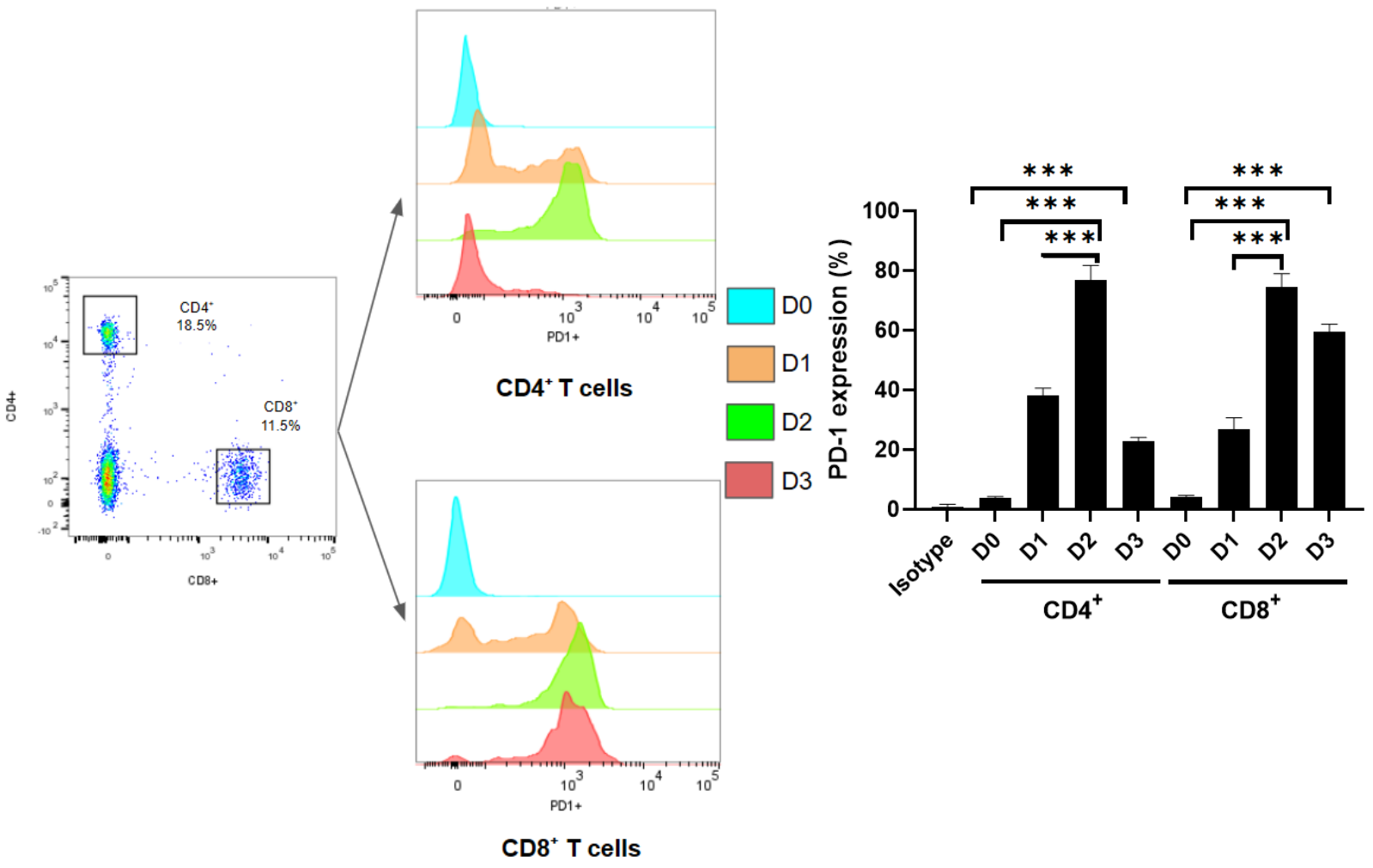


**Figure 18. Flow cytometry analysis was performed to assess PD-1 expression post-irradiation treatment in activated splenocytes.** Splenocytes were harvested and activated with anti CD3/CD28 plate bound activation. The samples were gated on viable singlets in the ly lymphocyte population. CD4+ T cells and CD8+ T cells (upper left panel) were then gated and assessed for surface expression of PD-1. (D0: day 0, D1: day 1, D2: day 2, D3: day 3, Isotype: PD-1 isotype control). N=3, Error bar= SD.

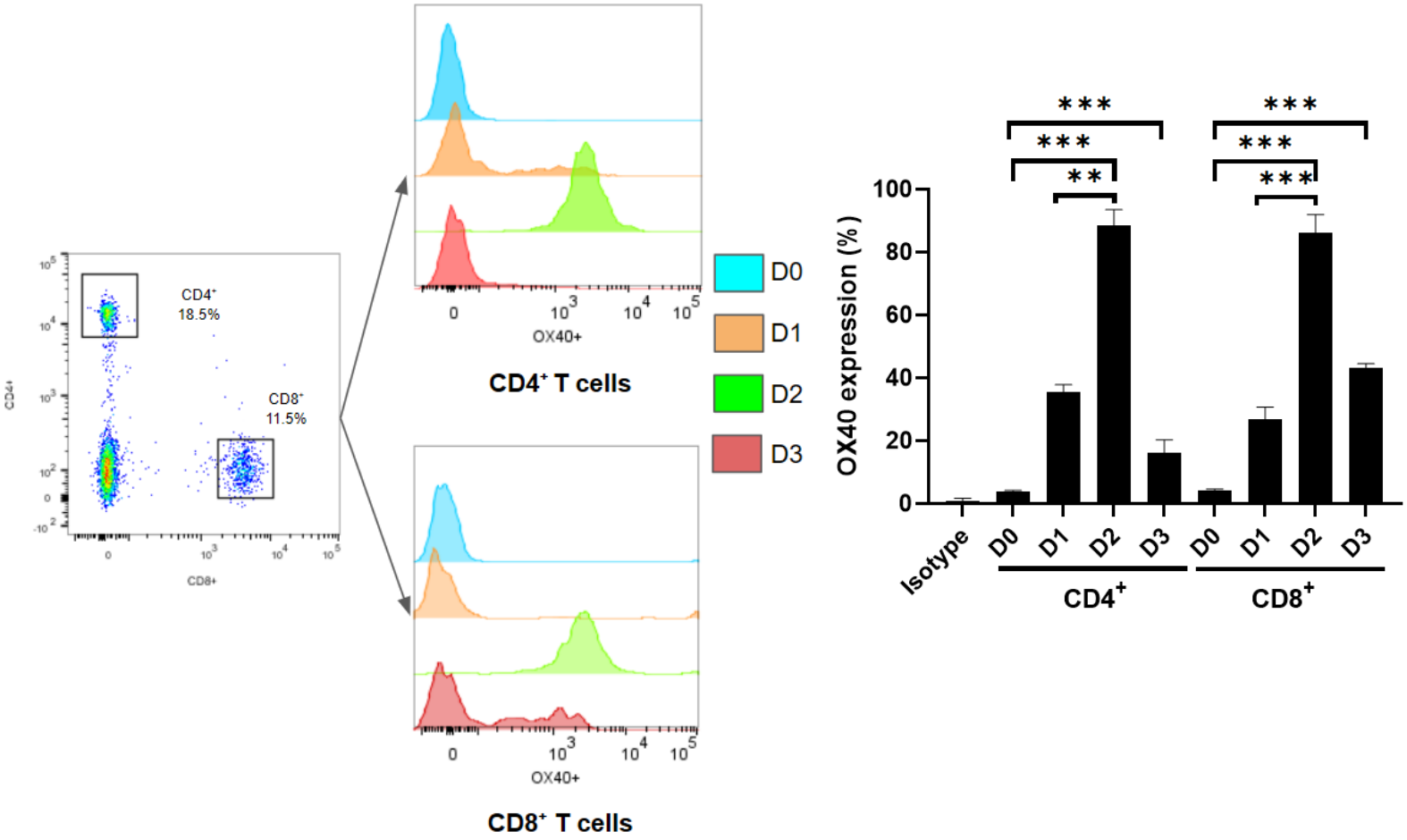


**Figure 19. Flow cytometry analysis was performed to assess OX40 expression post-irradiation treatment in activated splenocytes.** Splenocytes were harvested and activated with anti CD3/CD28 plate bound activation. Samples were collected starting day 0 and gated on viable singlets in the lymphocyte populations. CD4+ T cells and CD8+ T cells (upper left panel) were then gated form the viable lymphocytes and assessed for OX40 expression. (D0: day 0, D1: day 1, D2: day 2, D3: day 3, Isotype: OX-40 isotype control) N=3, Error bar= SD.

## 5.5 Discussion

Our aim with this experiment was to understand the expression patterns of PD-1 and OX40 on activated T lymphocytes and PD-L1 expression on irradiated hPSMA TRAMP-C2 cells. We harvested these cells after their specific treatments and analyzed them for different expression patterns through flow cytometry analysis.

The first step to assess PD-L1 expression in TRAMP-C2 cells was to generate a control that would yield high PD-L1 expression. Studies have shown that addition of IFNγ leads to increased PDL1 expression in murine cell lines such as MC-38 (colon adenocarcinoma) [164, 165]. I performed a dosage response experiment (data not shown) to determine the optimal IFNγ concentration that would result in high PD-L1 expression 24 hours post-treatment. Once this concentration was identified, I utilized 100 U/mL IFNγ as my positive control for this experiment. I wanted to evaluate if a radiation treatment would change the expression pattern of PD-L1 in TRAMP-C2 cells. To observe these changes, I analyzed TRAMP-C2 cells that were treated with irradiation using a linear accelerator (LINAC). The LINAC utilizes photon energy of 6 megavoltage (MV) to irradiate the cells. Although this emission is different from $^{177}$Lu-PSMA617, the focus of this thesis, this experiment acted as a preliminary step to understand if radiation could induce change in PD-L1 expression. In Chapter 3, I had tested different irradiation dosages to assess cell death in hPSMA TRAMP-C2 which helped me decide 20 Gy as my treatment dose for this experiment. We found an interesting expression pattern for PD-L1 in TRAMP-C2 post-treatment with 20 Gy irradiation. We found that there was a basal PD-L1 expression (~42%) in untreated hPSMA TRAMP-C2 cells, this expression increased significantly in hPSMA TRAMP-C2 cells treated with 20 Gy irradiation (~56%) (Figure 17, $p<0.001$). There have been studies done that show that irradiation increases PD-L1 expression [172, 173]. We found it fascinating was how quickly irradiation increased the expression [172,

173]. It would be vital to perform this experiment using $^{177}$Lu-PSMA617 as it would aid in understanding if a similar response can be observed. A rapid increase in PD-L1 expression could also point to a more immunosuppressive tumor microenvironment [152, 172, 173].

The next part of this experiment included analyzing the expression patterns of PD-1 and OX40 pre- and post- T cell activation. To evaluate these responses, I harvested splenocytes from the spleen of C57BL/6 wildtype mice. A small population of splenocytes were stained with Abs and fixed until the activated T lymphocytes were ready to be analyzed. The rest of the splenocytes were activated with CD3/CD28 plate-bound activation. For this experiment, the isotype control for the PD-L1 antibody was used to draw the population gate for positive expression. I found that PD-1 expression increased by day 1, reaching peak expression by day 2 and decreasing significantly by day 3 post-activation (Figure 18; $p<0.001$). A similar expression pattern was observed while examining OX40 expression. One interesting observation was noticed in PD-1 expression on day 3 post-activation (Figure 18). Even though both subsets reached peak expression day 2 post-activation, $CD4^+$ T cell subset showed a much sharper decrease in PD-1 expression than $CD8^+$ T cells (Figure 18). Previous studies have shown that PD-1 is not expressed on resting T cells but is expressed within 24 h after stimulation [85, 174]. One study showed a similar pattern where almost no PD-1 expression was observed on resting $CD3^+$ T cells. This PD-1 expression peaked at 48 h post-stimulation, followed by reduction in the following days [85]. This study did not examine specific $CD4^+$ or $CD8^+$ subsets but overall showed a much gradual reduction in PD-1 expression levels.

Another interesting observation was noted to be the kinetics involved with the expression of these checkpoint markers. According to these experiments, day 2 post-activation seems to be an important timepoint for expression of these checkpoint markers. Understanding the kinetics of

these checkpoint markers will play an important role in determining the administration of checkpoint inhibitors or agonists relative to $^{177}$Lu-PSMA617. However, it would be imperative to validate the kinetics of checkpoint molecule expression on tumors treated with$^{177}$Lu-PSMA617 *in vivo*.

Immunotherapies in PCa has been a holy grail since the advent of successful clinical responses with checkpoint inhibitors in other cancer settings. Currently there are two cancer vaccines targeting prostate tumor-associated antigens that have shown an overall benefit in patients with mCRPC [175, 176]. In one study, Sipuleucel-T showed no effect in progression-free survival but did show a median increase of 3.1 months in overall survival [175, 176]. The second study, PROSTVAC-VF, showed an increase in the median overall survival of 8.5 months and another study showed a 45% reduction in mortality [177]. Although these immunotherapies do seem to show an increase in overall survival, there is almost no effect on PSA levels or tumor volumes [175, 176, 177]. As explained in section 5.2, checkpoint inhibitors have had a mixed success in PCa. Clinical trials performed with anti-PD-1 and anti-CTLA-4 as monotherapies have shown minimal responses [178]. Compared to this, one study found that external beam radiation therapy (EBRT) for PCa resulted in a progression-free survival with a median of 24 months [179]. Another study found a 30-month progression-free survival rate of 42.6% after EBRT [180]. Although these studies put RT in a positive light, combinatorial modalities may be required for a better patient-outcome.

As explained earlier in section 5.2, the OX40-OX40L interaction acts as a co-stimulatory activation signal for T cells [87, 88]. Inducing this specific pathway may suggest a more effective treatment option than a checkpoint inhibitor. New developments targeting this interaction include anti-OX40 agonists which could be tested in the metastatic PCa setting. One

such clinical trial applied a combinatory approach with anti-OX40, radiation and cyclophosphamide. This study found transient decrease in PSA levels in 4/9 patients [86]. It also showed an increase in non-T reg $CD4^+$ T cells and $CD8^+$ T cells in peripheral blood [86]. This study also showed that combinatory approach with radiation and anti-OX40 treatment had a manageable safety and tolerability profile [86]. These results support further examination of a combinatorial approach using $^{177}$Lu-PSMA617 and an anti-OX40 agonist. Therefore, future studies could be readily conducted using the hPSMA TRAMP-C2 cell line I developed in chapter 2, to evaluate the effectiveness of $^{177}$Lu-PSMA617 combination with OX40 agonists.

In conclusion, understanding the patterns and levels of checkpoint molecule expression, of both the negative and positive regulatory molecules, is an important step towards *in vivo* studies.

# Chapter 6: Summary and Future Directions

## 6.1 Chapter Summaries

The objective of this thesis was to understand the mechanism of cell death and kinetics involved with $^{177}$Lu-PSMA617 radioligand therapy. In particular, I aimed to understand this by generating a mouse model that would allow me to investigate my objective. Understanding the mechanism behind $^{177}$Lu-PSMA617 induced cell death could help us improve the current treatment options available for patients with mCRPC.

In Chapter 2, I generated a DOX-inducible hPSMA TRAMP-C2 cell line that could be utilized to study hPSMA-targeted therapies such as $^{177}$Lu-PSMA617 radioligand therapy. To develop this cell line, we integrated the Lenti-X inducible system that consists of lentiviral components which allows for a controlled expression of hPSMA through DOX-induction. Using this system, we developed four hPSMA TRAMP-C2 clones that expressed hPSMA at various levels. Based on their expression, clones 14 and 19 were considered "medium" expressing clones while clones 1 and 16 were categorized as "high" expressing clones. I found that these clones only expressed hPSMA extracellularly after induction with DOX. We found low-level intracellular expression of hPSMA without DOX, but this was potentially attributed to the tetracyclines present in the culture medium. These clones were then tested for their binding response to a hPSMA-targeting ligand known as $^{18}$F-DCFPyL. We found that in DOX-induced cells, $^{18}$F-DCFPyL was able to bind to surface hPSMA. Once we verified this binding response *in vitro*, we wanted to investigate this response *in vivo*. We performed this by using male immunodeficient mice to investigate the uptake of $^{18}$F-DCFPyL in the tumor. We found that there was a significant difference in uptake between uninduced and DOX-induced mice. We saw no tumor-uptake of $^{18}$F-DCFPyL in mice not treated with DOX. These experiments showed that

no hPSMA was being expressed without DOX-induction. This chapter concluded with development of a hPSMA-TRAMP C2 cell line, verification of expression after DOX-induction and binding response to $^{18}$F-DCFPyL ligand, *in vitro* and *in vivo*.

One of the primary questions that remains from Chapter 2 is "how does this system translate in an immunocompetent mouse model?". The future directions for this chapter include understanding the immune component and how it responds to hPSMA TRAMP-C2 tumors. The group of researchers who first developed a mouse model to study $^{177}$Lu-PSMA617, Fendler, *et al.*, postulated that tumor rejection was only observed in cells expressing high levels of hPSMA [16]. They found no tumor rejections in cells with heterogenous PSMA expression [16]. This experiment provides support that hPSMA TRAMP-C2 cells can be used in an immunocompetent mouse model.

In Chapter 3, I investigated one of the possible mechanisms of cell death induced by $^{177}$Lu-PSMA617 rLT. The cells were treated with $^{177}$Lu-PSMA617 by our collaborators in Vancouver, BC. The collected lysates were then examined for apoptosis. These lysates were tested for caspase-3 cleavage [66]. We found evidence of caspase-3 cleavage starting one-day after treatment with $^{177}$Lu-PSMA617. This response was maintained until the last day of collection. This was an interesting observation as the association between $^{177}$Lu-PSMA617 and apoptosis has not been shown before in TRAMP-C2 cells. One of the key questions that remains from this chapter is "what other cell death mechanisms are involved with $^{177}$Lu-PSMA617 rLT?". I speculate that $^{177}$Lu-PSMA617 induces apoptosis through DNA damage and/or ER stress response. Further experiments should be performed to understand the degree of DNA damage and to understand other mechanisms that might be involved with $^{177}$Lu-PSMA617-induced cell death.

In Chapter 4, I examined if $^{177}$Lu-PSMA617 is capable of inducing an immunogenic cell death (ICD). As explained before, release of DAMPs such as calreticulin and HMGB1 are hallmarks of an immunogenic cell death [54, 55, 56,]. To investigate this, I initially treated hPSMA TRAMP-C2 cells with cyclophosphamide (CTX), a known ICD-inducer. The supernatants from the cells treated with CTX were examined for HMGB1 release. Once I verified the HMGB1 release with CTX, I performed a similar experiment using supernatants from hPSMA TRAMP-C2 cells treated with $^{177}$Lu-PSMA617. I found a steady increase in HMGB1 levels starting day 2 and increasing on day 4. This HMGB1 release showed evidence that $^{177}$Lu-PSMA617 can induce ICD in hPSMA TRAMP-C2 cells. I also generated DAMP-fluorescent reporter cell lines where HMGB1 and calreticulin (CRT) were expressed in tandem with fluorescent proteins such as GFP and mCherry, respectively. These HMGB1-GFP and CRT-mCherry cell lines can be utilized to visualize the translocation and release of these molecules from the cell. This can help understand the kinetics involved with the release and when the activation of the immune system occurs in response to this cell death. Understanding this can help us develop combinatory treatments utilizing immune-modulatory agents for patients with mCRPC as well as other cancer modalities.

In Chapter 5, I examined the expression patterns of checkpoint markers such as PD-L1, PD-1 and OX-40. These checkpoint markers play an important role in T cell stimulation and inhibition thus it is integral to understand their expression patterns [78, 79]. The most surprising result was the significant increase in PD-L1 expression just 24-hours after irradiation treatment. The expression pattern of PD-1 and OX-40 were similar; we saw an increase in expression on day 2 and sharp decrease by day 3 in both T cell subsets. It would be interesting to see if ICD can

change the expression pattern of these markers. We can utilize this knowledge to properly schedule the administration of checkpoint inhibitors/agonists.

## 6.2 Future Directions

The results of this thesis help us understand the mechanism of cell death and kinetics involved with $^{177}$Lu-PSMA617. Although $^{177}$Lu-PSMA617 has already been heavily investigated in clinical settings in Europe, the mechanistic knowledge is still lacking [96, 97]. Also, there are very limited pre-clinical mouse models that have been developed to study the effect of $^{177}$Lu-PSMA617 in PCa [16]. My thesis focused on bridging this gap in knowledge and developing the tools for an immunocompetent mouse model to study $^{177}$Lu-PSMA617 rLT and other hPSMA-targeted therapies.

The set of experiments performed in this thesis show support towards the development of a promising PCa mouse model. The study performed by Fender *et al* evaluated a mouse model to investigate the uptake of $^{177}$Lu-PSMA617 and evaluate the efficacy of the compound [16]. One limitation of this experiment is that PSMA was constitutively expressed on their particular cell lines. With my proposed system, the DOX-controlled expression of hPSMA provides a more complete immune competent model to study $^{177}$Lu-PSMA617 and other hPSMA-targeted therapies.

The first future experiment should ask the question “Does the combinatory approach with $^{177}$Lu-PSMA617 and checkpoint agonist have a better therapeutic efficacy then each treatment alone?”. Currently, we are interested in understanding the impact of utilizing a checkpoint agonist (anti-OX-40) in a pre-clinical PCa mouse model. The reason is checkpoint inhibitors such as anti-PD-L1 and anti-PD-1 have had limited success in regard to PCa. [89, 144, 164]. Studies with anti-OX-40 as part of the combinatory treatment with radiation in PCa have shown

promising results [86]. This warrants for a pre-clinical study evaluating the survival and anti-tumor response of a combinatory treatment with anti-OX-40 and $^{177}$Lu-PSMA617. Evaluating the responses of the combinatory treatment versus singular treatments alone can help us understand how these treatments will translate in the clinical settings.

In conclusion, the findings presented in this thesis have provided further knowledge in understanding $^{177}$Lu-PSMA617 rLT and developing the tools for pre-clinical PCa mouse model to evaluate hPSMA-targeted therapies. It is my hope that we can develop $^{177}$Lu-PSMA617 rLT in combination with other treatments using results outlined in this thesis, along with additional results from current and future research, to improve the survival of mCRPC patients.

# References


1. Attard, G., Richards, J., & de Bono, J. S. (2011). New strategies in metastatic prostate cancer: Targeting the androgen receptor signaling pathway. *Clinical Cancer Research: An Official Journal of the American Association for Cancer Research*, *17*(7), 1649–1657. https://doi.org/10.1158/1078-0432.CCR-10-0567
2. Drake, C. G., Sharma, P., & Gerritsen, W. (2014). Metastatic castration-resistant prostate cancer: New therapies, novel combination strategies and implications for immunotherapy. *Oncogene*, *33*(43), 5053–5064. https://doi.org/10.1038/onc.2013.497
3. *177Lu-PSMA-617 and Pembrolizumab in Treating Patients with Metastatic Castration-Resistant Prostate Cancer* (2016, June 23). https://www.cancer.gov/about-cancer/treatment/clinical-trials/search/v?id=NCI-2018-02993
4. Hofman, M. S., Emmett, L., Violet, J., Y Zhang, A., Lawrence, N. J., Stockler, M., Francis, R. J., Iravani, A., Williams, S., Azad, A., Martin, A., McJannett, M., ANZUP TheraP team, & Davis, I. D. (2019). TheraP: A randomized phase 2 trial of 177 Lu-PSMA-617 theranostic treatment vs cabazitaxel in progressive metastatic castration-resistant prostate cancer (Clinical Trial Protocol ANZUP 1603). *BJU International*, *124 Suppl 1*, 5–13. https://doi.org/10.1111/bju.14876
5. Hofman, M., Violet, J. A., Hicks, R. J., Ferdinandus, J., Thang, S. P., Iravani, A., Kong, G., Ravi Kumar, A., Akhurst, T. J., Mooi, J., Guo, C., Tran, B., Jackson, P., Scalzo, M., Eu, P., Williams, S., & Sandhu, S. K. (2019). Results of a 50-patient single-center phase II prospective trial of Lutetium-177 PSMA-617 theranostics in metastatic castrate-resistant prostate cancer. *Journal of Clinical Oncology*, *37*(7_suppl), 228–228. https://doi.org/10.1200/JCO.2019.37.7_suppl.228
6. Johnson, L. D., Nesslinger, N. J., Blood, P. A., Chima, N., Richier, L. R., Ludgate, C., Pai, H. H., Lim, J. T., Nelson, B. H., Vlachaki, M. T., & Lum, J. J. (2014). Tumor-associated autoantibodies

correlate with poor outcome in prostate cancer patients treated with androgen deprivation and external beam radiation therapy. *Oncoimmunology*, *3*. https://doi.org/10.4161/onci.29243

7. Jin, J.-K., Dayyani, F., & Gallick, G. E. (2011). Steps in prostate cancer progression that lead to bone metastasis. *International Journal of Cancer*, *128*(11), 2545–2561. https://doi.org/10.1002/ijc.26024
8. National Collaborating Centre for Cancer (UK). (2014). *Prostate Cancer: Diagnosis and Treatment*. National Collaborating Centre for Cancer (UK). http://www.ncbi.nlm.nih.gov/books/NBK247469/
9. Pinthus, J. H., Pacik, D., & Ramon, J. (2007). Diagnosis of prostate cancer. *Recent Results in Cancer Research. Fortschritte Der Krebsforschung. Progres Dans Les Recherches Sur Le Cancer*, *175*, 83–99. https://doi.org/10.1007/978-3-540-40901-4_6
10. Albertsen, P. C., Hanley, J. A., & Fine, J. (2005). 20-Year Outcomes Following Conservative Management of Clinically Localized Prostate Cancer. *JAMA*, *293*(17), 2095–2101. https://doi.org/10.1001/jama.293.17.2095
11. Siddiqui, M. M., Rais-Bahrami, S., Turkbey, B., George, A. K., Rothwax, J., Shakir, N., Okoro, C., Raskolnikov, D., Parnes, H. L., Linehan, W. M., Merino, M. J., Simon, R. M., Choyke, P. L., Wood, B. J., & Pinto, P. A. (2015). Comparison of MR/Ultrasound Fusion–Guided Biopsy With Ultrasound-Guided Biopsy for the Diagnosis of Prostate Cancer. *JAMA*, *313*(4), 390–397. https://doi.org/10.1001/jama.2014.17942
12. Litwin, M. S., & Tan, H.-J. (2017). The Diagnosis and Treatment of Prostate Cancer: A Review. *JAMA*, *317*(24), 2532–2542. https://doi.org/10.1001/jama.2017.7248
13. *Europe PMC*. (n.d.). Retrieved September 16, 2020, from https://europepmc.org/article/med/24531787

14. Bednarova, S., Lindenberg, M. L., Vinsensia, M., Zuiani, C., Choyke, P. L., & Turkbey, B. (2017). Positron emission tomography (PET) in primary prostate cancer staging and risk assessment. *Translational Andrology and Urology*

15. Sanli, Y., Sanli, O., Has Simsek, D., & Subramaniam, R. M. (2018). 68Ga-PSMA PET/CT and PET/MRI in high-risk prostate cancer patients. *Nuclear Medicine Communications*, *39*(10), 871–880. https://doi.org/10.1097/MNM.0000000000000888

16. Fendler, W. P., Stuparu, A. D., Evans-Axelsson, S., Lückerath, K., Wei, L., Kim, W., Poddar, S., Said, J., Radu, C. G., Eiber, M., Czernin, J., Slavik, R., & Herrmann, K. (2017). Establishing 177Lu-PSMA-617 Radioligand Therapy in a Syngeneic Model of Murine Prostate Cancer. *Journal of Nuclear Medicine*, *58*(11), 1786–1792. https://doi.org/10.2967/jnumed.117.193359

17. Current, K., Meyer, C., Magyar, C. E., Mona, C. E., Almajano, J., Slavik, R., Stuparu, A. D., Cheng, C., Dawson, D. W., Radu, C. G., Czernin, J., & Lueckerath, K. (2020). Investigating PSMA-Targeted Radioligand Therapy Efficacy as a Function of Cellular PSMA Levels and Intratumoral PSMA Heterogeneity. *Clinical Cancer Research*. https://doi.org/10.1158/1078-0432.CCR-19-1485

18. Barrio, M., Fendler, W. P., Czernin, J., & Herrmann, K. (2016). Prostate specific membrane antigen (PSMA) ligands for diagnosis and therapy of prostate cancer. *Expert Review of Molecular Diagnostics*, *16*(11), 1177–1188. https://doi.org/10.1080/14737159.2016.1243057

19. Chang, S. S. (2004). Overview of Prostate-Specific Membrane Antigen. *Reviews in Urology*, *6*(Suppl 10), S13–S18.

20. van der Toom, E. E., Axelrod, H. D., de la Rosette, J. J., de Reijke, T. M., Pienta, K. J., & Valkenburg, K. C. (2019). Prostate-specific markers to identify rare prostate cancer cells in liquid biopsies. *Nature Reviews. Urology*, *16*(1), 7–22. https://doi.org/10.1038/s41585-018-0119-5

21. Sumanasuriya, S., & De Bono, J. (2018). Treatment of Advanced Prostate Cancer-A Review of Current Therapies and Future Promise. *Cold Spring Harbor Perspectives in Medicine*, *8*(6). https://doi.org/10.1101/cshperspect.a030635

22. Komisarenko M, Martin LJ, Finelli A. (2018). *Active surveillance review: Contemporary selection criteria, follow-up, compliance and outcomes—Komisarenko—Translational Andrology and Urology*. Retrieved September 16, 2020, from http://tau.amegroups.com/article/view/18626/19083

23. Barocas, D. A., Alvarez, J., Resnick, M. J., Koyama, T., Hoffman, K. E., Tyson, M. D., Conwill, R., McCollum, D., Cooperberg, M. R., Goodman, M., Greenfield, S., Hamilton, A. S., Hashibe, M., Kaplan, S. H., Paddock, L. E., Stroup, A. M., Wu, X. C., & Penson, D. F. (2017). Association Between Radiation Therapy, Surgery, or Observation for Localized Prostate Cancer and Patient-Reported Outcomes After 3 Years. *JAMA*, *317*(11), 1126–1140. https://doi.org/10.1001/jama.2017.1704

24. Tourinho-Barbosa, R., Srougi, V., Nunes-Silva, I., Baghdadi, M., Rembeyo, G., Eiffel, S. S., Barret, E., Rozet, F., Galiano, M., Cathelineau, X., & Sanchez-Salas, R. (2018). Biochemical recurrence after radical prostatectomy: What does it mean? *International Braz J Urol: Official Journal of the Brazilian Society of Urology*, *44*(1), 14–21. https://doi.org/10.1590/S1677-5538.IBJU.2016.0656

25. Bill-Axelson, A., Holmberg, L., Filén, F., Ruutu, M., Garmo, H., Busch, C., Nordling, S., Häggman, M., Andersson, S.-O., Bratell, S., Spångberg, A., Palmgren, J., Adami, H.-O., Johansson, J.-E., & Scandinavian Prostate Cancer Group Study Number 4. (2008). Radical prostatectomy versus watchful waiting in localized prostate cancer: The Scandinavian prostate

cancer group-4 randomized trial. *Journal of the National Cancer Institute*, *100*(16), 1144–1154. https://doi.org/10.1093/jnci/djn255

26. Demaria, S., Golden, E. B., & Formenti, S. C. (2015). Role of Local Radiation Therapy in Cancer Immunotherapy. *JAMA Oncology*, *1*(9), 1325–1332. https://doi.org/10.1001/jamaoncol.2015.2756
27. Hindson, B., Turner, S., & Do, V. (2007). Palliative radiation therapy for localized prostate symptoms in hormone refractory prostate cancer. Australasian Radiology, 51(6), 584–588. https://doi.org/10.1111/j.1440-1673.2007.01897.
28. O'Neill, A. G. M., Jain, S., Hounsell, A. R., & O'Sullivan, J. M. (n.d.). Fiducial marker guided prostate radiotherapy: A review. *The British Journal of Radiology*, *89*(1068). https://doi.org/10.1259/bjr.20160296
29. Bottke, D., & Wiegel, T. (2010). Radiotherapy and Prostate Cancer: Quo Vadis? *European Urology Supplements*, *9*(3), 394–400. https://doi.org/10.1016/j.eursup.2010.02.013
30. Zelefsky, M. J., Pei, X., Chou, J. F., Schechter, M., Kollmeier, M., Cox, B., Yamada, Y., Fidaleo, A., Sperling, D., Happersett, L., & Zhang, Z. (2011). Dose escalation for prostate cancer radiotherapy: Predictors of long-term biochemical tumor control and distant metastases-free survival outcomes. *European Urology*, *60*(6), 1133–1139. https://doi.org/10.1016/j.eururo.2011.08.029
31. Skowronek, J. (2017). Current status of brachytherapy in cancer treatment – short overview. *Journal of Contemporary Brachytherapy*, *9*(6), 581–589. https://doi.org/10.5114/jcb.2017.72607
32. Yoshioka, Y., Suzuki, O., Otani, Y., Yoshida, K., Nose, T., & Ogawa, K. (2014). High-dose-rate brachytherapy as monotherapy for prostate cancer: Technique, rationale and perspective. *Journal of Contemporary Brachytherapy*, *6*(1), 91–98. https://doi.org/10.5114/jcb.2014.42026

33. Skowronek, J. (2013). Low-dose-rate or high-dose-rate brachytherapy in treatment of prostate cancer – between options. *Journal of Contemporary Brachytherapy*, *5*(1), 33–41. https://doi.org/10.5114/jcb.2013.34342

34. *Getting Oral or Systemic Radiation Therapy*. (n.d.). Retrieved September 16, 2020, from https://www.cancer.org/treatment/treatments-and-side-effects/treatment-types/radiation/systemic-radiation-therapy.html

35. Larson, S. M., Carrasquillo, J. A., Cheung, N.-K. V., & Press, O. W. (2015). Radioimmunotherapy of human tumours. *Nature Reviews. Cancer*, *15*(6), 347–360. https://doi.org/10.1038/nrc3925

36. Deshayes, E., Roumiguié, M., Thibault, C., Beuzeboc, P., Cachin, F., Hennequin, C., Huglo, D., Rozet, François & Kassab-Chahmi, Diana & Rebillard, Xavier & Nadine, Houede. (2017). Radium 223 dichloride for prostate cancer treatment. Drug Design, Development and Therapy. Volume 11. 2643-2651. 10.2147/DDDT.S122417.

37. Marques, P., Skorupskaite, K., George, J. T., & Anderson, R. A. (2000). Physiology of GNRH and Gonadotropin Secretion. In K. R. Feingold, B. Anawalt, A. Boyce, G. Chrousos, W. W. de Herder, K. Dungan, A. Grossman, J. M. Hershman, H. J. Hofland, G. Kaltsas, C. Koch, P. Kopp, M. Korbonits, R. McLachlan, J. E. Morley, M. New, J. Purnell, F. Singer, C. A. Stratakis, … D. P. Wilson (Eds.), *Endotext*. MDText.com, Inc. http://www.ncbi.nlm.nih.gov/books/NBK279070/

38. Crawford, E. D., Heidenreich, A., Lawrentschuk, N., Tombal, B., Pompeo, A. C. L., Mendoza-Valdes, A., Miller, K., Debruyne, F. M. J., & Klotz, L. (2019). Androgen-targeted therapy in men with prostate cancer: Evolving practice and future considerations. *Prostate Cancer and Prostatic Diseases*, *22*(1), 24–38. https://doi.org/10.1038/s41391-018-0079-0

39. Cattrini, C., Castro, E., Lozano, R., Zanardi, E., Rubagotti, A., Boccardo, F., & Olmos, D. (2019). Current Treatment Options for Metastatic Hormone-Sensitive Prostate Cancer. *Cancers*, *11*(9). https://doi.org/10.3390/cancers11091355

40. Antonarakis, E. S., Lu, C., Luber, B., Wang, H., Chen, Y., Zhu, Y., Silberstein, J. L., Taylor, M. N., Maughan, B. L., Denmeade, S. R., Pienta, K. J., Paller, C. J., Carducci, M. A., Eisenberger, M. A., & Luo, J. (2017). Clinical Significance of Androgen Receptor Splice Variant-7 mRNA Detection in Circulating Tumor Cells of Men With Metastatic Castration-Resistant Prostate Cancer Treated With First- and Second-Line Abiraterone and Enzalutamide. *Journal of Clinical Oncology*, *35*(19), 2149–2156. https://doi.org/10.1200/JCO.2016.70.1961

41. Small, E. J., Saad, F., Chowdhury, S., Oudard, S., Hadaschik, B. A., Graff, J. N., Olmos, D., Mainwaring, P. N., Lee, J. Y., Uemura, H., De Porre, P., Smith, A. A., Zhang, K., Lopez-Gitlitz, A., & Smith, M. R. (2019). Apalutamide and overall survival in non-metastatic castration-resistant prostate cancer. *Annals of Oncology*, *30*(11), 1813–1820. https://doi.org/10.1093/annonc/mdz397

42. Yeong C-H, Cheng M, Ng K-H. (2014) *Therapeutic radionuclides in nuclear medicine: Current and future prospects*. (n.d.). Retrieved September 16, 2020, from https://www.ncbi.nlm.nih.gov/pmc/articles/PMC4201313/

43. Ersahin, D., Doddamane, I., & Cheng, D. (2011). Targeted radionuclide therapy. *Cancers*, *3*(4), 3838–3855. https://doi.org/10.3390/cancers3043838

44. Friedberg, J. W., & Fisher, R. I. (2004). Iodine-131 tositumomab (Bexxar): Radioimmunoconjugate therapy for indolent and transformed B-cell non-Hodgkin's lymphoma. *Expert Review of Anticancer Therapy*, *4*(1), 18–26. https://doi.org/10.1586/14737140.4.1.18

45. Czerwińska, M., Bilewicz, A., Kruszewski, M., Wegierek-Ciuk, A., & Lankoff, A. (2020). Targeted Radionuclide Therapy of Prostate Cancer-From Basic Research to Clinical Perspectives. *Molecules (Basel, Switzerland)*, *25*(7). https://doi.org/10.3390/molecules25071743

46. Mettler F.A., Guiberteau M.J (2018) *Essentials of Nuclear Medicine and Molecular Imaging—7th Edition*. (n.d.). Retrieved September 16, 2020, from https://www.elsevier.com/books/essentials-of-nuclear-medicine-and-molecular-imaging/mettler/978-0-323-48319-3

47. Rahbar, K., Afshar-Oromieh, A., Jadvar, H., & Ahmadzadehfar, H. (2018). PSMA Theranostics: Current Status and Future Directions. *Molecular Imaging*, *17*, 1536012118776068. https://doi.org/10.1177/1536012118776068

48. Rahbar, K., Ahmadzadehfar, H., Kratochwil, C., Haberkorn, U., Schäfers, M., Essler, M., Baum, R. P., Kulkarni, H. R., Schmidt, M., Drzezga, A., Bartenstein, P., Pfestroff, A., Luster, M., Lützen, U., Marx, M., Prasad, V., Brenner, W., Heinzel, A., Mottaghy, F. M., … Krause, B. J. (2017). German Multicenter Study Investigating 177Lu-PSMA-617 Radioligand Therapy in Advanced Prostate Cancer Patients. *Journal of Nuclear Medicine: Official Publication, Society of Nuclear Medicine*, *58*(1), 85–90. https://doi.org/10.2967/jnumed.116.183194

49. Ahmadzadehfar, H., Eppard, E., Kürpig, S., Fimmers, R., Yordanova, A., Schlenkhoff, C. D., Gärtner, F., Rogenhofer, S., & Essler, M. (2016). Therapeutic response and side effects of repeated radioligand therapy with 177Lu-PSMA-DKFZ-617 of castrate-resistant metastatic prostate cancer. *Oncotarget*, *7*(11), 12477–12488. https://doi.org/10.18632/oncotarget.7245

50. Ahmadzadehfar, H., Essler, M., Schäfers, M., & Rahbar, K. (2016). Radioligand therapy with 177Lu-PSMA-617 of metastatic prostate cancer has already been arrived in clinical use. *Nuclear Medicine and Biology*, *43*(12), 835. https://doi.org/10.1016/j.nucmedbio.2016.08.003

51. Emmett, L., Willowson, K., Violet, J., Shin, J., Blanksby, A., & Lee, J. (2017). Lutetium $^{177}$ PSMA radionuclide therapy for men with prostate cancer: a review of the current literature and discussion of practical aspects of therapy. *Journal of medical radiation sciences*, *64*(1), 52–60. https://doi.org/10.1002/jmrs.227

52. Violet, J., Sandhu, S., Iravani, A., Ferdinandus, J., Thang, S. P., Kong, G., Kumar, A. R., Akhurst, T., Pattison, D. A., Beaulieu, A., Mooi, J., Guo, C., Kalff, V., Murphy, D. G., Jackson, P., Eu, P., Scalzo, M., Williams, S., Hicks, R. J., & Hofman, M. S. (2019). Long term follow-up and outcomes of re-treatment in an expanded 50 patient single-center phase II prospective trial of Lutetium-177 (177Lu) PSMA-617 theranostics in metastatic castrate-resistant prostate cancer. *Journal of Nuclear Medicine*, jnumed.119.236414. https://doi.org/10.2967/jnumed.119.236414

53. Kroemer, G., Galluzzi, L., Kepp, O., & Zitvogel, L. (2013). Immunogenic cell death in cancer therapy. *Annual Review of Immunology*, *31*, 51–72. https://doi.org/10.1146/annurev-immunol-032712-100008

54. Kepp, O., Senovilla, L., Vitale, I., Vacchelli, E., Adjemian, S., Agostinis, P., Apetoh, L., Aranda, F., Barnaba, V., Bloy, N., Bracci, L., Breckpot, K., Brough, D., Buqué, A., Castro, M. G., Cirone, M., Colombo, M. I., Cremer, I., Demaria, S., … Galluzzi, L. (2014). Consensus guidelines for the detection of immunogenic cell death. *Oncoimmunology*, *3*(9). https://doi.org/10.4161/21624011.2014.955691

55. Zhou, J., Wang, G., Chen, Y., Wang, H., Hua, Y., & Cai, Z. (2019). Immunogenic cell death in cancer therapy: Present and emerging inducers. *Journal of Cellular and Molecular Medicine*, *23*(8), 4854–4865. https://doi.org/10.1111/jcmm.14356

56. Michalak, M., Groenendyk, J., Szabo, E., Gold, L. I., & Opas, M. (2009). Calreticulin, a multi-process calcium-buffering chaperone of the endoplasmic reticulum. *The Biochemical Journal*, *417*(3), 651–666. https://doi.org/10.1042/BJ20081847

57. Tesniere, A., Apetoh, L., Ghiringhelli, F., Joza, N., Panaretakis, T., Kepp, O., Schlemmer, F., Zitvogel, L., & Kroemer, G. (2008). Immunogenic cancer cell death: A key-lock paradigm. *Current Opinion in Immunology*, *20*(5), 504–511. https://doi.org/10.1016/j.coi.2008.05.007

58. Liu P, Zhao L, Loos F, Iribarren K, Lachkar S, Zhou H (2017) *Identification of pharmacological agents that induce HMGB1 release*. Sci Rep. Retrieved September 16, 2020, from https://www.ncbi.nlm.nih.gov/pmc/articles/PMC5668281/

59. Apetoh, L., Ghiringhelli, F., Tesniere, A., Criollo, A., Ortiz, C., Lidereau, R., Mariette, C., Chaput, N., Mira, J. P., Delaloge, S., André, F., Tursz, T., Kroemer, G., & Zitvogel, L. (2007). The interaction between HMGB1 and TLR4 dictates the outcome of anticancer chemotherapy and radiotherapy. *Immunological reviews*, *220*, 47–59. https://doi.org/10.1111/j.1600-065X.2007.00573.x

60. Yang, H., Wang, H., Chavan, S. S., & Andersson, U. (2015). High Mobility Group Box Protein 1 (HMGB1): The Prototypical Endogenous Danger Molecule. *Molecular Medicine (Cambridge, Mass.)*, *21 Suppl 1*, S6–S12. https://doi.org/10.2119/molmed.2015.00087

61. Galluzzi, L., Buqué, A., Kepp, O., Zitvogel, L., & Kroemer, G. (2017). Immunogenic cell death in cancer and infectious disease. *Nature Reviews. Immunology*, *17*(2), 97–111. https://doi.org/10.1038/nri.2016.107

62. De Andrade Carvalho, H., & Villar, R. C. (2018). Radiotherapy and immune response: The systemic effects of a local treatment. *Clinics*, *73*(Suppl 1). https://doi.org/10.6061/clinics/2018/e557s

63. Galluzzi L, Maiuri MC, Vitale I, Zischka H, Castedo M, Zitvogel L. (2007). Cell death modalities: classification and pathophysiological implications. Cell Death Differ. 2007;14((7)):1237–43.

64. Barker, H. E., Paget, J. T. E., Khan, A. A., & Harrington, K. J. (2015). The tumour microenvironment after radiotherapy: Mechanisms of resistance and recurrence. *Nature Reviews. Cancer*, *15*(7), 409–425. https://doi.org/10.1038/nrc3958

65. Montico, B., Nigro, A., Casolaro, V., & Dal Col, J. (2018). Immunogenic Apoptosis as a Novel Tool for Anticancer Vaccine Development. *International Journal of Molecular Sciences*, *19*(2). https://doi.org/10.3390/ijms19020594

66. Elmore S. *(2007).* Apoptosis: A Review of Programmed Cell Death. *Toxicol Pathol*. Retrieved September 16, 2020, from https://www.ncbi.nlm.nih.gov/pmc/articles/PMC2117903/

67. *APOPTOSIS IN RADIATION THERAPY: A DOUBLE-EDGED SWORD | Experimental oncology*. (n.d.). Retrieved September 16, 2020, from https://exp-oncology.com.ua/article/3516/apoptosis-in-radiation-therapy-a-double-edged-sword

68. Zhu, J., Powis de Tenbossche, C. G., Cané, S., Colau, D., van Baren, N., Lurquin, C., Schmitt-Verhulst, A.-M., Liljeström, P., Uyttenhove, C., & Van den Eynde, B. J. (2017). Resistance to cancer immunotherapy mediated by apoptosis of tumor-infiltrating lymphocytes. *Nature Communications*, *8*(1), 1404. https://doi.org/10.1038/s41467-017-00784-1

69. Cohen, J. J. (1991). Programmed cell death in the immune system. *Advances in Immunology*, *50*, 55–85. https://doi.org/10.1016/s0065-2776(08)60822-6

70. D'Arcy, M. S. (2019). Cell death: A review of the major forms of apoptosis, necrosis and autophagy. *Cell Biology International*, *43*(6), 582–592. https://doi.org/10.1002/cbin.11137

71. Nagata, S. (2018). Apoptosis and Clearance of Apoptotic Cells. *Annual Review of Immunology*, *36*. https://doi.org/10.1146/annurev-immunol-042617-053010

72. Grabarek, J., Amstad, P., & Darzynkiewicz, Z. (2002). Use of fluorescently labeled caspase inhibitors as affinity labels to detect activated caspases. *Human Cell*, *15*(1), 1–12. https://doi.org/10.1111/j.1749-0774.2002.tb00094.x

73. Cohen, G. M. (1997). Caspases: The executioners of apoptosis. *The Biochemical Journal*, *326 ( Pt 1)*, 1–16. https://doi.org/10.1042/bj3260001

74. Martinvalet, D., Zhu, P., & Lieberman, J. (2005). Granzyme A induces caspase-independent mitochondrial damage, a required first step for apoptosis. *Immunity*, *22*(3), 355–370. https://doi.org/10.1016/j.immuni.2005.02.004

75. Boland, K., Flanagan, L., & Prehn, J. H. (2013). Paracrine control of tissue regeneration and cell proliferation by Caspase-3. *Cell Death and Disease*. https://doi.org/10.1038/cddis.2013.250

76. Fulda, S., & Debatin, K.-M. (2006). Extrinsic versus intrinsic apoptosis pathways in anticancer chemotherapy. *Oncogene*, *25*(34), 4798–4811. https://doi.org/10.1038/sj.onc.1209608

77. Parrish, A. B., Freel, C. D., & Kornbluth, S. (2013). Cellular mechanisms controlling caspase activation and function. *Cold Spring Harbor Perspectives in Biology*, *5*(6). https://doi.org/10.1101/cshperspect.a008672

78. Plesca, I., Tunger, A., Müller, L., Wehner, R., Lai, X., Grimm, M.-O., Rutella, S., Bachmann, M., & Schmitz, M. (2020). Characteristics of Tumor-Infiltrating Lymphocytes Prior to and During Immune Checkpoint Inhibitor Therapy. *Frontiers in Immunology*, *11*, 364. https://doi.org/10.3389/fimmu.2020.00364

79. Kurozumi, S., Fujii, T., Matsumoto, H., Inoue, K., Kurosumi, M., Horiguchi, J., & Kuwano, H. (2017). Significance of evaluating tumor-infiltrating lymphocytes (TILs) and programmed cell

death-ligand 1 (PD-L1) expression in breast cancer. *Medical Molecular Morphology*, *50*(4), 185–194. https://doi.org/10.1007/s00795-017-0170-y

80. Swann, J. (2007). JCI - Immune surveillance of tumors. *J Clin Invest*. https://www.jci.org/articles/view/31405
81. Mlecnik, B., Bindea, G., Pagès, F., & Galon, J. (2011). Tumor immunosurveillance in human cancers. *Cancer Metastasis Reviews*, *30*(1), 5–12. https://doi.org/10.1007/s10555-011-9270-7
82. Goswami, S., Aparicio, A., & Subudhi, S. K. (2016). Immune Checkpoint Therapies in Prostate Cancer. *Cancer Journal (Sudbury, Mass.)*, *22*(2), 117–120. https://doi.org/10.1097/PPO.0000000000000176
83. Akinleye, A., & Rasool, Z. (2019). Immune checkpoint inhibitors of PD-L1 as cancer therapeutics. *Journal of Hematology & Oncology*, *12*(1), 92. https://doi.org/10.1186/s13045-019-0779-5
84. Havel, J. J., Chowell, D., & Chan, T. A. (2019). The evolving landscape of biomarkers for checkpoint inhibitor immunotherapy. *Nature Reviews. Cancer*, *19*(3), 133–150. https://doi.org/10.1038/s41568-019-0116-x
85. Xing K, Gu B, Zhang P, Wu X. (2015). Dexamethasone enhances programmed cell death 1 (PD-1) expression during T cell activation: An insight into the optimum application of glucocorticoids in anti-cancer therapy. *BMC Immunology*. Retrieved September 16, 2020, from https://bmcimmunol.biomedcentral.com/articles/10.1186/s12865-015-0103-2
86. Kovacsovics-Bankowski, M., Chisholm, L., Vercellini, J., Crittenden, M., Lary, S., Curti, B., & Weinberg, A. (2013). Phase I/II clinical trial of anti-OX40, radiation and cyclophosphamide in patients with prostate cancer: Immunological analysis. *Journal for ImmunoTherapy of Cancer*, *1*(1), P255. https://doi.org/10.1186/2051-1426-1-S1-P255

87. Croft, M., So, T., Duan, W., & Soroosh, P. (2009). The Significance of OX40 and OX40L to T cell Biology and Immune Disease. *Immunological Reviews*, *229*(1), 173–191. https://doi.org/10.1111/j.1600-065X.2009.00766.x

88. Gramaglia, I., Weinberg, A. D., Lemon, M., & Croft, M. (1998). Ox-40 ligand: A potent costimulatory molecule for sustaining primary CD4 T cell responses. *Journal of Immunology (Baltimore, Md.: 1950)*, *161*(12), 6510–6517.

89. Fay, A. P., & Antonarakis, E. S. (2019). Blocking the PD-1/PD-L1 axis in advanced prostate cancer: Are we moving in the right direction? *Annals of Translational Medicine*, *7*(Suppl 1), S7. https://doi.org/10.21037/atm.2019.01.37

90. *The IFN-γ/PD-L1 axis between T cells and tumor microenvironment: Hints for glioma anti-PD-1/PD-L1 therapy | Journal of Neuroinflammation | Full Text*. (n.d.). Retrieved September 16, 2020, from https://jneuroinflammation.biomedcentral.com/articles/10.1186/s12974-018-1330-2

91. Barron, D. A., & Rowley, D. R. (2012). The reactive stroma microenvironment and prostate cancer progression. *Endocrine-Related Cancer*, *19*(6), R187-204. https://doi.org/10.1530/ERC-12-0085

92. Morrissey, C., & Vessella, R. L. (2007). The role of tumor microenvironment in prostate cancer bone metastasis. *Journal of Cellular Biochemistry*. https://onlinelibrary.wiley.com/doi/abs/10.1002/jcb.21214

93. Weinberg, A. D., Morris, N. P., Kovacsovics-Bankowski, M., Urba, W. J., & Curti, B. D. (2011). Science gone translational: The OX40 agonist story. *Immunological Reviews*, *244*(1), 218–231. https://doi.org/10.1111/j.1600-065X.2011.01069.x

94. Evans DE, Prell RA, Thalhofer CJ, Hurwitz AA, Weinberg AD. (2001). Engagement of OX40 enhances antigen-specific CD4(+) T cell mobilization/memory development and humoral immunity: comparison of alphaOX-40 with alphaCTLA-4. *J Immunol*, 167:6804–6811.

95. Fradet, Y., Klotz, L., Trachtenberg, J., & Zlotta, A. (2009). The burden of prostate cancer in Canada. *Canadian Urological Association Journal*, *3*(3 Suppl 2), S92–S100

96. Hofman, M., Violet, J. A., Hicks, R. J., Ferdinandus, J., Thang, S. P., Iravani, A., Kong, G., Ravi Kumar, A., Akhurst, T. J., Mooi, J., Guo, C., Tran, B., Jackson, P., Scalzo, M., Eu, P., Williams, S., & Sandhu, S. K. (2019). Results of a 50 patient single-center phase II prospective trial of Lutetium-177 PSMA-617 theranostics in metastatic castrate-resistant prostate cancer. *Journal of Clinical Oncology*, *37*(7_suppl), 228–228. https://doi.org/10.1200/JCO.2019.37.7_suppl.228

97. Baum, R. P., Kulkarni, H. R., Schuchardt, C., Singh, A., Wirtz, M., Wiessalla, S., Schottelius, M., Mueller, D., Klette, I., & Wester, H.-J. (2016). 177Lu-Labeled Prostate-Specific Membrane Antigen Radioligand Therapy of Metastatic Castration-Resistant Prostate Cancer: Safety and Efficacy. *Journal of Nuclear Medicine: Official Publication, Society of Nuclear Medicine*, *57*(7), 1006–1013. https://doi.org/10.2967/jnumed.115.168443

98. Chen, N., & Zhou, Q. (2016). The evolving Gleason grading system. *Chinese journal of cancer research = Chung-kuo yen cheng yen chiu*, *28*(1), 58–64. https://doi.org/10.3978/j.issn.1000-9604.2016.02.04

99. Kinsella, N., Helleman, J., Bruinsma, S., Carlsson, S., Cahill, D., Brown, C., & Van Hemelrijck, M. (2018). Active surveillance for prostate cancer: a systematic review of contemporary worldwide practices. *Translational andrology and urology*, *7*(1), 83–97. https://doi.org/10.21037/tau.2017.12.24

100. *Hormone Therapy for Prostate Cancer*. (n.d.). Retrieved September 16, 2020, from https://www.cancer.org/cancer/prostate-cancer/treating/hormone-therapy.html

101. Siddiqui, Z. A., & Krauss, D. J. (2018). Adjuvant androgen deprivation therapy for prostate cancer treated with radiation therapy. *Translational andrology and urology*, *7*(3), 378–389. https://doi.org/10.21037/tau.2018.01.06

102. Saad, F., & Hotte, S. J. (2010). Guidelines for the management of castrate-resistant prostate cancer. *Canadian Urological Association journal = Journal de l'Association des urologues du Canada*, *4*(6), 380–384. https://doi.org/10.5489/cuaj.10167

103. Heston, W. D. (1996). [Significance of prostate-specific membrane antigen (PSMA). A neurocarboxypeptidase and membrane folate hydrolase]. *Der Urologe. Ausg. A*, *35*(5), 400–407. https://doi.org/10.1007/s001200050041

104. Fung, E. K., Cheal, S. M., Fareedy, S. B., Punzalan, B., Beylergil, V., Amir, J., Chalasani, S., Weber, W. A., Spratt, D. E., Veach, D. R., Bander, N. H., Larson, S. M., Zanzonico, P. B., & Osborne, J. R. (2016). Targeting of radiolabeled J591 antibody to PSMA-expressing tumors: Optimization of imaging and therapy based on non-linear compartmental modeling. *EJNMMI Research*, *6*. https://doi.org/10.1186/s13550-016-0164-0

105. *PSMA PET and radionuclide therapy in prostate cancer*. (n.d.). Retrieved September 16, 2020, from https://www.ncbi.nlm.nih.gov/pmc/articles/PMC5123597/

106. Giovacchini, G., Giovannini, E., Riondato, M., & Ciarmiello, A. (2018). PET/CT With 68Ga-PSMA in Prostate Cancer: Radiopharmaceutical Background and Clinical Implications. *Current Radiopharmaceuticals*, *11*(1), 4–13. https://doi.org/10.2174/1874471010666171101121803

107. Kratochwil C, Giesel FL, Stefanova M, Benešová M, Bronzel M, Afshar-Oromieh A, Mier W, Eder M, Kopka K, Haberkorn U. (2016) PSMA-Targeted Radionuclide Therapy of Metastatic

Castration-Resistant Prostate Cancer with 177Lu-Labeled PSMA-617. *J Nucl Med*, 57(8):1170-6. doi: 10.2967/jnumed.115.171397. Epub 2016 Mar 16. PubMed PMID: 26985056.

108. Vatner, R. E., Cooper, B. T., Vanpouille-Box, C., Demaria, S., & Formenti, S. C. (2014). Combinations of immunotherapy and radiation in cancer therapy. *Frontiers in oncology*, *4*, 325. https://doi.org/10.3389/fonc.2014.00325

109. Foster, B. A., Gingrich, J. R., Kwon, E. D., Madias, C., & Greenberg, N. M. (1997). Characterization of prostatic epithelial cell lines derived from transgenic adenocarcinoma of the mouse prostate (TRAMP) model. *Cancer Research*, *57*(16), 3325–3330.

110. Takara Bio. (2017) *Lenti-X™ Tet-On® 3G Inducible Expression System*. 24.

111. Krueger, C., Pfleiderer, K., Hillen, W., & Berens, C. (2004). Tetracycline derivatives: Alternative effectors for Tet transregulators. *BioTechniques*, *37*(4), 546, 548, 550. https://doi.org/10.2144/04374BM04

112. O'Keefe, D. S., Bacich, D. J., Huang, S. S., & Heston, W. D. W. (2018). A Perspective on the Evolving Story of PSMA Biology, PSMA-Based Imaging, and Endoradiotherapeutic Strategies. *Journal of Nuclear Medicine: Official Publication, Society of Nuclear Medicine*, *59*(7), 1007–1013. https://doi.org/10.2967/jnumed.117.203877

113. Tönnesmann, R., Meyer, P. T., Eder, M., & Baranski, A.-C. (2019). [177Lu]Lu-PSMA-617 Salivary Gland Uptake Characterized by Quantitative In Vitro Autoradiography. *Pharmaceuticals*, *12*(1). https://doi.org/10.3390/ph12010018

114. Janiczek, M., Szylberg, Ł., Kasperska, A., Kowalewski, A., Parol, M., Antosik, P., Radecka, B., & Marszałek, A. (2017). Immunotherapy as a Promising Treatment for Prostate Cancer: A Systematic Review. *Journal of Immunology Research*, *2017*, 4861570. https://doi.org/10.1155/2017/4861570

115. Kwon, E. D., Drake, C. G., Scher, H. I., Fizazi, K., Bossi, A., van den Eertwegh, A. J. M., Krainer, M., Houede, N., Santos, R., Mahammedi, H., Ng, S., Maio, M., Franke, F. A., Sundar, S., Agarwal, N., Bergman, A. M., Ciuleanu, T. E., Korbenfeld, E., Sengeløv, L., … CA184-043 Investigators. (2014). Ipilimumab versus placebo after radiotherapy in patients with metastatic castration-resistant prostate cancer that had progressed after docetaxel chemotherapy (CA184-043): A multicentre, randomised, double-blind, phase 3 trial. *The Lancet. Oncology*, *15*(7), 700–712. https://doi.org/10.1016/S1470-2045(14)70189-5

116. van Kalmthout, L., Braat, A., Lam, M., van Leeuwaarde, R., Krijger, G., Ververs, T., Mehra, N., Bins, A., Hunting, J., & de Keizer, B. (2019). First Experience With 177Lu-PSMA-617 Therapy for Advanced Prostate Cancer in the Netherlands. *Clinical Nuclear Medicine*, *44*(6), 446–451. https://doi.org/10.1097/RLU.0000000000002561

117. Silvestri, I., Cattarino, S., Aglianò, A. M., Collalti, G., & Sciarra, A. (2015). Beyond the Immune Suppression: The Immunotherapy in Prostate Cancer. *BioMed Research International*, *2015*. https://doi.org/10.1155/2015/794968

118. Slee, E. A., Adrain, C., & Martin, S. J. (2001). Executioner caspase-3, -6, and -7 perform distinct, non-redundant roles during the demolition phase of apoptosis. *The Journal of Biological Chemistry*, *276*(10), 7320–7326. https://doi.org/10.1074/jbc.M008363200

119. Rathmell, J. C., & Thompson, C. B. (2002). Pathways of apoptosis in lymphocyte development, homeostasis, and disease. *Cell*, *109 Suppl*, S97–S107. https://doi.org/10.1016/s0092-8674(02)00704-3

120. Molecular mechanisms of cell death: recommendations of the Nomenclature Committee on Cell Death. (2018). *Cell Death & Differentiation* [Internet]. [cited 2020 Mar 20]. Available from: https://www.nature.com/articles/s41418-017-0012-4

121. Regulation of apoptosis in health and disease: the balancing act of BCL-2 family proteins | *Nature Reviews Molecular Cell Biology* [Internet]. [cited 2020 Mar 20]. Available from: https://www.nature.com/articles/s41580-018-0089-8

122. Poręba, M., Stróżyk, A., Salvesen, G. S., & Drąg, M. (2013). Caspase Substrates and Inhibitors. *Cold Spring Harbor Perspectives in Biology*, *5*(8), a008680. https://doi.org/10.1101/cshperspect.a008680

123. Timmer JC, Salvesen GS. 2007. Caspase substrates. Cell Death Differ 14: 66–72.

124. Pardo, J., Bosque, A., Brehm, R., Wallich, R., Naval, J., Müllbacher, A., Anel, A., & Simon, M. M. (2004). Apoptotic pathways are selectively activated by granzyme A and/or granzyme B in CTL-mediated target cell lysis. *The Journal of cell biology*, *167*(3), 457–468. https://doi.org/10.1083/jcb.200406115

125. Krautwald, S., Ziegler, E., Rölver, L., Linkermann, A., Keyser, K. A., Steen, P., Wollert, K. C., Korf-Klingebiel, M., & Kunzendorf, U. (2010). Effective blockage of both the extrinsic and intrinsic pathways of apoptosis in mice by TAT-crmA. *The Journal of biological chemistry*, *285*(26), 19997–20005. https://doi.org/10.1074/jbc.M110.122127

126. Chinnaiyan AM. (1999). The apoptosome: heart and soul of the cell death machine. *Neoplasia*. (1):5–15.

127. Kischkel FC, Hellbardt S, Behrmann I, Germer M, Pawlita M, Krammer PH. (1995) Cytotoxicity-dependent APO-1 (Fas/CD95)-associated proteins form a death-inducing signaling complex (DISC) with the receptor. *EMBO J.* 1995;14(22):5579–88.

128. Rai NK, Tripathi K, Sharma D, Shukla VK. (2005). Apoptosis: a basic physiologic process in wound healing. *Int J Low Extrem Wounds*.; 4(3):138–44.

129. Schuler M, Green DR. (2001). Mechanisms of p53-dependent apoptosis. *Biochem Soc Trans*.;29(Pt 6):684–8.

130. Kerr JF, Winterford CM, Harmon BV. (1994). Apoptosis. Its significance in cancer and cancer therapy. *Cancer*.;73(8):2013–26.

131. Evan GI, Vousden KH.(2001). Proliferation, cell cycle and apoptosis in cancer. *Nature*; 411: 342–348.

132. Liu J-j Lin M, Yu J-y, Liu B, Bao J-k. (2011). Targeting apoptotic and autophagic pathways for cancer therapeutics. *Cancer Lett* 300: 105–114

133. Hassan M, Watari H, AbuAlmaaty A, Ohba Y, Sakuragi N. (2014). Apoptosis and Molecular Targeting Therapy in Cancer. *BioMed Research International* 2014:1–23

134. A. G. Eliopoulos, D. J. Kerr, J. Herod. (1995). The control of apoptosis and drug resistance in ovarian cancer: influence of p53 and Bcl-2. *Oncogene*, 11:1217–1228

135. M. Kartalou and J. M. Essigmann. (2001). Recognition of cisplatin adducts by cellular proteins. *Fundamental and Molecular Mechanisms of Mutagenesis*, vol. 478, no. 1-2, pp. 1–21, 2001.

136. Baig S, Seevasant I, Mohamad J, Mukheem A, Huri HZ, Kamarul T. (2016). Potential of apoptotic pathway-targeted cancer therapeutic research: Where do we stand? *Cell Death & Disease.*7(1): e2058–e2058.

137. Fischer U, Schulze-Osthoff K. (2005). Apoptosis-based therapies and drug targets. *Cell Death Differ* 12(S1):942–61.

138. Roth W, Isenmann S, Naumann U, Kugler S, Bahr M, Dichgans J, Ashkenazi A and Weller M (1999). Locoregional Apo2L/TRAIL eradicates intracranial human malignant glioma xenografts in athymic mice in the absence of neurotoxicity. *Biochem. Biophys. Res. Commun*. 265: 479–4

139. Walczak H, Miller RE, Ariail K, Gliniak B, Griffith TS, Kubin M, Chin W, Jones J, Woodward A, Le T, Smith C, Smolak P, Goodwin RG, Rauch CT, Schuh JC and Lynch DH (1999) Tumoricidal activity of tumor necrosis factor-related apoptosis-inducing ligand in vivo. *Nat. Med*. 5: 157–163

140. Ashkenazi A, Pai RC, Fong S, Leung S, Lawrence DA, Marsters SA, Blackie C, Chang L, McMurtrey AE, Hebert A, DeForge L, Koumenis IL, Lewis D, Harris L, Bussiere J, Koeppen H, Shahrokh Z and Schwall RH (1999) Safety and anti-tumor activity of recombinant soluble Apo2 ligand.*J.Clin.Invest.*104: 155–162

141. Wu, J., & Waxman, D. J. (2018). Immunogenic chemotherapy: Dose and schedule dependence and combination with immunotherapy. *Cancer letters*, *419*, 210–221. https://doi.org/10.1016/j.canlet.2018.01.050

142. Scurr M, Pembroke T, Bloom A, Roberts D, Thomson A, Smart K. (2017). Low-Dose Cyclophosphamide Induces Antitumor T-Cell Responses, which Associate with Survival in Metastatic Colorectal Cancer. *Clin Cancer Res*. 23(22):6771–80.

143. Batty N, Yarlagadda N, Pili R. Major Response to Cyclophosphamide and Prednisone in Recurrent Castration-Resistant Prostate Cancer. (2013). *Journal of the National Comprehensive Cancer Network*. 1;11(8):911–5.

144. Chaudhary, B., & Elkord, E. (2016). Regulatory T Cells in the Tumor Microenvironment and Cancer Progression: Role and Therapeutic Targeting. *Vaccines*, *4*(3), 28. https://doi.org/10.3390/vaccines4030028

145. Amarante-Mendes, G. P., Adjemian, S., Branco, L. M., Zanetti, L. C., Weinlich, R., & Bortoluci, K. R. (2018). Pattern Recognition Receptors and the Host Cell Death Molecular Machinery. *Frontiers in Immunology*, *9*, 2379. https://doi.org/10.3389/fimmu.2018.02379

146. Land W. G. (2015). The Role of Damage-Associated Molecular Patterns (DAMPs) in Human Diseases: Part II: DAMPs as diagnostics, prognostics and therapeutics in clinical medicine. *Sultan Qaboos University medical journal*, *15*(2), e157–e170.

147. Gold, L. I., Eggleton, P., Sweetwyne, M. T., Van Duyn, L. B., Greives, M. R., Naylor, S. M., Michalak, M., & Murphy-Ullrich, J. E. (2010). Calreticulin: non-endoplasmic reticulum functions in physiology and disease. *FASEB journal: official publication of the Federation of American Societies for Experimental Biology*, 24(3), 665–683. https://doi.org/10.1096/fj.09-145482

148. Michalak M, Groenendyk J, Szabo E, Gold L I, Opas M. (2009). Calreticulin, a multi-process calcium-buffering chaperone of the endoplasmic reticulum. *Biochem J*. 417:651–666

149. Liu P, Zhao L, Loos F, Iribarren K, Lachkar S, Zhou H. (2017). Identification of pharmacological agents that induce HMGB1 release. Sci Rep [Internet]. [cited 2020 Aug 7];7. Available from: https://www.ncbi.nlm.nih.gov/pmc/articles/PMC5668281/

150. Yamazaki, T., Hannani, D., Poirier-Colame, V., Ladoire, S., Locher, C., Sistigu, A., Prada, N., Adjemian, S., Catani, J. P., Freudenberg, M., Galanos, C., André, F., Kroemer, G., & Zitvogel, L. (2014). Defective immunogenic cell death of HMGB1-deficient tumors: compensatory therapy with TLR4 agonists. *Cell death and differentiation*, *21*(1), 69–78. https://doi.org/10.1038/cdd.2013.72

151. Reisz, J. A., Bansal, N., Qian, J., Zhao, W., & Furdui, C. M. (2014). Effects of ionizing radiation on biological molecules--mechanisms of damage and emerging methods of detection. *Antioxidants & redox signaling*, *21*(2), 260–292. https://doi.org/10.1089/ars.2013.5489

152. Dudzinski SO, Cameron BD, Wang J, Rathmell JC, Giorgio TD, Kirschner AN. (2019) Combination immunotherapy and radiotherapy causes an abscopal treatment response in a mouse

model of castration resistant prostate cancer. *Journal for ImmunoTherapy of Cancer*. 14;7(1):218.

153. Shevtsov M, Sato H, Multhoff G, Shibata A. (2019). Novel Approaches to Improve the Efficacy of Immuno-Radiotherapy. *Front Oncol* [Internet; cited 2020 May 25]. Available from: https://www.frontiersin.org/articles/10.3389/fonc.2019.00156/full

154. Liu Y, Dong Y, Kong L, Shi F, Zhu H, Yu J.(2018). Abscopal effect of radiotherapy combined with immune checkpoint inhibitors. *J Hematol Oncol* [Internet; cited 2020 Aug 13];11. Available from: https://www.ncbi.nlm.nih.gov/pmc/articles/PMC6097415/

155. Ngwa W, Irabor OC, Schoenfeld JD, Hesser J, Demaria S, Formenti SC. (2018). Using immunotherapy to boost the abscopal effect. *Nat Rev Cancer*. May;18(5):313–22.

156. Wang, Xuan. Directed studies report. 2017 [cited 2020 Aug 24]

157. Mikyskova, R., Indrova, M., Stepanek, I., Kanchev, I., Bieblova, J., Vosahlikova, S., Moserova, I., Truxova, I., Fucikova, J., Bartunkova, J., Spisek, R., Sedlacek, R., & Reinis, M. (2017). Dendritic cells pulsed with tumor cells killed by high hydrostatic pressure inhibit prostate tumor growth in TRAMP mice. *Oncoimmunology*, *6*(12), e1362528. https://doi.org/10.1080/2162402X.2017.1362528

158. Kasikova L, Hensler M, Truxova I, Skapa P, Laco J, Belicova L. (2019). Calreticulin exposure correlates with robust adaptive antitumor immunity and favorable prognosis in ovarian carcinoma patients. *Journal for ImmunoTherapy of Cancer*. 20;7(1):312.

159. De Sousa Linhares A, Leitner J, Grabmeier-Pfistershammer K, Steinberger P. (2018). Not All Immune Checkpoints Are Created Equal. *Front Immunol* [Internet]. [cited 2020 May 25];9.

160. Arneth B. (2019). Tumor Microenvironment. *Medicina (Kaunas, Lithuania)*, *56*(1), 15. https://doi.org/10.3390/medicina56010015

161. Zhang, N., & Bevan, M. J. (2011). CD8(+) T cells: Foot soldiers of the immune system. *Immunity*, *35*(2), 161–168. https://doi.org/10.1016/j.immuni.2011.07.010

162. Dustin M. L. (2014). The immunological synapse. *Cancer immunology research*, *2*(11), 1023–1033. https://doi.org/10.1158/2326-6066.CIR-14-0161

163. Picardo, S. L., & Hansen, A. R. (2019). The PD-1/PD-L1 pathway in advanced prostate cancer-have we milked this cow? *Annals of Translational Medicine*, *7*(14), 346. https://doi.org/10.21037/atm.2019.05.86

164. Qian J, Wang C, Wang B, Yang J, Wang Y, Luo F. (2018). The IFN-γ/PD-L1 axis between T cells and tumor microenvironment: hints for glioma anti-PD-1/PD-L1 therapy. *Journal of Neuroinflammation* 15(1):290.

165. Juneja VR, McGuire KA, Manguso RT, LaFleur MW, Collins N, Haining WN. (2017). PD-L1 on tumor cells is sufficient for immune evasion in immunogenic tumors and inhibits CD8 T cell cytotoxicity. *J Exp Med*. 3;214(4):895–904.

166. Evans DE, Prell RA, Thalhofer CJ, Hurwitz AA, Weinberg AD. (2001). Engagement of OX40 enhances antigen-specific CD4(+) T cell mobilization/memory development and humoral immunity: comparison of alphaOX-40 with alphaCTLA-4. *J Immunol*. 167:6804–6811.

167. Olson, B. M., Jankowska-Gan, E., Becker, J. T., Vignali, D. A., Burlingham, W. J., & McNeel, D. G. (2012). Human prostate tumor antigen-specific CD8+ regulatory T cells are inhibited by CTLA-4 or IL-35 blockade. *Journal of immunology (Baltimore, Md.: 1950)*, *189*(12), 5590–5601. https://doi.org/10.4049/jimmunol.1201744

168. Ebelt, K., Babaryka, G., Frankenberger, B., Stief, C. G., Eisenmenger, W., Kirchner, T., Schendel, D. J., & Noessner, E. (2009). Prostate cancer lesions are surrounded by FOXP3+, PD-

1+ and B7-H1+ lymphocyte clusters. *European journal of cancer (Oxford, England : 1990)*, *45*(9), 1664–1672. https://doi.org/10.1016/j.ejca.2009.02.015

169. Kiniwa, Y., Miyahara, Y., Wang, H. Y., Peng, W., Peng, G., Wheeler, T. M., Thompson, T. C., Old, L. J., & Wang, R. F. (2007). CD8+ Foxp3+ regulatory T cells mediate immunosuppression in prostate cancer. *Clinical cancer research : an official journal of the American Association for Cancer Research*, *13*(23), 6947–6958. https://doi.org/10.1158/1078-0432.CCR-07-0842

170. Miller, A. M., Lundberg, K., Ozenci, V., Banham, A. H., Hellström, M., Egevad, L., & Pisa, P. (2006). CD4+CD25high T cells are enriched in the tumor and peripheral blood of prostate cancer patients. *Journal of immunology (Baltimore, Md: 1950)*, *177*(10), 7398–7405. https://doi.org/10.4049/jimmunol.177.10.7398

171. Calderhead, D. M., Buhlmann, J. E., van den Eertwegh, A. J., Claassen, E., Noelle, R. J., & Fell, H. P. (1993). Cloning of mouse Ox40: A T cell activation marker that may mediate T-B cell interactions. *The Journal of Immunology*, *151*(10), 5261.

172. Deng, L., Liang, H., Burnette, B., Beckett, M., Darga, T., Weichselbaum, R. R., & Fu, Y. X. (2014). Irradiation and anti-PD-L1 treatment synergistically promote antitumor immunity in mice. *The Journal of clinical investigation*, *124*(2), 687–695. https://doi.org/10.1172/JCI67313

173. Shen, X., Zhang, L., Li, J., Li, Y., Wang, Y., & Xu, Z. X. (2019). Recent Findings in the Regulation of Programmed Death Ligand 1 Expression. *Frontiers in immunology*, *10*, 1337. https://doi.org/10.3389/fimmu.2019.01337

174. Gibbons Johnson, R. M., & Dong, H. (2017). Functional Expression of Programmed Death-Ligand 1 (B7-H1) by Immune Cells and Tumor Cells. *Frontiers in immunology*, *8*, 961. https://doi.org/10.3389/fimmu.2017.00961

175. Higano CS, Schellhammer PF, Small EJ, Burch PA, Nemunaitis J, Yuh L, Provost N, Frohlich Placebo-controlled phase III trial of immunologic therapy with sipuleucel-T (APC8015) in patients with metastatic, asymptomatic hormone refractory prostate cancer. MW Cancer. 2009 Aug 15; 115(16):3670-9.

176. Plosker, G. L. (2011). Sipuleucel-T. *Drugs*, *71*(1), 101–108. https://doi.org/10.2165/11206840-000000000-00000

177. Madan, R. A., Arlen, P. M., Mohebtash, M., Hodge, J. W., & Gulley, J. L. (2009). Prostvac-VF: a vector-based vaccine targeting PSA in prostate cancer. *Expert opinion on investigational drugs*, *18*(7), 1001–1011. https://doi.org/10.1517/13543780902997928

178. Redman, J. M., Gulley, J. L., & Madan, R. A. (2017). Combining immunotherapies for the treatment of prostate cancer. *Urologic oncology*, *35*(12), 694–700. https://doi.org/10.1016/j.urolonc.2017.09.024

179. Triggiani, L., Alongi, F., Buglione, M., Detti, B., Santoni, R., Bruni, A., Maranzano, E., Lohr, F., D'Angelillo, R., Magli, A., Bonetta, A., Mazzola, R., Pasinetti, N., Francolini, G., Ingrosso, G., Trippa, F., Fersino, S., Borghetti, P., Ghirardelli, P., & Magrini, S. M. (2017). Efficacy of stereotactic body radiotherapy in oligorecurrent and in oligoprogressive prostate cancer: new evidence from a multicentric study. *British journal of cancer*, *116*(12), 1520–1525. https://doi.org/10.1038/bjc.2017.103

180. Patel, P. H., Chaw, C. L., Tree, A. C., Sharabiani, M., & van As, N. J. (2019). Stereotactic body radiotherapy for bone oligometastatic disease in prostate cancer. *World journal of urology*, *37*(12), 2615–2621. https://doi.org/10.1007/s00345-019-02873-w